Spring 2009

Master's Thesis 2009

Candidate: Chameera K Jayarathna

Title: Experimental and computational study of the effect of particle size distributions on the flow behavior in fluidized beds

Telemark University College
Faculty of Technology

Telemark University College
Faculty of Technology
M.Sc. Programme

MASTER'S THESIS, COURSE CODE FMH606

Student: **Chameera K Jayarathna**

Thesis title: **Experimental and computational study of the effect of particle size distributions of the flow behavior in the fluidized beds**

Signature: . . . . . .

Number of pages: 99

Keywords: **Bubbling fluidization, Bubble behavior, CFD simulations**, **Pressure distribution**

Supervisor: **Britt M. Halvorsen** sign.: . . . . . .

Censor: sign.: . . . . . .

Availability: **Open**

Archive approval (supervisor signature)**:** sign.: . . . . . **Date :** . . . . . .

Abstract:

The aim of the work of this thesis is to study the flow behavior of a fluidized bed with respect to different particle mixtures.

The efficiency of the fluidized bed reactors depends on the bubble distribution, bubble size and the bubble velocity in the reactor. The bubble behavior depends on the amount of excess air introduced to the reactor.

Set of experiments and simulations are performed related to the study. The experiments are performed in a circular fluidized bed with uniform air distribution. Mixtures of spherical glass particles with different compositions with respective to the size of the particles are used for the experiments. The mixtures consist of two different particle types mainly, which are referred as large and small particles in the thesis. The minimum fluidization velocity, bubble behavior in the bed, pressure distribution in the bed and the bed expansion are observed for the two particle types and their mixtures.

As the first part of the computational study, a set of simulations are performed to select the optimum grid size for the mesh to be used for rest of the computational work. The meshes are prepared using commercial software Gambit. The simulations are performed using the commercial software FLUENT 6.3.

Two dimensional simulations are selected after comparing the simulations time requirement. The optimum grid size is found as 3x3 mm in a two dimensional bed.

As the second part of the computational study, a set of simulations Corresponding simulations are performed using the same conditions as in the experiments. The mean particle diameter of the mixture is used to represent each of the particle mixtures which are used in the experiments.

The predicted results from the simulations are compared with the experimental results.

Some of the results from this work have accepted to be presented in the modeling and simulation conference, sims50 at Denmark in year 2009. The paper is attached as an appendix.

Contents

I Theoretical studies and phenomenon of fluidization **7**

1 Introduction **8**
1.1 The phenomenon of fluidization 8
1.2 Liquidlike behavior of a fluidized bed 9
1.3 Advantages and disadvantages of the fluidized beds for industrial operations . . . 9
1.4 Factors effecting on the fluidization 11
1.5 Industrial applications of fluidized beds 12
1.6 Researches and experiments done on bubbling fluidization 13
1.7 Computational fluid dynamics for fluidization 15

2 Fluidization and mapping of regimes **16**
2.1 Characterization of particles 16
2.2 Minimum fluidization velocity 17
2.2.1 Calculation of minimum fluidization velocity theoretically 18
2.3 Minimum bubbling velocity and fluidization index 19
2.4 Pressure drop along the bed 20
2.5 The Geldart classification of particles 22
2.6 Importance of analyzes 24

3 Multiphase modelling **26**
3.1 Basic approaches of multiphase modelling 26
3.1.1 Euler-Euler approach 26
3.1.2 Euler-Lagrange approach 27
3.1.3 Lagrangian - Lagrangian approach 27
3.1.4 Multiphase approaches in former researches 27
3.2 The Eulerian model and the start-up of the simulation 28
3.3 Fundamentals of computational fluid dynamics 29
3.4 Available functions in FLUENT 29
3.4.1 Mass and momentum conservation equations 29
3.4.2 Drag models 30
3.4.3 Function for solid pressure 31
3.4.4 Radial distribution function 31
3.4.5 Functions for frictional viscosity 32
3.4.6 Functions for frictional pressure 32
3.4.7 Functions for granular viscosity 32
3.4.8 Granular bulk viscosity function 33
3.4.9 General equation for granular temperature 33

II Experimental and computational studies of flow behavior in bubbling fluidized bed 34

4 Experimental studies of bubbling fluidized bed 35
4.1 Lab scale experimental set up . . . 35
4.2 Preparation of particle samples for the experiments . . . 38
4.3 Experimental studies . . . 39
4.4 Observations from the experimental studies . . . 41
4.4.1 Volume fractions of the particle phases . . . 41
4.4.2 Minimum fluidization velocities, minimum bubbling velocity and expanded bed height . . . 42

5 Computational studies in bubbling fluidized beds 43
5.1 Optimum grid size verification . . . 43
5.1.1 Mesh preparation using Gambit . . . 43
5.1.2 Initializing the computer simulations in Fluent and determine the suitable mesh . . . 46
5.2 Simulating the bubbling fluidized bed with selected mesh . . . 46

6 Analysis of the results from experimental and computational studies 49
6.1 Bed expansion (experimental) . . . 49
6.2 Studies based on the minimum fluidization velocity . . . 50
6.2.1 Calculations of minimum fluidization velocity . . . 50
6.2.2 Analysis of all experimental, computational and theoretical minimum fluidization velocities . . . 51
6.3 Void fraction variations . . . 52
6.4 Analysis of fluidized bed behavior based on simulations . . . 55
6.5 Pressure variation of the observations with computations . . . 61

7 Conclusion for computational and experimental studies of bubbling fluidized bed 69

III Observations from experiments & simulations 74

A Experimental observations of bed expansion 75

B Experimental observations of void fractions 76

C Experimental observations of U_{mf} and U_{mb} 77

D Experimental observations of pressure variations along the bed with superficial air velocity 78

E Computational observations of pressure variations along the bed with superficial air velocity 82

F Comparison of experimental and computational pressure variations along the bed 86

G Particle size distribution 93

H Calculations of Umf **94**
H.1 For small particles 94
H.2 For large size particles 94

I Observations of excess air velocity **96**

Preface

Fluidization has became important engineering process over many years. There are many researches carried out on fluidization around the world. Telemark University College is playing an important role on these researches. I'm glad that, I had this opportunity to contribute for those researches with my master thesis. Dr.(Mrs.). Britt M. Halvorsen is a major character in the field of research on fluidization at Telemark University College (TUC). I am very lucky to have her as my supervisor for my thesis.

This report is enriched with the results from 91 simulations and experiments for 7 samples of particles. Since it takes a considerably long time to have data from 91 simulations, I hope these results will be useful for future research work. All the results are illustrated in the appendix.

Telemark University College provides excellent support for the students for their thesis work. I had enough computer facilities and other resources to continue my research studies without any obstacles. It is important to have enough computer facilities to run Fluent simulations, which take hours to run. I really appreciate the facilities provided by the library of TUC by providing all the literature requirements.

"*Fluidization Engineering, 2nd edition*" by Kunii D. et al and "*Multiphase Flow and Fluidization*" by Gidaspow D. et al have provided enough theoretical knowledge related to fluidization and its simulation. It was very important to follow up all the publications by Dr (Mrs). Britt Halvorsen and her PhD research. Former master student Ariyarathna S. has done some interesting research and some publication under her master thesis. I'm glad that, I had all of these resource people around me to make my thesis a success.

I am thankful to Dr (Mrs). Britt Halvorsen for her excellent supervision and all the other authors of the literature I have used. In addition I'm thanking to all the staff at TUC who has provided me enough resources to finish this report successfully. Finally, I thank to my family and friends who was backing me all the time and made me strong.

Chameera K Jayarathna

Nomenclature

A_t	Cross sectional area of tube	$[\mathrm{m}^2]$
C_D	Drag coefficient	
C_{fr}	Coefficient of friction between particles of two solid phases	
D_p, d	Particle diameter	$[\mathrm{m}]$
D_c	Equivalent column diameter	$[\mathrm{m}]$
e	Coefficient of restitution	
$\vec{F}_q$	External body force	$[\mathrm{N\,m^{-2}}]$
$\vec{F}_{lift,q}$	Lift force	$[\mathrm{N\,m^{-2}}]$
$\vec{F}_{vm,q}$	Virtual mass force	$[\mathrm{N\,m^{-2}}]$
g	Acceleration of gravity	$[\mathrm{m\,s^{-2}}]$
g_o	Radial distribution function	
G_m	Fluid mass velocity	$[\mathrm{kg\,h^{-1}\,m^{-2}}]$
G_{mf}	Fluid mass velocity at minimum fluidization	$[\mathrm{kg\,h^{-1}\,m^{-2}}]$
h	Specific enthalpy of phase	$[\mathrm{kJ/\,kg}]$
h_s	Static bed height	$[\mathrm{m}]$
h_{pq}, h_{qp}	Interphase enthalphy	$[\mathrm{kJ/\,kg}]$
I_{2D}	Second invariant of the deviatoric stress tensor	$[\mathrm{s^{-2}}]$
K	Interphase momentum exchange coefficient	$[\mathrm{kg\,s^{-1}}]$
L_{mf}	Height of the bed at minimum fluidization	$[\mathrm{m}]$
$\dot{m}$	Rate of mass transfer from one phase to another	$[\mathrm{kg\,s^{-1}}]$
p	Pressure	$[\mathrm{Pa}]$
p_s	Solid pressure	$[\mathrm{Pa}]$
$\vec{q}$	Heat flux	$[\mathrm{W\,m^{-2}}]$
Q	Heat exchange between the phases	$[\mathrm{J}]$
$\vec{R}_{pq}$	Interphase force	$[\mathrm{N\,m^{-2}}]$
Re_s	Relative Reynolds number	
S_q	Source term	
t	Time	$[\mathrm{s}]$
u_o	Superficial air velocity	$[\mathrm{m\,s^{-1}}]$
U_{mf}	Minimum fluidization velocity	$[\mathrm{m\,s^{-1}}]$
U_{mb}	Minimum bubbling velocity	$[\mathrm{m\,s^{-1}}]$
$\vec{v}$	Velocity of a phase	$[\mathrm{m\,s^{-1}}]$
$\vec{v}_{qp}$	Interphase velocity	$[\mathrm{m\,s^{-1}}]$
v_{rs}	Terminal velocity of the solid phase	$[\mathrm{m\,s^{-1}}]$
W	Weight of the particle	$[\mathrm{kg}]$

Greek Letters

Δp	Pressure drop across bed	$[\mathrm{Pa}]$
ε	Void fraction	
ε_{mf}	Void fraction at minimum fluidization	
ρ_s	Particle density	$\left[\mathrm{kg\,m^{-3}}\right]$
ρ_g	Gas density	$\left[\mathrm{kg\,m^{-3}}\right]$
ρ_{rq}	Phase reference density	$\left[\mathrm{kg\,m^{-3}}\right]$
$\bar{\tau}$	Stress-strain tensor	$[\mathrm{Pa}]$
α	Phase volume fractions	
μ_l	Shear velocity of fluid phase	$[\mathrm{Pa\,s}]$
μ_{fr}	Frictional viscosity	$[\mathrm{Pa\,s}]$
$\mu_{s,kin}$	Kinetic viscosity	$[\mathrm{Pa\,s}]$
$\mu_{s,\mathrm{col}}$	Collisional viscosity	$[\mathrm{Pa\,s}]$
Θ	Granular temperature	$\left[\mathrm{m^2\,s^{-2}}\right]$
ϕ	Angel of internal friction	
λ_s	Granular bulk viscosity	$[\mathrm{Pa\,s}]$

Part I

Theoretical studies and phenomenon of fluidization

Chapter 1

Introduction

Fluidization is the operation by which solid particles are transformed into a fluidlike state through suspension in a gas or a liquid [1]. This operation contains several different characteristics of fluidization and those are privileges to achieve many engineering goals.

1.1 The phenomenon of fluidization

There are different states in a fluidized bed according to the behavior of the solids and fluids in the bed. Fluid in the fluidized bed may be a liquid or a gas. In general, fluidization can be divided simply into two classes: homogeneous fluidization and bubbling fluidization. The homogeneous fluidization appears in liquid-solid systems and in gas-solid systems with Geldart A particles when the superficial gas velocity is in the range of the minimum fluidization velocity to the minimum bubbling velocity. Bubbling fluidization appears in gas-solid systems when the superficial gas velocity is greater than the minimum bubbling velocity. In this work only the bubbling fluidization in gas-solid systems is considered.

The fluidized bed is called a fixed bed, when the fluid is flowing upward through the bed of fine particles with a lower flow rates while the fluid penetrating via the void spaces of the particles without moving those. A fixed bed is shown in the Figure 1.1.a. When the flow rate is increasing, the particles start to move away from each other in restricted regions with small vibration and such a bed is called as expanded bed [1].

When the fluid flow rate keep on increasing after a certain time all the particles start to suspend in the upward-flowing fluid. In this situation, the vertical component of all the forces acting on the particles is zero. The reason is that the frictional forces between the particles and the fluid compensate the weight of the particles [1]. This is the minimum fluidization state of a particle bed and is considered as a just fluidized bed (Figure 1.1.b). If the fluid in a fluidized bed is a liquid an increase in the flow rate after the minimum fluidization state usually gives smooth, progressive expansion of the bed (Figure 1.1.c). Generally, the gas-solid systems have a different behavior. Therefore it is hard to observe this type of beds in the gas-solid systems, since it needs special conditions as very fine particles with high dense gases at high pressure. It is possible to observe the creation of gas bubbles which are moving upwards in the particle bed when the flow rate is increased beyond the minimum fluidization in gas-solid systems. From this point onwards the system becomes unstable, agitation becomes violent and the particles gain strong moments. There is not much expansion of the bed can be observed beyond its volume at the minimum fluidization. This type of beds are called an aggregative fluidized bed, a heterogeneous fluidized

bed or mostly as a bubbling fluidized bed (Figure 1.1.d) [1]. The bubbling beds occur only with high density solids fluidized by low density fluids.

In a gas-solid system, normally the gas bubbles tends to join together and grow as they rise. In a bed with a small diameter, the rising bubbles may ultimately large enough to cover the whole diameter of the bed if the bed is deep enough. In such a situation the fine particles existing in the bed flow smoothly down wards along the wall of the bed. This is called an axial slugging (Figure 1.1.e). There is another type called a flat slugging beds. Where the bubbles are pushing the accumulated particles upwards by acting similar to a piston. Then the particles rain down from the slug and finally disintegrate. This unstable oscillatory motion is repeated and the slugging is very frequent for a long, narrow fluidized beds.

A fluidized bed which is at slugging state, can be converted in to a turbulent fluidized bed by increasing the gas flow rate even further. In such a case the terminal velocity of the solid is exceeded, the upper surface of the bed disappears and entrainment become significant. In a turbulent bed, it is possible to observe various sizes of particle clusters and voids throughout the particle bed as shown in Figure 1.1.g. With a supplementary air flow rate solids are carried out of the bed with the gas flow and this is called a lean-phase fluidized bed (Figure 1.1.h)[1].

1.2 Liquidlike behavior of a fluidized bed

Both gas and liquid fluidized beds are considered as dense phase fluidized beds as long as there are clear surfaces and upper limits [1]. Such fluidized beds are similar to liquids in many ways. As an examples a large, light object can easily be pushed in to a bed and, on release, it will pop up and float on the surface. The upper surface of the particle bed will adjust and stay horizontally even if the bed is Inclined. Also the particles will flow like a liquid from a hole in the bed surface as shown in Figure 1.2.c.

If two dense phase fluidized beds with different beds heights are connected; the heights get equalized demonstrating the liquid like behavior as shown in Figure 1.2.d. In addition due to the liquidlike behavior it possible to observe that the pressure difference between two points in the particle bed is approximately equals to the static head between the two points.

The liquidlike behavior allows various contacting phenomenon and gives exclusive properties to the bed and advantages for the fluidization. Those contacting schemes include countercurrent, crosscurrent and solid circulation between two beds [1].

1.3 Advantages and disadvantages of the fluidized beds for industrial operations

Gas-solid fluidized beds are extensively used in the process industry because of their advantageous properties. Fluidized beds are having following advantages;

The smooth, liquidlike behavior of the particles in fluidized beds facilitates automatically controlled operations with uncomplicated handling. Fluidized beds can provides isothermal conditions due to rapid mixing of the bed hence the operation can be controlled simply and consistently. Normally fluidized beds have large safety margins to stay away from temperature runaways for highly exothermic reactions. That is due to the resistance for large temperature increments by rapid mixing of solids. By circulating the solids between two fluidized beds it is possible to remove or add a huge amount of heat produced or needed in large reactors. Fluidized beds are superior for large scale industries. Besides the above factors, the fluidized beds have an excellent mass and heat transfer conditions due to high contact area between phases compared

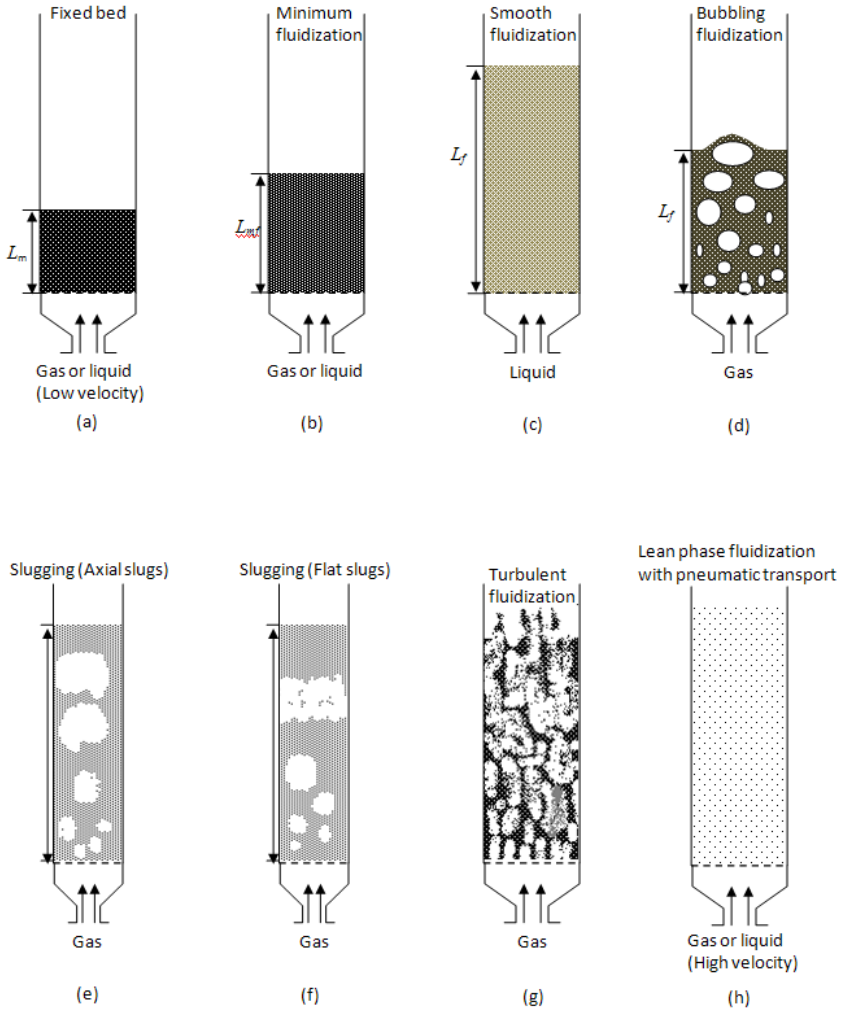

Figure 1.1: Various forms of contacting of a batch of solid by fluid

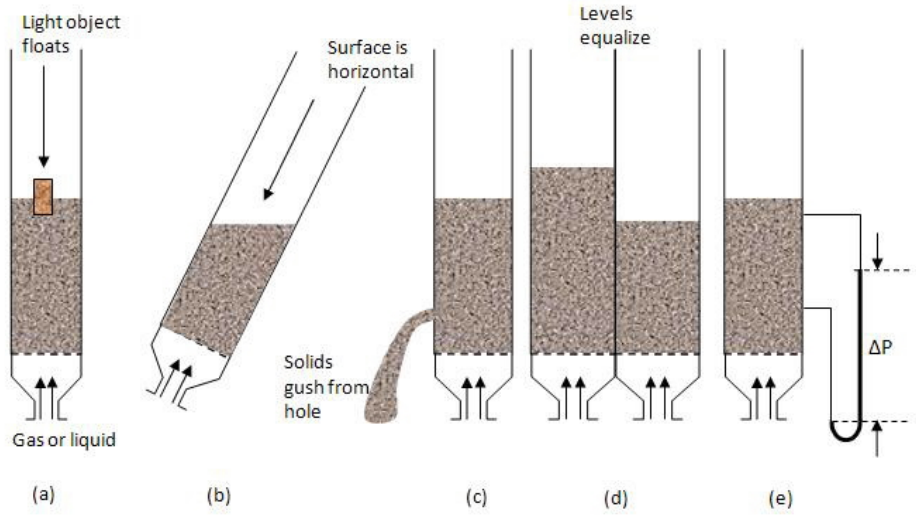

Figure 1.2: Liquidlike behavior of gas fluidized beds

to other methods. Heat exchangers consists of fluidized beds required relatively small surface areas due to the high rate of heat transfer between fluidized bed and an immersed object [1].

The fluidized bed applications cover a wide range of physical and chemical processes. In order to obtain the desired product specifications, maximize the efficiency and enhance the process safety, it is important to select an appropriate gas-solid contacting mode in the fluidized bed.

There are some disadvantages in fluidized beds. It has nonuniform resident time due to rapid mixing of solids in the bed. This might lead to production failures such as non-consistent product and inefficient plant performance. In addition to that dangerous situations can rise due to the erosions of pipes and vessels caused by the abrasion of particles. The temperature could be required to lower down in noncatalytic operations at high temperature, due to agglomeration and sintering of fine particles. Consequently this will reduce the reaction rate considerably.

Based on the special advantages on top of few disadvantages, fluidized beds are used successfully in many industrial operations.

1.4 Factors effecting on the fluidization

Fluidization engineering deals with many contacting methods but mainly on dense-phase systems. There are several factors which can affect the sustain fluidization.

The size and size distribution of solid particles is an important factor for sustain fluidization. Basically, if there is moisture or tacky, the fine particles in the bed tend to clump and agglomerate; thus the bed must be agitated to maintaining the enhanced fluidization. It is possible to do the agitation mechanically or by sending a high air flow through the bed. The uniformly sized solids often fluidize defectively and due to bumping, spouting and slugging, those can cause serious structural damages to the bed. In such situations, it is important to add some smaller particles to the bed to work as a lubricant. Normally for the large particle fluidization happen in a narrow range of gas flow rates. Therefore shallower beds must be used.

The fluid-solid density ratio holds an important role in the case of fluidization. Normally, the liquid-solid systems show homogeneous fluidization and gas-solid systems fluidize heterogeneous fluidization. But deviation from the standards can occur if low density particles are used with dense gases or high density particles with low dense liquids.

Also there are many other factors which might considerably effect the fluidization such as vessel geometry, gas inlet arrangement, type of solid used, and whether the solids are free flowing or likely to agglomerate.

1.5 Industrial applications of fluidized beds

Fluidized bed is the key method for many industrial physical and chemical applications because of its special properties and advantages. It is mostly used in the fuel industries for coal gasification and also to produce gasoline from other petroleum fractions and natural synthesis gases. Fluidized beds are used also for incineration of solid waste and fluidized combustion of coal.

Fluidized beds are highly recommended specially for highly exothermic and temperature sensitive reactions due to the outstanding temperature uniformity. Some of the very successful applications of fluidized bed's in this area are the production of Phthalic Anhydride by the catalytic oxidation of Naphthalene or Ortho-Xylene, the production of Alkyl Chloride and the Sohio process for producing Acrylonitrile [1].

Fluidized beds are having a remarkable ability to transform heat rapidly and maintain a uniform temperature. Therefore it has been used widely for heat exchangers. Heat exchanger operations required a massive rate of heat transfer which is possible to provide by fluidized beds of fine particles.

Fluidized beds are used for the process called granulation in urea production, where a shallow fluidized bed is combined with numerous spouted beds. The fluidized beds are widely used for the case of plastic coating on metal objects due to the lower operating cost. The coating methods with fluidized bed's can be used for objects with rough and highly dipped surfaces and its coating is much thicker than paint [1]. Fluidized beds can be used not only for plastic coating but also for coating of object and growth of particles such as salt coating on dry fluidized particles. Subsequent drying of the liquid layer then gives an efficient coating process. Same procedure can be used for growing particles with use of salt solution or slurries of fine solid powder. Size and size distribution of growth particles can be controlled by the seed particles by adjusting the concentration of solid in liquid.

Many industries are broadly using fluidized beds for the drying operations, because of their exceptional properties like large capacity, low construction cost, easy operability, and high thermal efficiency [1]. It is suitable for any kind of wet solid materials which can be fluidized under hot gas. Iron and steel industries are using huge fluidized beds to drying coal before feeding in to their coke oven and small but very efficient and expensive fluidized beds are used in pharmaceutical industries.

In the case of adsorption, multistage fluidized beds are used to remove dilute components from large flows of carrier gas. This process can become superior to conventional fixed bed processes. The dilute component is absorbed periodically by carbon particles and it is desorbed later using steam. In addition fluidized beds are using for carbon activation. It is possible to carry on this carbon activation process by low temperature (800-900 ^0C) endothermic gasification with hot combustion gas of wooden materials. This process contains a multi stage fluidized bed unit as it gives more uniform residence time distribution for the solids and helps to recover heat for the gasification by secondary combustion of CO and H_2 produced from solids.

Catalytic cracking of fluid (FCC), fluid coking and flexi coking, thermal cracking, calcina-

tions, polymerization of olefins, roasting sulfide ores, producing silicon for the semiconductor and solar cell industries, chlorination and fluorination of metal oxides, reduction of iron oxide, and biofluidization are other frequent applications which are using fluidized beds [1].

1.6 Researches and experiments done on bubbling fluidization

There are many ongoing and completed researches based on experimental studies of bubbling fluidized beds due to their enormous industrial usage. The researches are based on the measurements systems, bubble behavior, solid effect, mixing properties, minimum and bubbling fluidization velocity, etc.

Caicedo et al [2] studied minimum fluidization velocities for gas-solid 2D beds. Fluidization experiments were carried out in a two-dimensional fluidized bed with different height, weight of the bed and for different particle sizes. Minimum fluidization velocity was found to be a function of bed weight, particle diameter and column width. Sing et al [3] performed a set of experiments to prediction the minimum bubbling velocity, fluidization index and range of particulate fluidization for gas-solid fluidization in cylindrical and non-cylindrical beds. A uniform fluidization exists between minimum fluidization velocity and minimum bubbling velocity. The experiments were performed to determination the minimum bubbling velocity and fluidization index for non-spherical particles in cylindrical and non-cylindrical beds. Equations were developed for the prediction of minimum bubbling velocity for gas–solid fluidization in cylindrical and non-cylindrical (viz. semi-cylindrical, hexagonal and square) beds for non-spherical particles fluidized by air at ambient conditions. Based on the experimental data it was concluded that under similar operating conditions the minimum bubbling velocity and the fluidization index are maximum in the case of either semi-cylindrical conduit or hexagonal conduit for most of the operating conditions and minimum in case of square one.

A very interesting investigation was done by Lin et al [4]. They have studied about the effect of particle size distribution on minimum fluidization velocity at high temperature. They have used four particle size distributions of silica for fluidization in air at atmospheric pressure between 700 and 900 ^0C. The experimental results revealed a minimum in the minimum fluidization velocity value near 800 ^oC. They consider the reason might be that the interparticle forces would have been changed as temperature rises and increased the minimum fluidization velocity. Girimonte R et al, [5] also studied the minimum bubbling velocity of fluidized beds operating at high temperatures.

Wirsum M. et al [6] found some valuable information regarding particle mixing in bubbling fluidized beds of binary particle systems. The mixing and segregation behavior of spherical solids between 20 and 40 μm in diameter in a bubbling fluidized bed of quartz sand was investigated. The experimental system used is a cold-air fluidized bed with binary systems of particles. Time average segregation patterns of the solid mixtures were obtained from single particle trajectories measured by a newly developed experimental procedure. The technique related with magnetic system was proposed and it is generally suitable to locate metallic spheres in three dimensions inside non-transparent and non-metallic media. Experimental results indicated that segregation of large flotsam particles is apparent in bubbling fluidized bed systems particularly at low superficial velocities, in coarse particle systems and for low densities of the debris particles.

Rasul M.G. et al [7] investigated the segregation potential in binary gas fluidized beds. Some smoothly fluidized binary mixtures exhibit no tendency to segregate under a particular combination of solids and fluid volume fractions. In these cases the equilibrium mixture remains stable, even in the absence of mixing forces. The conditions corresponding to segregation potential free

mixtures could be theoretically predicted from the physical properties of the system, and have been validated for liquid fluidized systems. They have shown that the same approach may be applied to gas fluidized beds of fine particles.

Wang Y. et at [8] did an experiment to find the impacts of solid properties and operating conditions on the performance of gas-solid fluidization systems. The characteristics of gas-solids two-phase flow and fluidization in terms of the flow structures and the apparent behavior of particles and fluid particle interactions are closely linked to physical properties of the particles, operating conditions and bed configurations. They have discussed both positive and negative impacts of particle sizes, bubbles, clusters, and column walls on the fluidized-bed reactor performance to assist the development of useful strategies for the design of fluidized-bed reactors.

Werther J. et al [9] investigated regarding measurement techniques in fluidized beds. Measurement techniques are extremely important to study fluidization properties. Quantities that need to be measured in gas fluidized-bed systems include solids volume concentrations, solids velocities and solids mass flows, the vertical and horizontal distribution of solids inside the system, the lateral distribution of the fluidizing gas, temperatures and gas concentrations. They have presented the information about available measuring techniques, including the techniques for temperature and pressure drop measurements. Practical applications and also the limitations of these techniques are outlined. More sophisticated techniques such as measurements of local solids mass flows, heat transfer probes for the detection of defluidized zones and solids flows inside fluidized-bed reactors and capacitance probes for solids concentration and velocity measurements under high-temperature conditions were presented with their research paper. Hayhurst A.N. et al [10] have studied mass transfer coefficient and Sherwood number for carbon spheres burning in bubbling fluidized beds.

Many researchers have studied pressure measurement systems and the pressure distributions in the bubbling fluidized beds. Ommen J.R. et al [11] carried out their research on the topic of optimal placement of probes for dynamic pressure measurements in large-scale fluidized beds. They have sampled pressure data at sufficiently high frequency and could yield much information about the hydrodynamic state of a fluidized bed. Experiments and simulations were performed to determine the intensity decrease as local pressure waves propagate from their origin. A new spectral method was applied to determine the degree of coherence for pressure signals measured at two different positions in a fluidized bed. Kim S.H. et al [12] have analyzed the pressure drop fluctuations in circulating fluidized beds. The characteristics of pressure drop fluctuation in a circulating fluidized bed with fine polymer particles were investigated. The measurements of time series of the pressure drop were carried out. Effects of coarse particles and relative humidity of air on the flow behavior of polymer powders-air suspension in the riser were observed. The analysis of pressure fluctuations by statistical and chaos theory gave qualitative and the quantitative information of flow behavior in file circulating fluidized bed.

Park S.H. et al [13] studied experimental, statistical and stochastic studies of pressure fluctuations in a three-phase fluidized bed with a moderately large diameter. Hydrodynamic properties of bubbling flow through a three-phase fluidized bed with a moderately large diameter have been characterized with statistical and stochastic analyses of a comprehensive set of experimentally measured pressure fluctuations in the bed. They have revealed that the hydrodynamic properties of a three-phase Fluidized bed with a moderately large column in terms of pressure fluctuations are strongly affected by the flow rates of both the fluidizing gas and liquid.

1.7 Computational fluid dynamics for fluidization

The simulations are another approach to get required information without performing experiments. It is a developing area where reasonable predictions can be done and efficient way without wasting resources and without the risks that have to be taken while doing real time experiments. The computational fluid dynamics (CFD) is becoming an upcoming method to explore the complicated fluid dynamics in gas–solid fluidized bed since Davidson first analyzed single-bubble motion in an infinite fluidized bed.

In CFD models, there are three main approaches which can be used to simulate a fluidized bed; those are Eulerian–Lagrangian, Eulerian–Eulerian and Lagrangian-Lagrangian approaches. The former considers the solid phase at a particle level, whilst the latter treats both gas and solid phases as interpenetrating continuous media. The bubbling fluidization, especially for Geldart B particles, was extensively investigated using either Eulerian–Lagrangian or Eulerian–Eulerian CFD models in the past 30 years. Most of Eulerian–Lagrangian simulations for homogeneous fluidization were conducted in two-dimensional beds due to the lack of computer resources and complexity of the theoretical models. It is clear that the Eulerian–Lagrangian method is computationally too intensive to apply at an engineering scale, even in the near feature.[14].

Chapter 2

Fluidization and mapping of regimes

Fluidized bed can form different type of conditions while the bed of solid particles is suspended by the up flowing air flow, mainly smoothly fluidizing, bubbling, slugging and spouting. Fluidized beds behave differently when the gas velocity, gas properties and solid properties are varied. The state of fluidization starts at the point of minimum fluidization when the drag force on the particles becomes equal to the weight of the bed. At the onset of fluidization the bed is more or less uniformly expanded and as the gas velocity is increased further, bubbles appear in the bed. The gas velocity at which the first bubbles appear on the surface of the bed is the minimum bubbling velocity. The regime of non-bubbling fluidization is bounded by the minimum fluidization velocity U_{mf} and the minimum bubbling velocity U_{mb}. In this regime all the gas passes between the particles without forming bubbles and the bed smoothly expands with a more or less uniform bed structure. The operational range of the non-bubbling fluidization regime is quite narrow and at ambient conditions the non-bubbling regime exists only in fluidized beds with Geldart A powders. In fluidized beds of coarse solids bubbles tend to appear as soon as the gas velocity reaches the minimum fluidization velocity.

2.1 Characterization of particles

In the case of experimental studies of fluidization mostly the spherical particles are used due to ease of calculations. That is because there is no ambiguity to measure the size of the spherical particles. When it comes to non-spherical, it becomes more questionable. Following method is used for calculating non-spherical particle diameter (equivalent spherical diameter) ,d_{sph}.

According to Kunii et al [1], equivalent spherical diameter ,d_{sph} diameter of a sphere having the same volume as the particle. There are many measurements for non-spherical particles; most common parameter is the sphericity, ϕ_s, defined as follows,

$$\phi_s = \left(\frac{\text{Surface of sphere}}{\text{Surface of particle}} \right)_{\text{of same volume}}$$

In this study two types of spherical glass particles were used within the range of particle diameter of $100\mu m$-$200\mu m$ and $400\mu m$-$600\mu m$. These particles are regular in shape the density is known and particles are non porous.

According to this definition $\phi_s = 1$ for spheres and $0 < \phi_s < 1$ for all other particle shapes.

When it comes to fluidization it is important to determined the void fraction, ε . The bed voidage can be calculate by using the particle density and the weight.

2.2 Minimum fluidization velocity

When a fluid is passing through a bed of fine particles, it starts to drag the particles to upward. With the increased velocity there is a point that all the particles are just suspended by the upward flowing fluid and all the vertical forces on the particles became counter balance with each other. The bed is considered to be just fluidized and is referred as minimum fluidization. Superficial velocity of the fluid at this stage is called as minimum fluidization velocity, U_{mf}.

When the fluidization occurs,

$$\begin{pmatrix} \text{drag force by} \\ \text{upward moving gas} \end{pmatrix} = \begin{pmatrix} \text{weight of the} \\ \text{particle} \end{pmatrix}$$

or

$$\begin{pmatrix} \text{pressure} \\ \text{drop} \\ \text{across bed} \end{pmatrix} \begin{pmatrix} \text{cross} \\ \text{sectional} \\ \text{area of tube} \end{pmatrix} = \begin{pmatrix} \text{volume} \\ \text{of the bed} \end{pmatrix} \begin{pmatrix} \text{fraction} \\ \text{consisting} \\ \text{of solids} \end{pmatrix} \begin{pmatrix} \text{specific} \\ \text{weight} \\ \text{of solids} \end{pmatrix}$$

or, with Δp_b (pressure drop across bed) always positive,[1]

$$\Delta p_b A_t = W = A_t L_{mf}(1-\varepsilon_{mf})[(\rho_s - \rho_g)g] \tag{2.1}$$

by rearranging the above formula,

$$\frac{\Delta p_b}{L_{mf}} = (1-\varepsilon_{mf})(\rho_s - \rho_g)g \tag{2.2}$$

In general, for isotropic-shaped solids the following relation gives a quadratic in U_{mf}[1]

$$\frac{1.75}{\varepsilon_{mf}^3 \phi_s}\left(\frac{d_p U_{mf}\rho_g}{\mu}\right)^2 + \frac{150\,(1-\varepsilon_{mf})}{\varepsilon_{mf}^3 \phi_s^2}\left(\frac{d_p U_{mf}\rho_g}{\mu}\right) = \frac{d_p^3 \rho_g\left(\rho_s - \rho_g\right)g}{\mu^2} \tag{2.3}$$

or

$$\frac{1.75}{\varepsilon_{mf}^3 \phi_s}\,\mathrm{Re}_{p,mf}^2 + \frac{150\,(1-\varepsilon_{mf})}{\varepsilon_{mf}^3 \phi_s^2}\,\mathrm{Re}_{p,mf} = Ar \tag{2.4}$$

Where the Archimedes number is defined as,

$$Ar = \frac{d_p^3 \rho_g\left(\rho_s - \rho_g\right)g}{\mu^2} \tag{2.5}$$

In the case of small particles , Eq.2.3 simplifies to,

$$u_{mf} = \frac{d_p^2\left(\rho_s - \rho_g\right)g}{150\mu}\frac{\varepsilon_{mf}^3 \phi_s^2}{(1-\varepsilon_{mf})}, \quad \mathrm{Re}_{p,mf} < 20 \tag{2.6}$$

And for the very large particles [1],

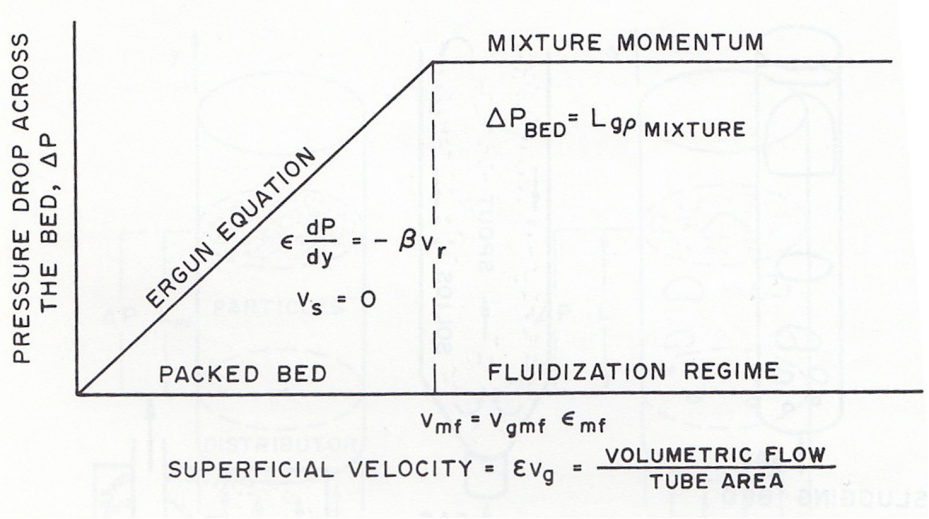

Figure 2.1: Determination of minimum fluidization

$$u_{mf}^2 = \frac{d_p\left(\rho_s - \rho_g\right) g}{1.75\rho_g}\varepsilon_{mf}^3\phi_s, \quad \mathrm{Re}_{p,mf} < 1000 \tag{2.7}$$

There are special procedures to find U_{mf} if void fraction, ε_{mf} or equivalent spherical diameter, ϕ_s are not known. In this study Ergun equation was used to calculate minimum fluidization as ε_{mf} is not known.

2.2.1 Calculation of minimum fluidization velocity theoretically

Calculating the minimum fluidization velocity, U_{mf} by using the above mentioned method is impossible with using an estimated void fraction. Because of this reason Ergun equation can be use to calculate the minimum fluidization velocity as mentioned below. Calculation of the minimum fluidization velocity theoretically could be done using a graphical method or numerical calculations. Minimum fluidization velocity can be found from the intersection of the pressure drop versus the spherical velocity curve and the pressure drop equals the weight of the bed line [15], see Figure 2.1.

Wong A.C.Y. et al [16] shows that it is more realistic to predict the minimum fluidization velocity depending on the angle of repose. In addition the minimum fluidization velocity can be calculated by using some extensions of the conservation equations. For that gas-wall friction and solid stress transmitted by the particles are neglected so that the buoyancy equals to the drag at the minimum fluidization conditions. Also it has taken in to consideration the fact that the velocity of solids is zero at the minimum fluidization.

In spherical case for small particles, Eq.2.3 can be re-written as [15],

$$U_{mf} = \varepsilon_{mf} \cdot v_{mf} = \frac{d_p^2 \cdot \Delta\rho \cdot g}{150 \cdot \mu_g}\left(\frac{\phi_s^2 \cdot \varepsilon_{mf}^3}{1 - \varepsilon_{mf}}\right) \tag{2.8}$$

For spherical particles of uniform size it is not unreasonable to expect the porosity at the minimum fluidization to be close to the porosity of a bed packed with spheres in a cubic mode, with

$\varepsilon_{mf} = 1 - \frac{\pi}{6} = 0.476$ [15]

Eq. 2.8 can be further simplified for small particles[15],

$$\left(\frac{\phi_s^2 \cdot \varepsilon_{mf}^3}{1-\varepsilon_{mf}}\right) \cong \frac{1}{11}$$

$$\therefore \quad U_{mf} = \frac{d_p^2 \cdot \left(\rho_s - \rho_g\right) \cdot g}{1650 * \mu_g}, \ \mathrm{Re}_{mf} < 20 \tag{2.9}$$

2.3 Minimum bubbling velocity and fluidization index

In a gas-solid system the fluidization velocity at which the bubbles are first observed is called the minimum bubbling velocity, $U_{mb.}$ In a gas-solid system minimum bubbling velocity and the minimum fluidization velocity are slightly the same for Geldart B particles ($> 100\mu m$)[1].

$$u_{mb} \backsimeq u_{mf} \tag{2.10}$$

The ratio of minimum bubbling velocity to minimum fluidization velocity, U_{mb}/U_{mf}, is known as the fluidization index, which gives a measure of the degree to which the bed can be expanded uniformly. This ratio tends to be relatively high for Geldart Group A powders and for gas of high density reported by Davidson and Harrison [17]. Unlike the minimum fluidization velocity, the minimum bubbling velocity was correlated for the first time in the late 1970s and until now the only widely accepted correlation appears to be that of Abrahamsen and Geldart. They examined the effect of properties of gases and powders on the homogeneous bed expansion and the ratio U_{mb}/U_{mf}.Abrahamsen and Geldart [18] correlated the values of minimum bubbling velocity for twenty three different powders. They have observed that U_{mb}/U_{mf} was strongly dependent on the weight fraction of particles smaller than $45\mu m$.Abrahamsen and Geldart [18] correlated the values of minimum bubbling velocity with the properties of gases and particles as follows:

$$U_{mb} = 2.07exp(0.716P_{45\mu m})\left(\frac{x_p \rho_g^{0.06}}{\mu^{0.347}}\right) \tag{2.11}$$

Where $P_{45\mu m}$is the fraction of powder less than $45\mu m$. Minimum fluidization velocity for particles less than $100\mu m$ is given by Baeyens equation [1],

$$U_{mf} = \frac{\left(\rho_s - \rho_g\right)^{0.934} g^{0.934} x^{1.8}}{1100\mu^{0.87}\rho_g^{0.066}} \tag{2.12}$$

The fluidization Index is the ratio of minimum bubbling velocity to minimum fluidization velocity. Dividing the Abrahamsen equation by the Baeyens equation gives the following correlation,

$$U_{mb}/U_{mf} = \frac{2300\rho_g^{0.13}\mu^{0.52}exp(0.716P_{45\mu m})}{\bar{d_p}^{0.8}\left(\rho_s - \rho_g\right)^{0.93}} \tag{2.13}$$

The higher the ratio is more the amount of gas that the bed can hold between the minimum fluidization and bubbling point. This means that for a correct initial aeration rate between these two values the bed will be less likely to form bubbles for a small increase in velocity and less likely to deareate due to a reduction in velocity.

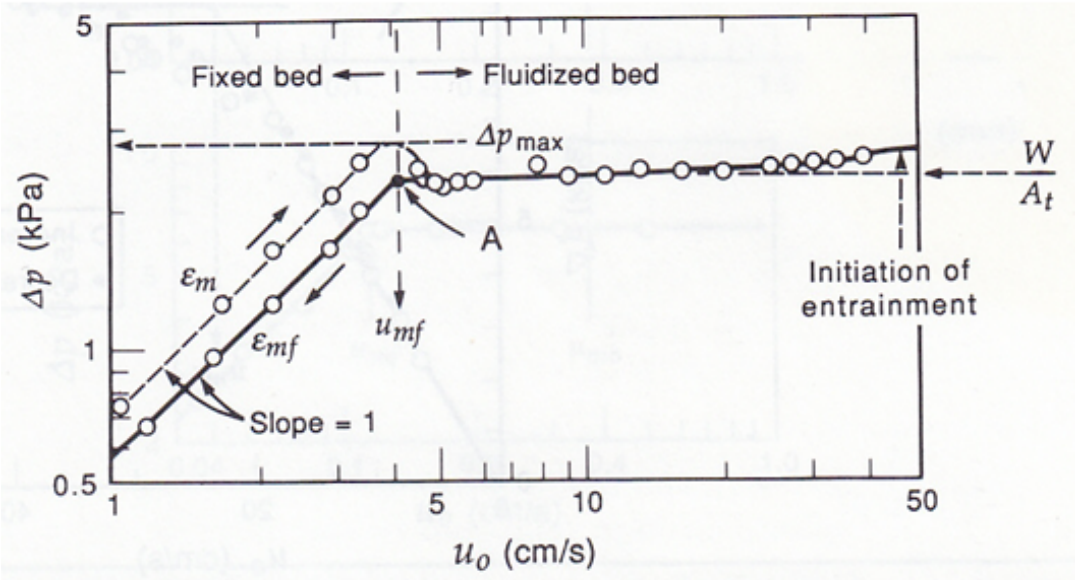

Figure 2.2: Pressure drop vs superficial air velocity for uniformly sized sharp sand gives ideal textbook behavior [1]

2.4 Pressure drop along the bed

The pressure drop, Δp in a fluidized bed is mainly effected by the air flow rate (superficial air velocity, u_o). The Δp vs u_o diagram is particularly useful as a rough indication of the quality of fluidization, specially when visual observations are not possible.

Pressure can be computed as the sum of the contributions from the momentum of the gas and the solids. In addition to that, in a dense flow or in dilute flow with a layer of solids at the wall, the pressure drop may have to be corrected for the effect of the normal solids at the wall, this pressure drop may have to be corrected for the effect of the normal solid stress transmitted by that contact of solid particles. Algebraically the Δp is obtained, with no solid stress, [15]

$$\left(\frac{dp}{dx}\right)_{total} = \left(\frac{dp}{dx}\right)_{momentum} + \left(\frac{dp}{dx}\right)_{friction} + \left(\frac{dp}{dx}\right)_{elevation} \tag{2.14}$$

According to Kunii et al [1], at small size (small particles with $155\mu m$ mean diameter) particle conditions, the pressure drop is approximately proportional to the gas flow rate for the relatively low air flow rates and usually reaches a maximum pressure drop $\Delta p_{\max}$, which is slightly higher than the static pressure of the bed. With more air flow the pressure, drop to the static pressure of the bed due to increments of the void fraction from ε_m to ε_{mf}. After the minimum fluidization stage, the bed will expand and start to generate bubbles. Theoretically the pressure drop should be constant after this point even with a little bit higher air flow rates. According to Kunii et al [1], Δp vs u_o diagram for uniformly sized sharp sand are shown in the Figure 2.2.

When the gas velocity decreases, the fluidized particles form a loose fixed bed of voidage ε_{mf}. In the case of wide size distribution of particles, while increasing the air flow rate, smaller particles tend to slip in to voidage in between bigger particles and fluidize, but the larger particles

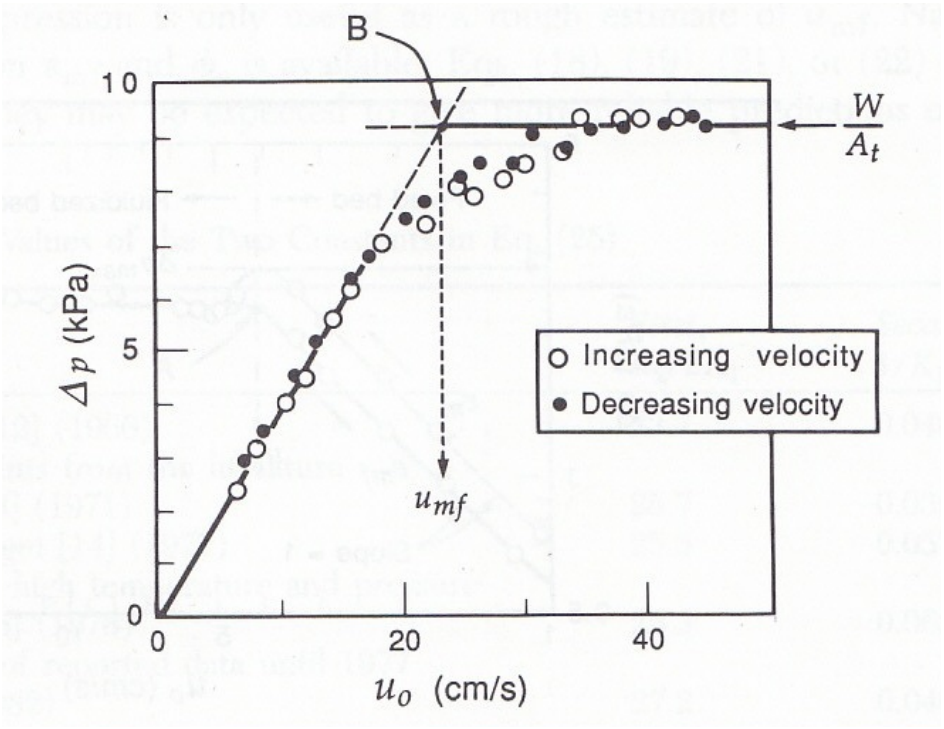

Figure 2.3: For a wide distribution of solids, the onset of fluidization is geadual but is defined as point B; Dolomite, $D_p = 180 - 1400\mu m$ [1]

will remain stationary. This called as partial fluidization and it gives a slight Δp, but all the solid particles will eventually be fluidized by increasing the gas flow rate, and Δp approaches its maximum. According to Kunii et al [1], this maximum value is equal to fraction of bed weight to cross section of the bed, $W/A_{t.}$ as shown in Figure 2.3 [1]. How ever this characteristics are dependant on the particle sizes and size distributions.

2.5 The Geldart classification of particles

There are numerous attempts to predict the mode of fluidization and the transition from one form to another. At the very beginning Reynold's number and Froude's number were used to consider the interparticle forces in the vicinity of bubbles. Empirical solutions and formation of bubbles based on stability theories were also considered for a better prediction. Geldart approached in a different way and he focused on the characteristics of the particles that make them fluidized in one way or another, but his approach was simple, has great generalizing power, and is very useful.

Geldart carefully observed the fluidization of small and larger particles and classified the particles in to four different particle groups. The four groups have clearly recognizable type of particle behaviors. This classification is clear and very convenient. Figure 2.4 [1] gives a graphical explanation of Geldart particle classification based on mean particle diameter $\bar{d}_p \mu m$ and density difference of solid and gas $(\rho_s - \rho_g) kg/m^3$ in gas-solid systems.

The fluidization properties of a powder in air may be predicted by analyzing in which group it lies. It is important to note that at operating temperatures and pressures above ambient conditions, a powder may appear in a different group from that which it occupies at ambient conditions. This is due to the effect of gas properties on the grouping and may have serious implications as far as the operation of the fluidized bed is concerned. Table 2.1 [19] presents a summary of the typical properties of the different powder classes.

Geldart C particle group consists of cohesive or very fine powders. Normal fluidization is extremely difficult as the interparticle forces are greater than the forces from the gas flow. In addition to that the Geldart C particles are difficult to fluidize in small diameter beds as these particles tend to rise as a plug of solids [1]. Some of the member of this particle group are talc, flour and starch.

The Geldart A particles have a small mean particle size and/or low particle density($<\sim 1400 kgm^{-3}$). The particle in this group shows smooth and easy fluidization characteristics at low gas velocities. The bubbles appear in the particle bed at gas velocities higher than minimum bubbling velocity. The particle bed expands considerably before the bubbles appears in the bed. Geldart A particles are having some unique properties in bubbling fluidization. The bubbles have a maximum size, typically less than $10cm$ even for a very large vessel. The gross circulation of the solids occur even with a few bubbles present in the bed. This circulation is specially evidant in large particle beds. If the bubbles achieve the vessel diameter, they turn in to axial slugs.

Mostly the Geldart B particles are within the range of 40-500μm and 1400-4000kgm^{-3} in mean particle diameter and density [1]. This type of beds behave differently at higher gas velocities, in such cases small bubbles form at the distributor and grow and coalesce as they rise through the bed. The bubbles size is roughly independent of the mean particle size. The size of the bubbles increases as it moves away from the distributor. The bubble growth shows a rough linear dependancy on the distance above the distributor. With time the bubble velocities exceed gas velocity, $U_0 - U_{mf}$. Vigorous bubbling encourages the gross circulation of solids. Minimum fluidization velocity of the Geldart B particles is slightly similar to the minimum bubbling velocity.

Table 2.1: Geldart's classification of powders [19]

GROUP →	GROUP C	GROUP A	GROUP B	GROUP D
Most obvious characteristic	Cohesive. difficult to fluidize	Ideal for fluidization. Exhibits range of non-bubbling fluidization	Starts bubbling at Umf	Coarse solids
Typical solids	Flour, Cement	Cracking catalyst	Building Sand	Gravel, Coffee beans
PROPERTY ▼				
Bed Expansion	Low because of chanelling	High	Moderate	Low
De-aeration rate	Initially fast, then exponential	Slow, linear	fast	Fast
Bubble Properties	No bubbles - only channels	Bubbles split and coalesce. Maximum bubble size.	No limit to size	No limit to size
Solids Mixing	Very low	High	Moderate	Low
Gas Backmixing	Very low	High	Moderate	Low
Spouting	No	No	Only in shallow	Yes, even in deep beds

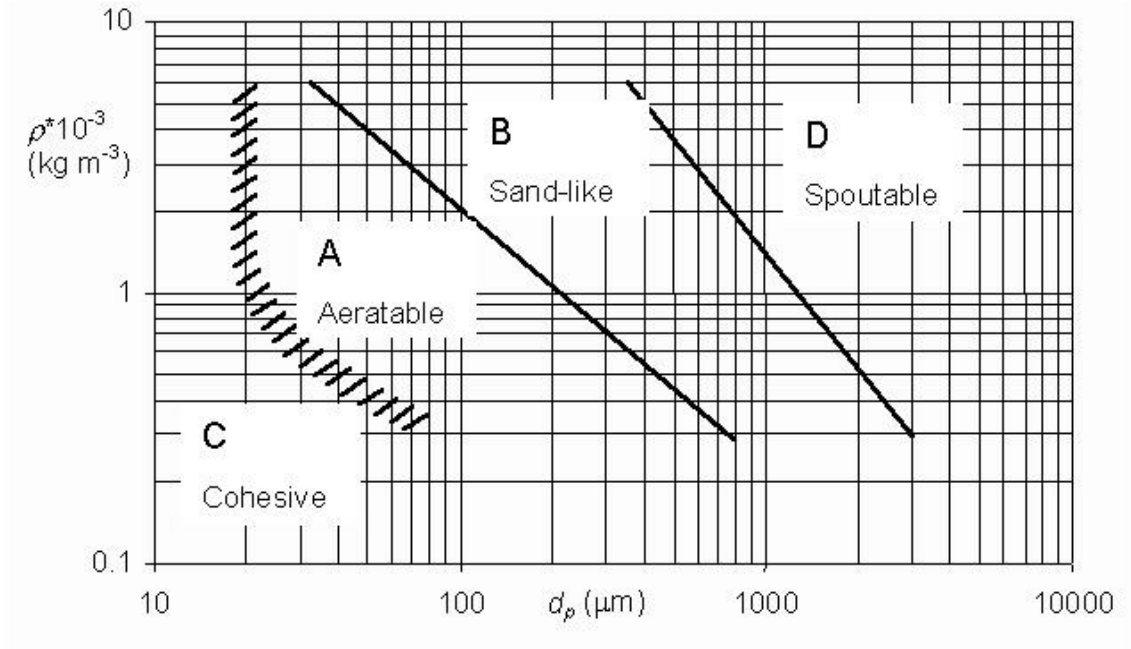

Figure 2.4: Geldart's classification of powders according to fluidization properties [1]

The Geldart D particles are spoutable, or large and/or dense particles [19]. The beds of these particles are difficult to fluidize, they behave unsteady while giving large bubbles or severe channeling or spouting behavior if the gas distribution is uneven. The large particle beds (Geldart D) are not very common but still used in some industries like processing agricultural products, in chemical agglomeration, and in the reaction of composite pellets using this type of needs for more efficient production. It is very costly to fabricate and to maintain such beds. It consumed enormous amount of gas compared to other fluidized bed operations. In such cases, one may want to use spouted beds, since they need much less gas.

The bubbles coalesce rapidly and grow to large size. Those bubbles rise slower than the rest of the gas flowing through the emulsion. The dense phase has a low voidage. When the bubble size approaches the bed diameter, flat slugs can be observed. These solids spout easily, whereas Geldart B solids do not [1].

2.6 Importance of analyzes

Analyzing the fluidized bed systems is very important due to frequent usage of the fluidized beds for different operations. Fluidized beds are widely used in a range of industrial applications as described in chapter 1. It is vital to achieve high quality and efficient fluidization conditions to maintaining the cost effective and high quality production. Different kind of particles are used in fluidized beds depending on the requirement. Fine particle mixtures with broads particle size distribution can be fluidized in a wide range of gas flow rates, permitting flexible operations with deep, large beds. On the contrary, beds of large uniformly sized solids often fluidized poorly, with bumping, spouting, and slugging, which may cause serious structural damage in large beds

and finally a waste of enormous amount of money.

Several other features may also affect for enhanced fluidization such as vessel geometry, physical properties of gas inlet and solids powder material used and its flow properties. Because of that it is vital to have an excellent understanding on the subject of fluidization and its dynamics. As a focal role in fluidization, bubbling fluidization is holding a competitive position with circulation fluidization. That emphasize the importance of studying about the dynamics and other properties of the bubbling fluidized beds. As declared in above segments the most significant property of fluidized beds is the large contact area between phases in the beds, which enhance the heat and mass transfer as well as the chemical reactions.

The efficiency of the bubbling fluidized beds are dependant on the bubble size, bubble frequency, bubble distribution and bubble velocity of the bed. The bubble characteristics are very important in the design of fluidized beds; they govern hydrodynamics and efficiency of the operation for which the bed is used. It is a great importance to study how those things depending on the particle size distribution. Simulations with satisfactory results are an obligation for this type of studies. A comparison between the simulated and experimental results will help for enhanced conclusions.

Chapter 3

Multiphase modelling

Computational fluid dynamics (CFD) has initiated a new chapter in fluid engineering and it has become an alternative method to experimental investigation for predicting the fluid dynamics in gas-solid fluidized beds. It has improved a lot within past decade since Davidson first analyzed single-bubble motion in an infinite fluidized bed [14]. With this tremendous improvement it is easy to have further insight of the multiphase flows than what can be seen in bare eye. At least two phases are present even in bubbling fluidized beds; the solids and the gas. According to that multiphase modeling has to be used if a simulation to be carried out on bubbling fluidized beds. Basic approaches for multiphase modeling and the available models in FLUENT are presented in this chapter.

3.1 Basic approaches of multiphase modelling

There are generally three kinds of models in two-phase flow simulation; Eulerian–Eulerian model, Eulerian–Lagrangian model and Lagrangian–Lagrangian model. The former considers the solid phase at a particle level, whilst the latter treats both gas and solid phases as interpenetrating continuous media [14].

3.1.1 Euler-Euler approach

In Eulerian–Eulerian model continuous medium model is used. This model has a long history going through different stages including non-slip model, little-slip two fluid model, slip-diffusion two-fluid model and the recently developed particle dynamics two-fluid model based on particle collision theory. Here different phases are treated separately. Physics quantities of both phases are described with conservation law of mass, momentum and energy in Eulerian coordinate. According to the concept the volume occupied by one phase cannot be taken by another phase. The phase volume fractions are considered for the analysis. Phase volume fractions are assumed to be continuous functions of space and time. There sum is equal to unity. Those set of equations are closed by using the kinetic theory of granular flow or other constitutive relations that are obtained from empirical information.

These models can compute effectively and treat boundary condition easily. It is applied in macroscopic analysis in high concentration flow while there is an inevitable disadvantage of lacking of detail transient information of phase interactions [20].

3.1.2 Euler-Lagrange approach

In Eulerian–Lagrangian model gas phase is regarded as continuum phase by solving the time-averaged Navier-Stokes equations. The particles are considered as dispersed phase. The dispersed phase is solved by considering a large number of particles, bubbles or droplets. It is considered that the dispersed phase can exchange momentum, mass, and energy with the fluid phase. The path that a particle, bubbles or a droplet follows is calculated individually. That is done at specified intervals during the fluid phase calculations. According to above features this approach is inappropriate for the modeling fluidized beds, or any application where the volume fraction of the secondary phase (sum of the secondary phases) is not negligible. Motion of continuous phase is studied in Eulerian coordinate while particle motion is tracked in Lagrangian coordinate, which is called Particles Trajectory Model [20].

3.1.3 Lagrangian - Lagrangian approach

In Lagrangian–Lagrangian model continuous flow can be calculated by discrete vortex method (DVM) and particle trajectories are obtained by particle motion equation. Then instantaneous fluctuations in shear flow field can be captured and simulated, which can reproduce the pairing, aggregation as well as interaction between the particles in unsteady flow such as turbulent shear layer. These methods have a strong advantage in simulation of high Reynolds number shear flow across a bluff body , which are most promising numerical simulation methods to be applied to engineering practice compared with direct numerical simulation and large eddy simulation [21].

3.1.4 Multiphase approaches in former researches

Enormous number of research studies were done using the multiphase approaches. Euler-Euler approach and Euler-Lagrange approach are used very often according to the requirement. Langrange-Langrange approach was rarely used, specially for the simulations in the cases with high Reynolds numbers.

The bubbling fluidization, specially for Geldart B particles, was extensively investigated using either Eulerian–Lagrangian or Eulerian–Eulerian CFD models in the past 30 years [22 & 23]. Most of Eulerian–Lagrangian simulations for homogeneous fluidization were conducted in two-dimensional beds due to the lack of computer resources and complexity of the theoretical models. A case study was carried out by Ye et al. [24], who investigated the effect of particle and gas properties on the fluidization quality. However, their calculations were carried out with 36,000 particles, and adopted time steps in the order of 10^5 and 10^6 s for gas and solid phases, respectively. Boemer et al [25] have developed a computer code to simulate the fluid dynamics of fluidized beds using Eularian approach.

N.Xia et al [26] used the Eulerian - Eulerian approach which represents each phase as an interspersed continuum. The transport equation for granular temperature is solved and hyperbolic tangent function is used to provide a smooth transition between the plastic and viscous regimes for the solid phase. Patil et al [21 &27] have used Eulerian - Eulerian approach with two different closure models. Those are constant viscosity model and a model based on the kinetic theory of granular flow. They have compared the simulated results of the two models with each other and also with the experimental results.

Eulerian - Eulerian approach with MFIX software programme was used by B. Halverson [28] in her simulations of bubbling fluidized bed. S.Ariyarathna [29], performed several simulations for her master thesis; using Eulerian - Eulerian multiphase approach for two dimensional fluidized bed. She has finalized a best combination of models available in the commercial software called Fluent 6.3.

Lu Huilin et al [30] has used both approaches separately and showing the results as a comparison with the experiments. Details of particle collision information were obtained through tracing particle motions based on Eulerian–Lagrangian approach coupled with the discrete hard sphere model. A CFD model based on kinetic theory of granular flow and Euler-Euler approach was used to simulate flows in bubbling gas-solid fluidized beds.

At same time many researchers were using Euler-Langrange approach. Recently a common used mode is the bonding-sliding collision model proposed by Lun and Bent [31], in which particle velocity after collision is calculated by impulse. Hoomas et al. [32] studied the growth of bubbles, combination, broken and other phenomena in fluidized bed, in which gas-phase is treated by $k-\varepsilon$ model while particle interaction is described by the hard-sphere model. Recently, Y. Tsuji et al [33] made a lot of researches on the numerical simulation of gas-solid flow using DEM methods, such work is mainly aimed at fluidized bed and circulating fluidized bed. Chidambaram et al [34] studied features of the temporal stability of particle-laden mixing layers under uniform particle loadings and evaluated the Eulerian–Lagrangian (particle tracking) methodology with linear stability analysis. Excellent agreement was observed for the instability growth rates. Study results have been demonstrated its strong potential predictable performance in simulating gas-solid two-phase flow, which is expected to describe the flow characteristics of particles in gas-solid two-phase flow in detail. However, there is one common feature in these methods: present simulations are mainly for large particle, small-scale devices and short term calculation, which are dominated by computer capacity and speed.

The selection of particle collision model plays an important role in Lagrangian–Lagrangian approach. In about two decades ago, Thomas et al [35], Maxey and Riley [36] and Auton [37] derived particle collision model in succession, which was used by Sene [38] and Yang [39], respectively, to get the particle trajectories in Rankine vortex and plane shear layer.

3.2 The Eulerian model and the start-up of the simulation

Fluent contains three types of multiphase models following the Eulerian - Eulerian approach; volume of fluid (VOF) model, the mixture model and the Eulerian model. The Eulerian model is the most complex multiphase model in FLUENT [40] within all three models. It is the most suitable model for granular flows [29]. Following the Eulerian model will be used with unsteady conditions in the simulations related to this study of bubbling fluidized beds.

The Eulerian model gives a set of n number of equations as it solves continuity and momentum equations for each phase. Pressure and momentum exchange coefficients couples the set of equations. The kinetic theory to introduce the properties of granular flows is used. Type of the mixture, the momentum transfer between phases is also modeled. Eulerian multiphase model is applicable for bubble columns, risers, particle suspension, and fluidized beds.

It is possible to use any number of secondary phases in the simulations with Eulerian model, but it is strictly depending on available memory capacity and convergence procedure of the system. This model is going to be extreamly useful when it comes to the simulations of the bubbling fluidized beds. A simulation can be initialized while introducing the particle size distribution of the granular material. After selecting the Eulerian model as the multiphase model, models for other parameters like drag coefficient, solids pressure, granular viscosity, etc also have to be selected. There are number of models available in FLUENT for most of those parameters. Ariyarathna,S. [29] has finalized the best combination of all the models and the parameters in her master thesis. Those combinations were used here in all the simulations.

3.3 Fundamentals of computational fluid dynamics

CFD is the analysis of systems involving fluid flow, heat transfer and associated phenomena such as chemical reactions by means of computer-based simulations. This is a well growing and very powerful technique which is using for wide range of industrial and non-industrial application areas, such as aircraft and shipping industry, power plant (combustion, IC engines, wind), turbo machinery, electronic engineering , chemical and process industry, weather prediction, biomedical engineering (Predict the blood flow behavior). CFD codes are structured with numerical algorithms which can tackle fluid flow problems including liquid-solid or gas-solid fluidization.

For the CFD simulations, it is important to have a mathematical basis for fluidization, which is already containing in CFD codes. Mathematical basis was developed for a comprehensive general purpose model of fluid flow and heat transfer from the basic principles, conservation of mass, momentum and energy. This leads to the governing equations of fluid flow and a discussion of the required auxiliary conditions; initial and boundary conditions.

In fluidization behavior of the fluid flow is analyzed by using the microscopic properties such as velocity, pressure, density, temperature and volume fraction, and their space and time derivatives. These may be thought of as average over suitable large numbers of molecules. In CFD these properties are analyzed in a fluid particle or point in a fluid (smallest possible element). All the mathematical equations were developed based on this fluid element.

Mass conservation and momentum conservation are important for all the fluidization simulations, but energy equation is not involving else if there is any temperature variations in the system. All the experiments explained in this report are done in the ambient temperature and assume there is no any temperature variations in the particles due friction. Assume temperature is constant.

In the simulation, the continuity equation and momentum equation will be solved for each face. Volume fraction of each phase will be calculated by solving the continuity equation. Those equations are presented below in their general format for a case that has n number of phases.

3.4 Available functions in FLUENT

After selecting the Eulerian model as the multiphase model, models for other parameters like drag coefficient, solids pressure, granular viscosity, etc also have to be selected. There are number of models available in FLUENT for most of those parameters and those have presented in the up coming subsection.

3.4.1 Mass and momentum conservation equations

As mentioned above, in the simulation, the continuity equation, momentum equation. Volume fraction of each phase will be calculated by solving the continuity equation. Those equations are presented below in their general format for a case that have n number of phases.

Mass conservation equation

[29]

$$\frac{1}{\rho_{rq}}\left(\frac{\partial}{\partial t}\left(\alpha_q\rho_q\right)+\nabla.\left(\alpha_q\rho_q\overrightarrow{v_q}\right)=\sum_{p=1}^{n}\left(\dot{m}_{pq}-\dot{m}_{qp}\right)\right) \tag{3.1}$$

Fluid-Solid momentum equation

For the sth solid phase [29],

$$\frac{\partial}{\partial t}\left(\alpha_s \rho_s \overrightarrow{v_s}\right) + \nabla.\left(\alpha_s \rho_s \overrightarrow{v_s}\overrightarrow{v_s}\right) = -\alpha_s \nabla p - \nabla p_s + \nabla.\overline{\overline{\tau_s}} + \alpha_s \rho_s \overrightarrow{g} + \sum_{l=1}^{N}\left(K_{ls}\left(\overrightarrow{v_l} - \overrightarrow{v_s}\right) + \dot{m}_{ls}\overrightarrow{v_{ls}} - \dot{m}_{sl}\overrightarrow{v_{sl}}\right) + \left(\overrightarrow{F_s} + \overrightarrow{F_{lift,s}} + \overrightarrow{F_{vm,s}}\right) \tag{3.2}$$

The momentum exchange between the phases is defined by the exchange coefficient K_{ls} which is included in the momentum equation. The exchange coefficient can be either fluid-solid or solid-solid when it is related to the bubbling fluidized beds with more than two phases.

3.4.2 Drag models

A Drag function is included in most of the exchange coefficients. It means the exchange coefficient varies according to the drag coefficient that is been used. There are three types of drag functions available in fluent; Syamlal-O'Brien Model, wen and Yu model and Gidaspow model. Syamlal-O'Brien model for fluid-solid exchange is used in the simulations. This model can be use when the solid shear stresses are defined according to Syamlal et al [29],

$$K_{ls} = \frac{\alpha_s \rho_s \left(\frac{C_D \operatorname{Re}_s \alpha_l}{24 v_{r,s}^2}\right)}{\tau_s} \tag{3.3}$$

$$C_D = \left(0.63 + \frac{4.8}{\sqrt{\operatorname{Re}_s / v_{r,s}}}\right)^2 \tag{3.4}$$

K_{ls} and C_D are the momentum exchange coefficient between the fluid and solid phases and the drag coefficient respectively. α_s and ρ_s are the phasic volume fraction of the liquid, the solid phase.

The Wen & Yu model fluid-solid exchange is given as [29],

$$K_{ls} = \frac{3}{4} C_D \frac{\alpha_s \alpha_l \rho_l \left|\overrightarrow{v_s} - \overrightarrow{v_l}\right|}{d_s} \alpha_l^{-2.65} \tag{3.5}$$

$$C_D = \frac{24}{\alpha_l \operatorname{Re}_s}\left[1 + 0.15\left(\alpha_l \operatorname{Re}_s\right)^{0.687}\right] \tag{3.6}$$

The Gidaspow model fluid-solid exchange is given as [29],

$$K_{ls} = \frac{3}{4} C_D \frac{\alpha_s \alpha_l \rho_l \left|\overrightarrow{v_s} - \overrightarrow{v_l}\right|}{d_s} \alpha_l^{-2.65}, \ \alpha_l > 0.8 \tag{3.7}$$

$$C_D = \frac{24}{\alpha_l \operatorname{Re}_s}\left[1 + 0.15\left(\alpha_l \operatorname{Re}_s\right)^{0.687}\right] \tag{3.8}$$

The Syamlal-O'Brien model for solid-solid exchange is given as [29],

$$K_{sl} = \left[\frac{3\left(1 + e_{ls}\right)\left(\frac{\pi}{2} + C_{fr,ls}\frac{\pi^2}{8}\right)\alpha_s \rho_s \alpha_l \rho_l \left(d_s + d_l\right)^2 g_{0,ls}}{2\pi\left(\rho_l d_l^3 + \rho_s d_s^3\right)}\right]\left|\overrightarrow{v_l} - \overrightarrow{v_s}\right| \tag{3.9}$$

3.4.3 Function for solid pressure

There are three models for defining the solids pressure, available in FLUENT named as Lun, Syamlal O,Brien and Mahamadi. The value of solids pressure calculated with use of the specified model is to be used as the pressure gradient in the momentum equation. Ma-hamadi equation is used for the simulations.

The Mahamadi equation is given as [29],

$$p_s = \alpha_s \rho_s \Theta_s \left[(1 + 4\alpha_s g_{0,ss}) + \frac{1}{2} \left[(1 + e_{ss}) \left(1 - e_{ss} + 2\mu_{fric} \right) \right] \right] \tag{3.10}$$

This is equation is very suitable in case of more than one solid phase.

The Equation by Lun is given as [29],

$$p_s = \alpha_s \rho_s \Theta_s + 2\rho_s (1 + e_{ss}) \alpha_s^2 g_{0,ss} \Theta_s \tag{3.11}$$

The Syamlal O'Brien equation is given as [29],

$$p_s = 2\rho_s (1 + e_{ss}) \alpha_s^2 g_{0,ss} \Theta_s \tag{3.12}$$

3.4.4 Radial distribution function

Three models that represent the radial distribution function are also available in FLUENT. Any one of those can be used to define the readial distribution coefficient, which is to be used in the solid-solid exchange coefficient of the momentum equation. According to Ariyarathna S et al [29] Mahamadi radial distribution function is the most appropriate function to use with all four available radial distribution functions in Fluent.

The Ma-ahmadi function is given as [29],

$$g_{0,ll} = \frac{1 + 2.5\alpha_s + 4.59\alpha_s^2 + 4.52\alpha_s^3}{\left(1 - \left(\frac{\alpha_s}{\alpha_{s,\max}} \right)^3 \right)^{0.678}} + \frac{1}{2} d_l \sum_{k=1}^{N} \frac{\alpha_k}{\rho_k}, \alpha_s = \Sigma_{k=1}^{n} \alpha_k \tag{3.13}$$

Here d_l is the diameter of the l^{th} solid phase particles. α_k and ρ_k are the phasic volume and physical density of each phase.

The Arastoopour function is given as [29],

$$g_{0,ll} = \frac{1}{\left(1 - \frac{\alpha_s}{\alpha_{s,\max}} \right)} + \frac{3}{2} d_l \sum_{k=1}^{N} \frac{\alpha_k}{\rho_k}, \alpha_s = \Sigma_{k=1}^{n} \alpha_k \tag{3.14}$$

The Lun function is given as [29],

$$g_{0,ll} = \left[1 - \left(\frac{\alpha_s}{\alpha_{s,\max}} \right)^{1/3} \right]^{-1} + \frac{1}{2} d_l \sum_{k=1}^{N} \frac{\alpha_k}{\rho_k}, \alpha_s = \Sigma_{k=1}^{n} \alpha_k \tag{3.15}$$

The Syamlal O'Brien function is given as [29],

$$g_{0,ll} = \frac{1}{(1 - \alpha_s)} + \frac{3 \left(\sum_{k=1}^{N} \frac{\alpha_k}{\rho_k} \right)}{(1 - \alpha_s)^2 (d_j + d_k)} d_k d_l, \alpha_s = \Sigma_{k=1}^{n} \alpha_k \tag{3.16}$$

3.4.5 Functions for frictional viscosity

The term called solids stress tensor is also required to solve the momentum equation. The solids stress tensor contains collisional and translational viscosities as well as the frictional viscosity. So that three frictional viscosity models available in Fluent. In addition to the available models there is a possibility to use a user defined model or even set the parameters as constants. Also it can be set that there is no frictional viscosity effecting on the solid phases. The Schaeffer function is used to express the frictional viscosity.

The Schaeffer function is given as [29],

$$\mu_{,frictional} = \frac{p_s \sin\phi}{\sqrt[2]{I_{2D}}} \tag{3.17}$$

$\mu_{,frictional}$, ϕ and I_{2D} are the frictional viscosity, the angle of internal friction and the second invariant of the deviatoric stress tensor.

The Johnson and Jackson function is given as [29],

$$\mu_{,frictional} = p_{frictional} \sin\phi \tag{3.18}$$

3.4.6 Functions for frictional pressure

Frictional pressure term is embodied in the frictional viscosity. Also it is possible to use an user defined model as well as the term can be set as that there is no frictional pressure available. There are containing 3 different functions in Fluent for the frictional pressure. Based-ktgf function is used in the simulations.

The Based-ktgf function is given as [29],

$$p_{,frictional} = \frac{\mu_{,frictional} * \sqrt[2]{I_{2D}}}{\sin\phi} \tag{3.19}$$

Where $p_{,frictional}$ is the frictional pressure.

The Johnson and Jackson function is given as [29],

$$P_{friction} = 0.1\alpha_s \frac{(\alpha_s - \alpha_{s,\min})^n}{(\alpha_{s,\max} - \alpha_s)^p}, \quad n = 2, \quad p = 3 \tag{3.20}$$

The Syamlal O'Brien function is given as [29],

$$\mu_{s,kin} = \frac{\alpha_s d_s \rho_s \sqrt{\Theta_s \pi}}{6(3 - e_{ss})} \left[1 + \frac{2}{5}(1 + e_{ss})(3e_{ss} - 1)\alpha_s g_{0,ss}\right] \tag{3.21}$$

3.4.7 Functions for granular viscosity

There is two basic function and Syamlal O'Brien function is used for the simulations.

The Syamlal O'Brien function is given as[29],

$$\mu_{s,kin} = \frac{\alpha_s d_s \rho_s \sqrt{\Theta_s \pi}}{6(3 - e_{ss})} \left[1 + \frac{2}{5}(1 + e_{ss})(3e_{ss} - 1)\alpha_s g_{0,ss}\right] \tag{3.22}$$

The Gidaspaw function is given as [29],

$$\mu_{s,kin} = \frac{100 d_s \rho_s \sqrt{\Theta_s \pi}}{96\alpha_s (1 + e_{ss}) g_{0,ss}} \left[1 + \frac{4}{5} g_{0,ss}\alpha_s (1 + e_{ss})\right]^2 \tag{3.23}$$

3.4.8 Granular bulk viscosity function

The Lun function is given as[29],

$$\lambda_s = \frac{4}{3}\alpha_s \rho_s d_s g_{0,ss} \left(1 + e_{ss}\right) \left(\frac{\Theta_s}{\pi}\right)^{1/2} \tag{3.24}$$

3.4.9 General equation for granular temperature

There is a general equation for granular temperature available in FLUENT. Just the term k_{Θ_s} varies depending on the model which is selected for the granular viscosity. It is possible to set the value as a constant, or can set it to be found algebraically. And also a user defined model can be used too. When the option algebraic is used for the granular temperature the convection and diffusion terms are neglected in the general equation [29].

$$\frac{3}{2}\left[\frac{\partial}{\partial t}\left(\rho_s \alpha_s \Theta_s\right) + \nabla.\left(\alpha_s \rho_s \overrightarrow{v_s} \Theta_s\right)\right] = \left(-p_s \overline{\overline{I}} + \overline{\overline{\tau_s}}\right) : \nabla \overrightarrow{v_s} + \nabla.\left(k_{\Theta_s} \nabla \Theta_s\right) - \gamma_{\Theta_s} + \phi_{ls} \tag{3.25}$$

When it is together with Syamlal O'Brien model as the Granular viscosity model [29],

$$k_{\Theta,s} = \frac{15\rho_s d_s \alpha_s \sqrt{\Theta_s \pi}}{4\left(41 - 33\eta\right)}\left[1 + \frac{12}{5}\eta^2\left(4\eta - 3\right)\alpha_s g_{0,ss} + \frac{16}{15\pi}\left(41 - 33\eta\right)\eta\alpha_s g_{0,ss}\right] \tag{3.26}$$

Where,

$$\eta = \frac{1}{2}1 + e$$

When combined with Gidaspaw model as the Granular viscosity model following combination can be observed [22],

$$k_{\Theta,s} = \frac{150\rho_s d_s \sqrt{\Theta\pi}}{384\left(1 + e_{ss}\right) g_{0,ss}}\left[1 + \frac{6}{5}\alpha_s g_{0,ss}\left(1 + e_s\right)\right]^2 + 2\rho_s \alpha_s^2 d_s \left(1 + e_{ss}\right) g_{0,ss}\sqrt{\frac{\Theta_s}{\pi}} \tag{3.27}$$

Part II

Experimental and computational studies of flow behavior in bubbling fluidized bed

Chapter 4

Experimental studies of bubbling fluidized bed

The aim of the experimental study is to analyze how, different fractions of particle sizes influence on the minimum fluidization velocity and the bed expansion and comparing the results with the computations. In addition to that , the dependency of the pressure distribution along the particle bed is studied from difference systems for a range of velocities.

Experimental studies are carried out using a three dimensional lab scale fluidized bed set up, which is in the Telemark university college premises. Spherical glass powder particles with difference mean diameters are used for the experiments. A special method is used to prepare particle samples for more accurate results. Pressure fluctuations along the bed are observed and recorded for several air flow rates. Experimental studies are performed for several particle mixtures with different mean diameters.

4.1 Lab scale experimental set up

The experimental set up was built at the Telemark University College for its research purposes in 2008. This lab scale unit includes three different sections; a computer based pressure measurement unit, air supply unit and the fluidized bed.

The bed is made out of a transparent Lexane plastic cylindrical pipe and there are two different sections. The upper section is 1.4m long and the bed area is 0.072m in diameter. The lower section is made of a 0.1m long pipe with the same diameter. This section works as a uniform air distributor. There is a porous metal plate in between the upper bed and the air distributing section. The experimental rig is shown in Figure 4.1 and Figure 4.2.

A pressure reduction valve is used in the air supply unit to control the gas flow. The gas flow is measured via a digital flow meter as shown in the Figure 4.1. The Inlet of the pressure reduction valve is connected to the air supply. Pressure reduction valve can only be controlled manually.

The pressure is measured from nine locations along the bed as shown in the Figure **??** and Table 4.2. This pressure measuring system is supported by commercial process control software called Labview. Since the Labview program is very flexible, it is possible to change the pressure reading frequency. For all the experiments performed during this study, the pressure measurements are taken at for each 0.5 seconds .

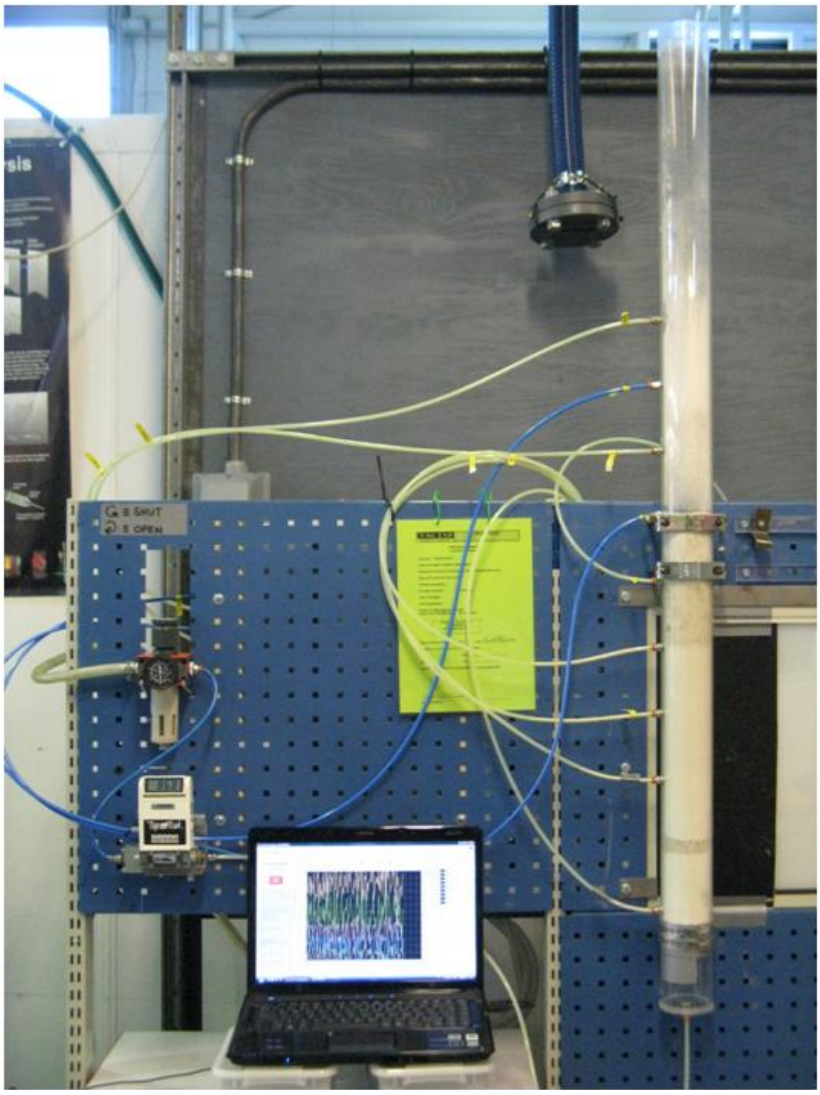

Figure 4.1: Bubbling fluidized bed with complete experimental setup

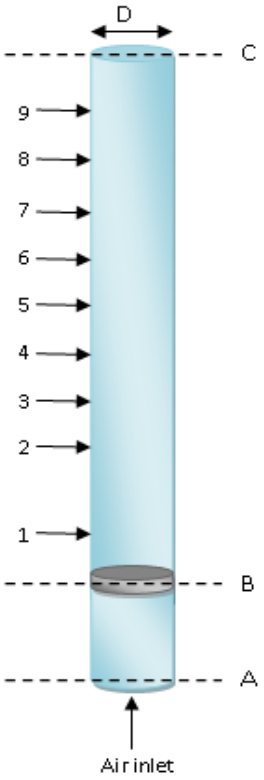

Figure 4.2: Pressure reading points along the bed

Table 4.1: Information about the bed and the pressure reading position

Point Number	**Distance from point B (cm)**
01	3.5
02	23.5
03	33.5
04	43.5
05	53.5
06	63.5
07	73.5
08	83.5
09	93.5
Cylindrical bed diameter (D) = 7.2cm	
Bed Height (BC) = 140cm	
Height of the air distributor (AB) = 10cm	

Table 4.2: Particle data

Particles (Spherical glass)		
Density	$2485 kg/m^3$	
Powder, particle range	100˜200 μm (small)	400˜600 μm (Large)
Mean particle size [μm]	$154 \mu m$	$488 \mu m$

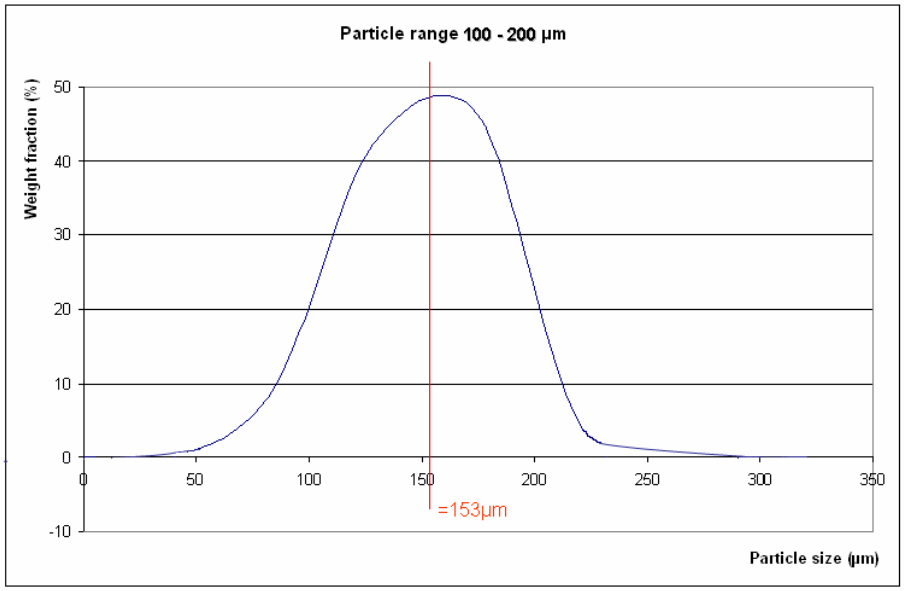

Figure 4.3: Extraction of the mean diameter from the particle size distribution of the sample of particles which is in the range 100 - 200 μm [29]

4.2 Preparation of particle samples for the experiments

Glass particles with two different mean particle sizes are used in this study. The particles have the size range of 100˜200 μm (small particles) and 400˜600 μm (large particles). The particle density is 2485 kg/m^3. Parameters of the bed and particles are presented in Table 4.2. Ariyarathna S. et al [29] performed experiments to analyze the particle size distribution for several particle samples. Particle size distribution of each particle samples are shown in the Figure 4.3 and Figure 4.4.

It is vital to assure the correct proportion of the different particle types in the particle mixture, which are used in each of the experiments for an accurate outcome. The proportion is usually taken as volume fraction. The volume occupied by the particles can be reduced by making those more compact for some extent without crushing them. According to that measuring the particle volumes at normal conditions is not a suitable method. It is important to use the identical particle volumes at the same compact condition if the bed expansion is to be analyzed. The bed expansion is an important observation for analyzing the behavior of the bubbling fluidized beds. One of the most suitable methods for making samples is by using the volumes at the maximum compact condition (without crushing them) of the powder materials. Maximum compact volume

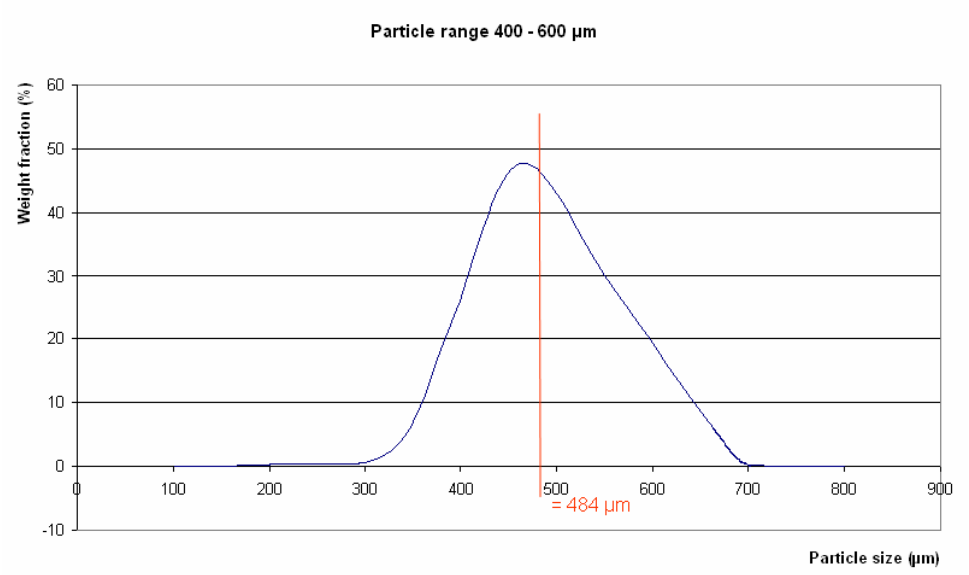

Figure 4.4: Extraction of the mean diameter from the particle size distribution of the sample of particles which is in the range 400 - 600 μm [29]

can be achieved via soft vibrations. Figure 4.5 has shown the changes of the powder volume with the time while vibrating the system.

The vibration process is performed for small and large particles separately. Bulk density (Weight of a unit particle volume) for the maximum compacted powder samples are measured . Based on the bulk density values the samples are prepared by weighing the required amount for each compact volume. Optimum compact volume for all seven samples is 2000ml. According to the experiment , the weight of one liter of small particles is $1665g$ and the weight of one liter of large particles is $1785g$. Required particle volume for each sample can be calculate by using the required particle volume and the bulk density of small or large particles.

Experiments are performed with 100% small particles, 100% large particles and mixtures of small particles with 20, 40, 50, 60 and 80% of large particles. All the particle samples, which are two liters in size, are weighted and well mixed prior to the experiments. At a time one compact mixture is freely filled into the bed. Composition of all the particle samples are shown in Table 4.3.

4.3 Experimental studies

Each powder mixture is used to performe a separate experiment. The minimum fluidization velocity and the minimum bubbling velocities are recorded. Readings of the bed expansions at minimum fluidization conditions are taken manually and pressure variations along the bed are investigated for several air flow rates as mention below.

A well mixed powder samples of two liters of a compact mixture is filled into the bed before starting the each experiments. The bed is filled with particles by using a plastic funnel. This method is used for all the sample. Particles have freely fallen in to the bed. Bed height is measured and recorded soon after the filling is completed. Here in this report this height is

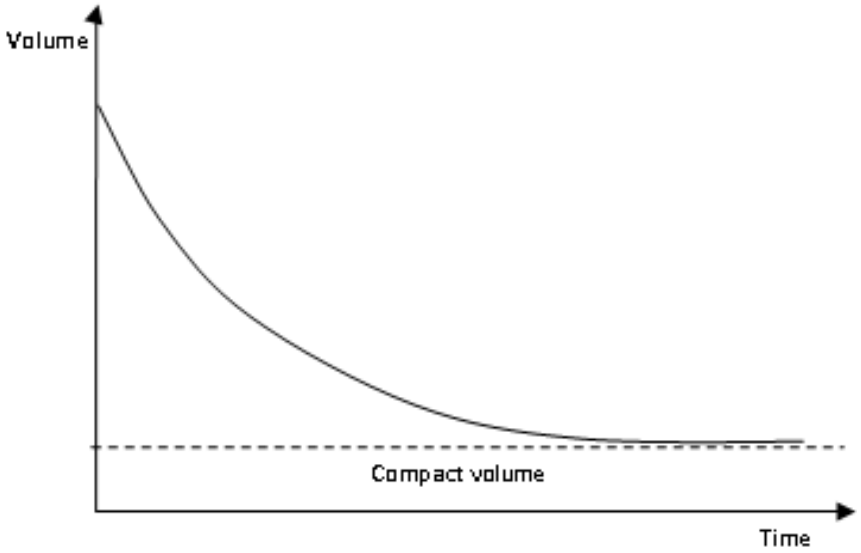

Figure 4.5: Volume varition of the powder while vibration

Table 4.3: Composition of glass particles in the mixture

Sample No.	% of Large particles	Small particles			Large Particles		
		Weight [g]	Particle Volume [ml]	Volume [ml]	Weight [g]	Particle Volume [ml]	Volume [ml]
1	0	3330	1340	2000	0	0	0
2	20	2664	1072	1600	714	287	400
3	40	1998	804	1200	1428	575	800
4	50	1665	670	1000	1785	718	1000
5	60	1332	536	800	2142	862	1200
6	80	666	268	400	2856	1149	1600
7	100	0	0	0	3570	1437	2000

mention as the filled bed height or as initial bed height.

The experiments are started by slowly opening the pressure reduction valve and send the air through the particle bed. A digital air flow meter is used, and the flow rates are observed continuously. The flow rates are recorded at minimum fluidization and minimum bubbling conditions. The digital flow meter is measuring the flow rate in standard liter pr. minute (Sl/min). A computational pressure reading programme is started at minimum fluidization condition. The bed height are measured again and recorded. After 30 seconds, the pressure reduction value is further opened and the pressures at the minimum bubbling conditions are recorded. Again after 30 seconds the air flow is increased up to the closest multiple of 5 and pressure is recorded. As an example, if the minimum bubbling flow rate is 12.5 Sl/min, the flow rate is increased to 15 Sl/min. The flow rate is increased by intervals of 5 Sl/min up to 75 Sl/min, and the pressure along the bed height is recorded for all the flow rates. An increase in flow rate of 5 Sl/min corresponds to an increase of superficial velocity of 0.02 m/s. Experimental studies were performed for all the different powder mixtures and the pressures are measured and recorded.

Prior cleaning of the fluidized bed is necessary to keep the constant volume and reduce the experimental errors. Experimental studies are done for all the particles samples and the data were recorded.

4.4 Observations from the experimental studies

The main observations from the experiments are the pressure variations along the bed, bed height, minimum fluidization velocity and the minimum bubbling velocity. Based on the observations void fraction and the volume fractions of the particle phases are calculated.

4.4.1 Volume fractions of the particle phases

Initial void fractions are calculated based on the weight and initial volume of the bed. The particle weight and the initial bed height are shown in the Table 4.3 and Table 4.4 respectively. The volume and the volume fractions of small and large particles are calculated as shown below. Following calculations are performed for the particle sample with 50% large particles.

$$\text{Volume of the particles } = \frac{\text{Total small/ large particle mass}}{\text{Particle density}}$$

$$\text{Volume fraction of the particles } = \frac{\text{Volume of the particles of small/large particles}}{\text{Bed volume}}$$

$$\text{Bed volume } = \text{ Initial bed height} \cdot \text{Bed cross section}$$

$$\text{Volume of the small particles} = \left(\frac{1665 \cdot 10^{-3}}{2485}\right)$$

$$\text{Volume of the large particles} = \left(\frac{1785 \cdot 10^{-3}}{2485}\right)$$

$$\text{Volume fraction of small particles} = \frac{\left(\frac{1665 \cdot 10^{-3}}{2485}\right)}{0.511 \cdot \pi \cdot 0.036^2} = 0.32$$

$$\text{Volume fraction of large particles} = \frac{\left(\frac{1785 \cdot 10^{-3}}{2485}\right)}{0.511 \cdot \pi \cdot 0.036^2} = 0.35$$

Table 4.4: Initial bed heights and the volume fractions of large and small particles

% of Large particles	**Bed Height** [m]	**Volume fraction of small particles**	**Volume fraction of large particles**
0	0.540	0.61	0
20	0.518	0.51	0.14
40	0.510	0.39	0.28
50	0.511	0.32	0.35
60	0.513	0.26	0.41
80	0.532	0.12	0.53
100	0.548	0	0.64

Table 4.5: Minimum fluidization velocities and the expanded bed height at minimum fluidization conditions

% of Large particles	**Expanded bed height** [m]	**Minimum fluidization velocity,**U_{mf} $[m/s]$	**Minimum bubbling velocity,**U_{mb} $[m/s]$
0	0.558	0.025	0.029
20	0.530	0.028	0.030
40	0.521	0.031	0.032
50	0.524	0.039	0.045
60	0.530	0.053	0.059
80	0.539	0.080	0.083
100	0.554	0.153	0.158

4.4.2 Minimum fluidization velocities, minimum bubbling velocity and expanded bed height

Superficial air velocity is extracted from air flow which unit was in $Sl/\min$ and shown in the Table 4.5. Bed height is measured at minimum fluidization conditions.

Averaged pressure reading are shown in the appendix D.

Chapter 5

Computational studies in bubbling fluidized beds

5.1 Optimum grid size verification

Fluidized bed simulations are extreamly time consuming operations, specially 3D simulations with multiple particles phases. Around 70 simulations are needed to cover the experimental data. The large number of simulations take much time and resources. If very small control volumes is used, even 2D simulations are time consuming. It important to use bit larger control volumes. Then there is a problem with the accuracy of the final results. So it is vital to find an optimum mesh size which can offer time effective and more precise data.

Several 2D mesh files are prepared by using the mesh preparation software called Gambit. Sizes of the smallest control volumes of the 2D mesh is 2×2 mm, which is a very small mesh size compared to the total volume and it has more potential to give more accurate results. A 3D mesh is also prepared with slightly the same size of control volumes. The aim of this experiments is to prepare some more 2D mesh files with bigger control volumes and finalize the optimum grid size by analyzing the simulated results.

5.1.1 Mesh preparation using Gambit

"Fluent" is the general name for the collection of computational fluid dynamics (CFD) programs sold by Fluent, Inc. Gambit is the program used to generate the grid or mesh for the CFD solver.

Several 2D mesh files are prepared by using Gambit. The width of the mesh is 0.072 m and the height is 1.2m. One of the prepared meshes is shown in Figure 5.1. The dimensions of the enclose control volumes are taken as x and y and those values are varied as mentioned in Table 5.2. Face of the 2D fluidized bed is meshed by using "Quad" as the elements and "Map" as the type. Boundary types are specified as shown in Table 5.1. Both 2D and 3D meshes are made as wire frame meshes using gambit and exported to FLUENT.

3D mesh is designed in Gambit by selecting a cylinder of 0.072m in diameter and 1.2m in height. Boundary layer of the bottom face is meshed by dividing the circumference in to fifty and including five separate layers as shown in Figure 5.2. The Boundary types are defined according to the same concept as with 2D mesh. The length of a control volume for y direction is $2mm$. Bottom face of the 3D fluidized bed is meshed by "Quad" as elements and "Pave" as the type.

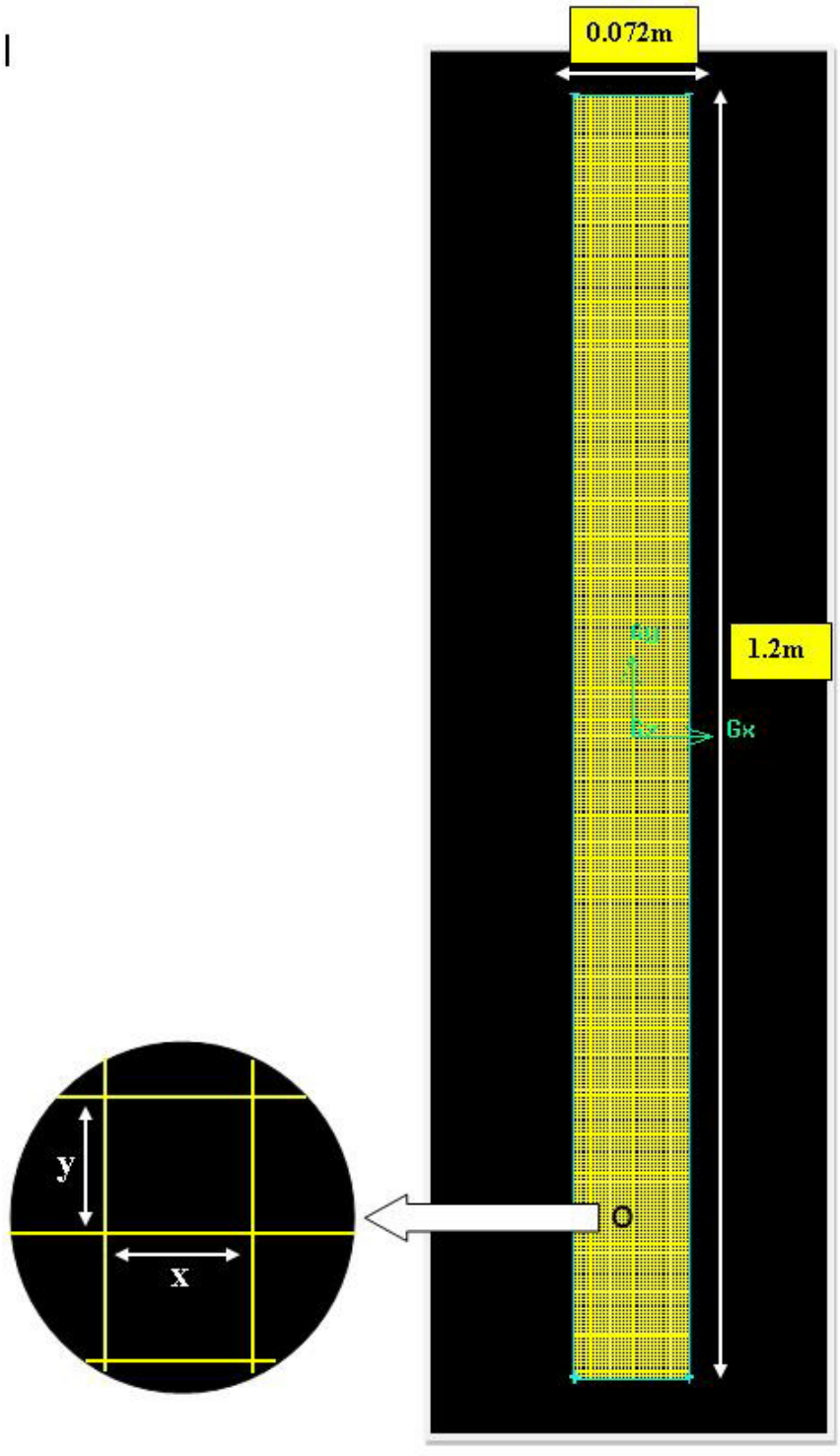

Figure 5.1: Two dimensional grid prepared by using Gambit

Table 5.1: Boundary types used for making the grid in Gambit

Boundary Type	
Bottom of the bed	Velocity inlet
Top of the bed	Pressure outlet
Rest of the boundaries	Pressure outlet

Table 5.2: Grid information

Mesh No.	**Mesh type**	**x** [mm]	**y** [mm]
1	2D	2	2
2	2D	2	3
3	2D	3	3
4	2D	3	4
5	2D	4	4
6	3D, $(2\pi r/50)$ for the boundary Layer, Pave mesh, $2mm$ for y direction		

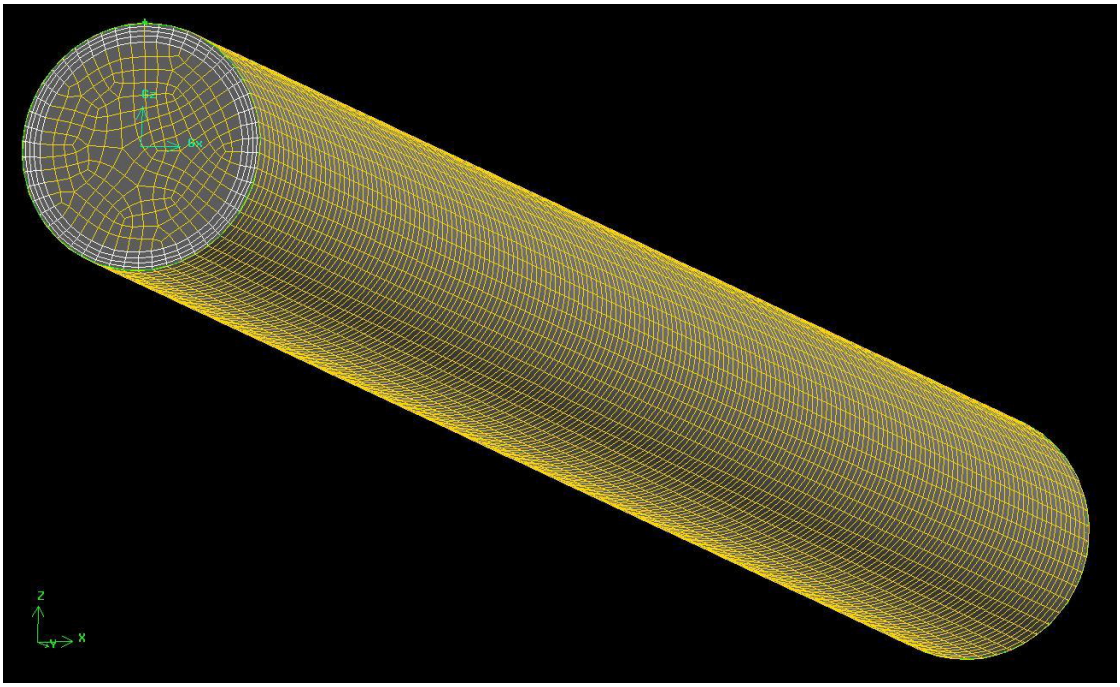

Figure 5.2: 3D mesh for the fluidized bed simulations

Table 5.3: combinations of models for simulating the bubbling fluidized beds

Model		**Selection**
Drag Model	$\Longrightarrow$	Syamlal O'Brien
Granular Viscosity	$\Longrightarrow$	Syamlal O'Brien
Granular Bulk Viscosity	$\Longrightarrow$	Constant
Frictional Viscosity	$\Longrightarrow$	Schaeffer
Frictional Pressure	$\Longrightarrow$	Based-ktgf
Solid Pressure	$\Longrightarrow$	Ma-ahmadi
Radial Distribution Function	$\Longrightarrow$	Ma-ahmadi
Rest of the models	$\Longrightarrow$	Use default settings

5.1.2 Initializing the computer simulations in Fluent and determine the suitable mesh

Simulations are started by loading the mesh files in to Fluent. In order to take readings eleven points are assigned along the bed from bottom to the top. When it comes to settings for monitoring, record type is selected as "Facet Average", which gives the average value of the measurement around the assinged point. The volume fractions are recorded for each 10 iterations. The simulation are performed for 2 phases (gas & solid). The solid phase is large glass particles with $488\mu m$ in mean diameter. Gravity and the atmospheric pressure are applied as operating conditions. Volume fractions of the solid was inserted as 0.6. Superficial air velocity is given as $0.28m/s$. Ariyarathna S et al [29] has recommended a combinations of models for simulation of bubbling fluidized beds, and these models are shown in the Table 5.3.

.

Simulations are performed for $0.4m$ initial bed height. The bed height is marked by using the "Region adaption". 7000 iterations are carried out with 0.001 seconds as "Time step size" (7 seconds). A similar procedure is followed to run simulations using all the prepared meshes including the 3D mesh. Simulations are performed to find the optimum mesh. The 3D simulation took significant amount of time compared 2D simulations to simulate seven seconds. Because of that, the mesh analysis is narrowed down to 2D simulations. Therefore the comparison is done to select a 2D mesh which can offer the same required qualities. The last 3 seconds of the simulation results are averaged and used for the comparison. Averaged solid volume fraction measurements are plotted in the Figure 5.3.

All the curves are compared with the 2D, results from the simulations with 2×2 mm mesh. When the grid sizes are smaller the accuracy is higher and the bigger the grid size lesser the time for the simulations. Mesh with 3×3mm is selected as the optimum mesh and it is used for rest of the simulations performed during this study.

5.2 Simulating the bubbling fluidized bed with selected mesh

The selected optimum mesh is used for further simulation work. Nine new point are assigned on the grid. The positions of those points are exactly the same as the positions of the pressure sensors in the actual fluidized bed. Total pressure is measured by the sensors. The same values are used for the bed heights and the volume fractions as in the experiments. Multiple solid phases are used based on the composition of the particle mixture. Air velocities and the particle compositions are changed according to the experiments performed earlier in the study. Rest

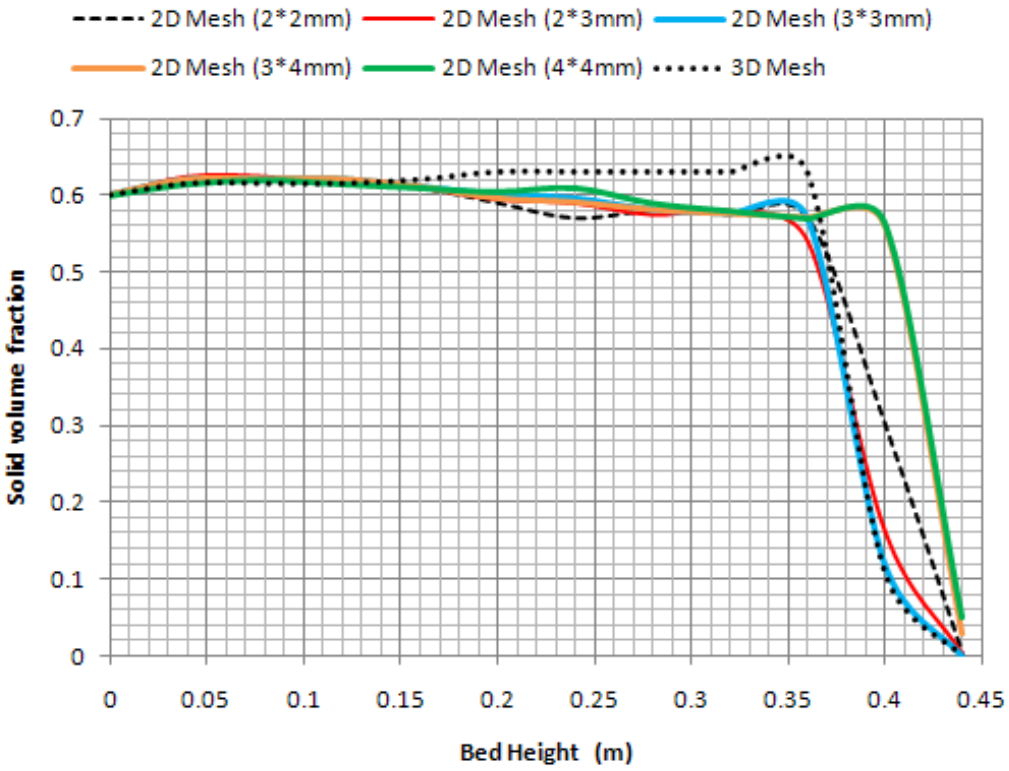

Figure 5.3: Obtained results from the grid resolution test

of the setting are the same as mentioned earlier in this chapter. Simulations are run for seven seconds and the results are averaged the same manner as in earlier simulations. Animated movies are created for each of the simulations for analytical requirements. The pressure values recorded from the simulations are presented in appendix E.

Chapter 6

Analysis of the results from experimental and computational studies

6.1 Bed expansion (experimental)

Bed expansions are measured in the experiments performed for 100% small particles, 100% large particles and 5 different mixtures of small and large particles. The small particles have a range of particle sizes from 100-200 μm mean diameter of 154 μm. According to Geldart characterization diagram, the particles are characterized as Group B particles, but very close to Group A particles. Due to inter-particle forces, Group A particles expand significantly before bubbles appear.

Inter-particle forces are due to wetness, electrostatic charges and Van der Waals forces [24]. For Group B particles the inter-particle forces are negligible, and the bed expansion is at minimum fluidization velocity is rather low [1].

The bed height as a function of fraction of large particles is shown in Figure 6.1. The curves present the initial bed height and the bed height at minimum fluidization. Initially two liters of well mixed and maximum packed particles are filled into the experimental rig. This corresponds to a initial bed height of 491 mm as plotted with a dotted line. During the filling, the powder expanded, and the initial height of the bed therefore varies with the concentration of small and large particles. The initial bed height is 540 mm for 100% small particles and decreases to about 510 mm for mixtures with 40, 50 and 60% large particles, and increases to 548 mm for 100% large particles. The difference between maximum packed powder and bed height after filling are significant for all the mixtures, about 50, 20 and 60 mm for 100% small, 40-60% large and 100% large respectively. For the small particles this is due to the inter-particle forces as described above. The large particles are getting random packed during the filling, and the void fraction increases compared to maximum packing. In the mixtures, the properties of small and large particles influence on each other. The large particles settle and is randomly packed, and the small particles fill the spaces between the large particles.

The bed expansion for the small particles at minimum fluidization velocity is about 20 mm. About the same bed expansion is also observed for the mixtures with 20, 40, 50 and 60% large particles. This indicates that the fluidization properties in a fluidized bed reactor are significantly influenced of the smallest particles in the mixture. The bed expansion for 80 and 100% large particles is about 6 mm. This is a rather low bed expansion, which is typical for Group B

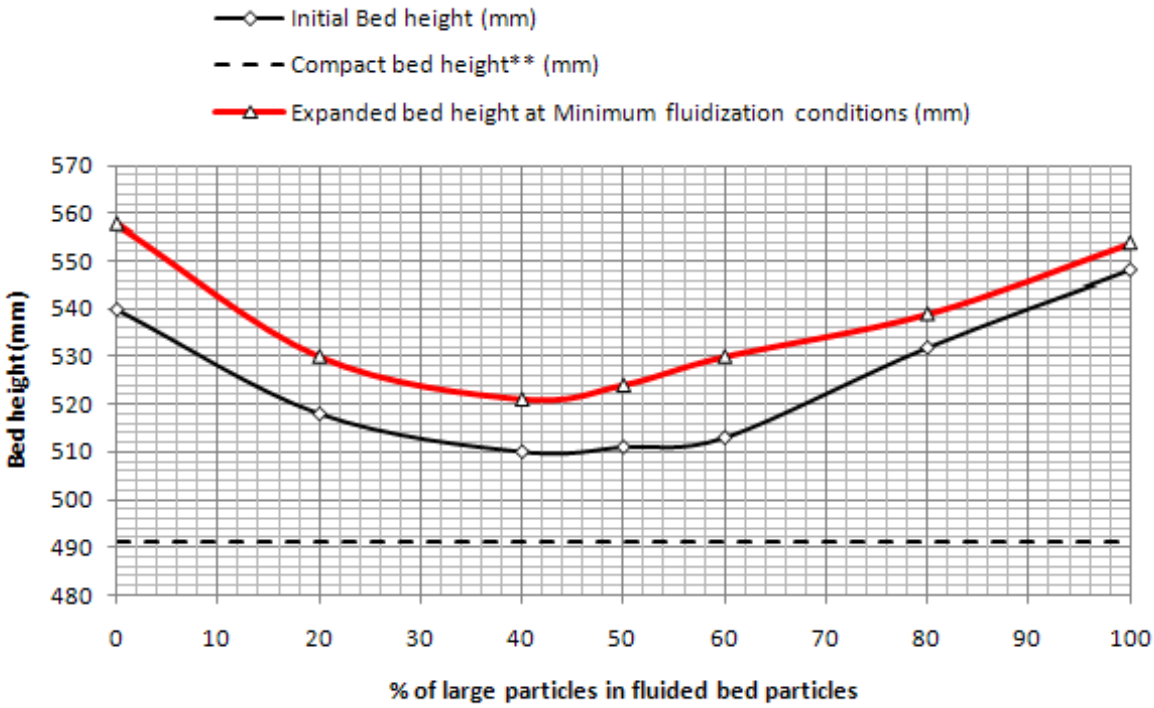

Figure 6.1: Initial bed height and the bed height at minimum fluidization with respect to the composition of particle mixture

particles.

6.2 Studies based on the minimum fluidization velocity

6.2.1 Calculations of minimum fluidization velocity

In this study the analytical method explained in chapter 2 has used to calculate the minimum fluidization velocities of each of the particle groups used in the study . Those are two groups and have referred as small and large particle groups. Densities of the glass particles and the gas are $2485kg/m^3$ and $1.2kg/m^3$ respectively. Viscosity of the gas is taken as $1.8 * 10^{-5}Pa.s$.Examples for Minimum fluidizations calculations are shown in appendix H.

According to Ariyarathna S et al [29] mean particle diameter for small particles is 154 μm.Calculated theoretical minimum fluidization velocity is $0.192\,19ms^{-1}$.It is necessary to calculate the mean particle diameter for each of the mixture to calculate the minimum fluidization velocity. The mean particle diameter of each particle group and their weight fractions are used to calculate the mean particle diameter for each particle samples.

$$D_p = \left(D_{p_{small}} x_{small} + D_{p_{large}} x_{large}\right) \tag{6.1}$$

The mean particle diameters are given in the Table 6.1 which are calculated using Eq.6.1.

Table 6.1: Weight fractions of small and large particles and the mean particle diameter for each particle sample

$D_{psmall} = 154\mu m$ & $D_{plarge} = 488\mu m$					
Sample No.	**Large particles** %	**Weight fraction** (Small)	**Weight fraction** (Large)	[μm]**Mean particle Diameter**	U_{mf} $[m/s]$
1	0	1	0	154	0.019
2	20	0.78	0.22	227.5	0.042
3	40	0.58	0.42	294.3	0.071
4	50	0.48	0.52	327.7	0.088
5	60	0.38	0.62	361.1	0.107
6	80	0.19	0.81	424.6	0.148
7	100	0	1	488	0.195

By using the mean particle diameters of the mixtures, the minimum fluidization velocity for each mixture are calculated using Eq.2.9, and presented in Table 6.1.

6.2.2 Analysis of all experimental, computational and theoretical minimum fluidization velocities

Minimum fluidization velocities are recorded from experiments, simulations and theoretical calculation for the same set of particle mixture. The experiments are performed by starting with low velocities and increase the velocity until the minimum fluidization velocity is obtained and the powder starts to float. Corresponding simulations are performed, using the minimum fluidization velocities found from the experiments as the start. Higher velocities are used till the bed fluidized if the bed does not fluidized with the velocity found by the experiment. Large number of simulations are performed to keep the difference between each velocity value a minimum. The minimum fluidization velocity is found using the highest velocity value which does not fluidized the bed.The comparison between the experimental and computational results is presented in Figure 6.2.

The experimental minimum fluidization velocity is about 0.025 m/s for 100% small particles and 0.15 m/s for 100% large particles. For the mixtures the minimum fluidization velocities increase from 0.027 to 0.039 m/s when the fraction of large particles is increased from 20 to 50%. Again when its come to 60 and 80% large particles, minimum fluidization velocities are 0.05 and $0.08m/s$. The minimum fluidization velocity is almost doubled when the fraction of large particles are increased from 80 to 100% large particles. This shows that the smallest particles in the mixture influence strongly on the fluidization behavior.

The results from the simulations show the same tendency as the experimental results. The minimum fluidization velocity for 100% small particles is 0.05 m/s. When the fraction of large particles are changed from 0 to 40% no change in minimum fluidization velocity are observed. The minimum fluidization velocity increases slightly when the volume fraction of large particles is increased from 40 to 80%. The computational minimum fluidization velocities are 0.055, 0.06 and 0.075 for 50, 60 and 80% large particle mixtures respectively. The simulation with 100% large particles gives a minimum fluidization velocity of 0.255 m/s. This is more than three times the fluidization velocity observed for the mixture with 80% large particles. Predicted theoretical minimum fluidization velocity based on Ergun equation, is different from both Observations and computations. May be this is due to the assumptions, which are made while calculating the theoretical minimum fluidization velocity.

The comparison between the experimental and computational results shows that the minimum fluidization velocities are strongly influenced of the smallest particles in the mixture. The computational minimum fluidization velocity is about double of the experimental fluidization velocity for small particles and mixtures with low concentrations of large particles. For the mixture with 50% large particles the deviation is smaller, and for the 60 and 80% mixtures the deviation between experimental and computational results are less than 10%. The difference between the experimental and computational minimum fluidization velocity is significant for the large particles.

The large deviation between the simulations and experiments for 100% small and 100% large particles can be explained by the difference in particle distribution. The small and the large particles used in the experiments are not mono sized particles but powders with a particle range of 100-200 μm and 400-600 μm respectively. This means that in the experiments many particle sizes are included, and this influence on the fluidization properties. In the simulations with 100%small and 100%large particles, the bed contains mono sized particles, and this influence on the void fractions, packing of the bed and thereby on the fluidization properties. The minimum void fraction is significantly higher for mono sized particles than for a mixture of particle sizes. Higher void fraction in the bed requires a higher gas velocity to get the particles fluidized. To get a better agreement between simulations and experiments for the small and large particles, the simulations for these cases can be run with multiple particle phases to give a particle size distribution that corresponds to the experimental powder.

More than two particle phases can also be included in the simulations of the mixtures. The deviation between the computational and experimental results may also partly be due to that the simulations are performed in a two dimensional system.

According to the Geldart classification all of these particle mixtures are belongs to Geldart B. Minimum fluidization velocity and minimum bubbling velocity for Geldart B particles are relatively same [1]. Which is shown in Figure 6.3.

6.3 Void fraction variations

All the particle samples are having an identical maximum compact volume as mentioned in above chapters. The volume of the particles has expanded when it is filled smoothly in to the fluidized bed. Figure 6.4 shows the void fractions and the compositions of large and small particles in the mixtures. It is possible to observe that the samples with only small and only large particles have higher void fractions than the particle mixtures with both large and small particles.

This may be due to the repulsive forces between the small particles [24]; which means that they are having some barriers to reduce the voids as shown in Figure 6.5(a). The large particle can not reduce the voids in between those particles, because of their geometry as shown in Figure 6.5(b). The repulsive forces are not longer significant for large particles as much as for small particles.

In the mixtures of both small and large particles, lower void fractions can be observed. The mixtures which showed lower void fractions are observed for the mixtures with 50% to 90% large particles. The minimum void fraction is found for the mixture of 70% large and 30% small particles. That means the mixtures of both large and small particles are more packed than the mono size particle samples. It might be there is less space in between particles In the mixtures with more large particles than the mixtures with more small particles as shown in Figure 6.5 (c) & (d).

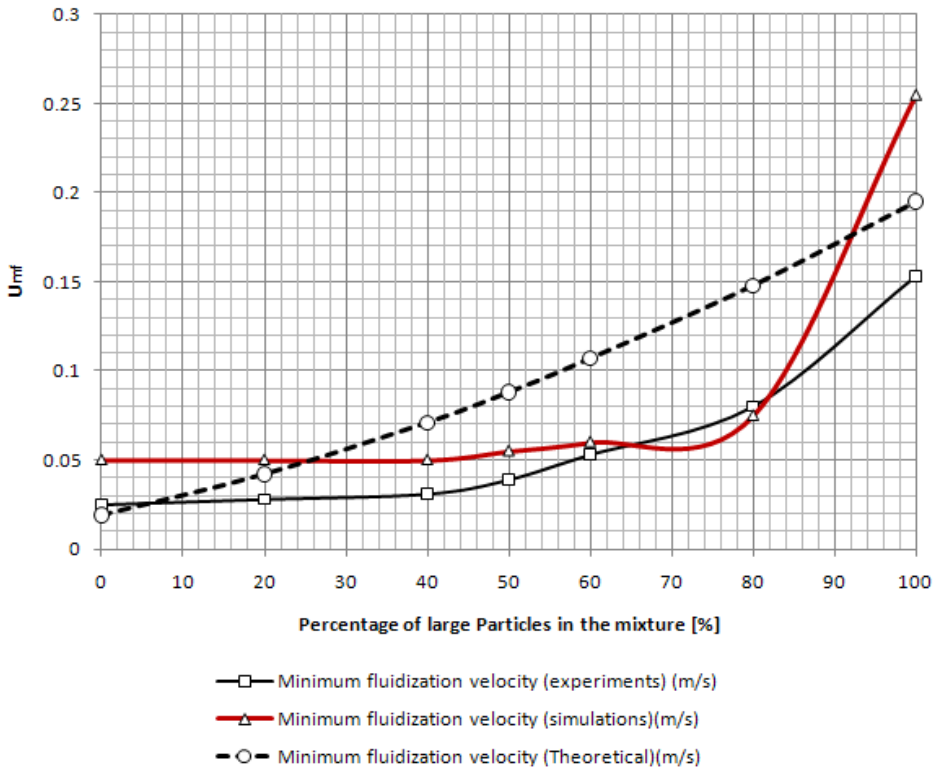

Figure 6.2: Experimental, computational and theoretical minimum fluidization velocity

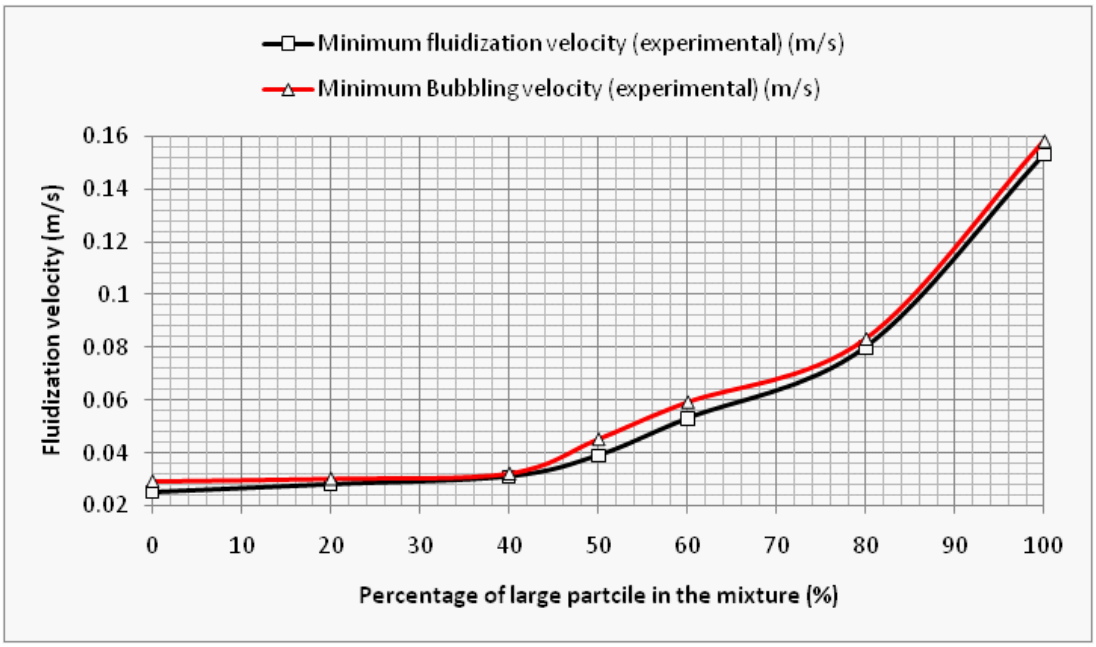

Figure 6.3: Variations of U_{mf} and U_{mb}

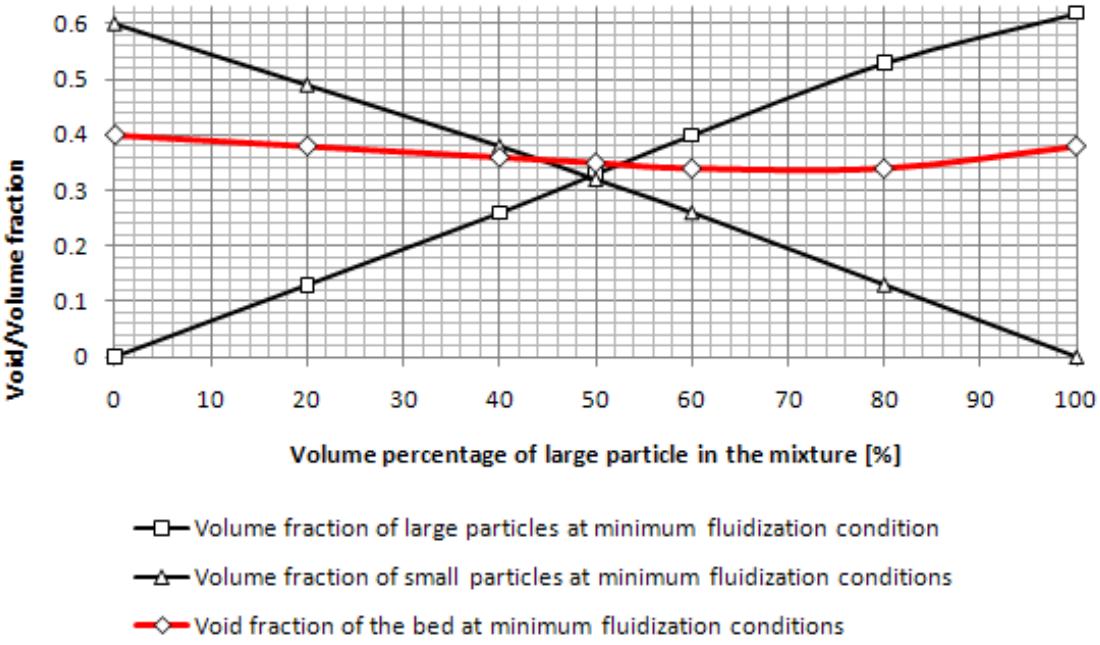

Figure 6.4: Void fractions and compotions of particles as a function of contained lagre particle percentage

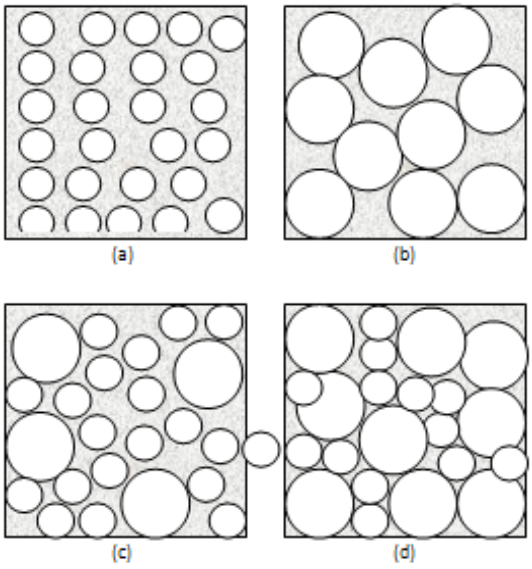

Figure 6.5: Possible particle positioning with 2 difference size of particles

6.4 Analysis of fluidized bed behavior based on simulations

Figure 6.6 contains the simulated fluidized bed of only small particles for three difference air flow rates. There is no bed expansion for 0.029 m/s of air flow rate. This is the experimental minimum fluidization velocity for the corresponding particle sample and computational minimum fluidization velocity is 0.05 m/s. The bed expansion is almost doubled when the velocity is increased to 0.307 m/s. It is possible to observe large air bubbles and higher bed expansions for the samples with 0%, 20% and 40% large particle mixtures as shown in Figures 6.6, 6.7 and 6.8.

Figure 6.9 shows the bed behavior and the volume fraction of small particles in the fluidized bed after 7 seconds for different superficial air velocities. These simulations are performed for a mixture of 50% small and 50% large particles and initial bed height is $0.511m$. Volume fractions for large and small particle phases are 0.32 and 0.35. These conditions are the same as the initial conditions used in the experiment with the same particle mixture.

The experimental minimum fluidization value for this particle mixture is $0.039m/s$, but the minimum fluidization velocity from the simulation is 0.055 m/s. Computational minimum fluidization velocity value is bit higher than the experimental minimum fluidization velocity. The deviation can be due to the several different particle phases contained in the real mixture as mentioned earlier.

In the simulation with $0.039m/s$ of air velocity and the sample with for 50% large particle, the air flow rate is a lower value and the gas merely percolates through the void spaces between stationary particles. This means the bed is at fixed bed conditions. At the next simulation the air flow of $0.045m/s$ is used, particles moved apart and they moved in restricted regions. This time the bed has converted to an expanded bed and possible to observe a little increment of bed height. Bed has started to fluidized when the air flow is increased to 0.055m/s. At higher velocity ($0.102m/s$ and $0.143m/s$) slugging started and the bed height is increased further, gas bubbles coalesce and grow as they rise. In a deep enough bed of small diameter they may eventually

Table 6.2: Bed information at minimum fluidization conditions

Large particle percentage [%]	**Initial bed height** [mm]	**Volume fraction of large particles**	**Volume fraction of small particles**
0	540	0	0.61
20	518	0.14	0.51
50	511	0.35	0.32
60	513	0.41	0.26
80	532	0.53	0.12
100	548	0.64	0

become large enough to spread across the vessel[1]. Finally the bed has turned in to a turbulent fluidization at higher velocities about $0.266m/s$ and $0.307m/s$ air velocities. Which means the terminal velocity of the solids exceeded, the upper surface of the bed disappears, entrainment becomes appreciable, and instead of bubbles, one observes a turbulent motion of solid clusters and voids of gas of various size and shapes.

Excess air velocity is the superficial air velocity relative to the minimum fluidization velocity [1]. Excess air velocity has increased with increased air flow. Higher excess air velocity means the higher air thrust on particles and increase the force on particles opposite to the gravity. Due to this reason bed is expanding while increasing the air flow [1].

At the slugging condition bubbles are moving upward by using a zigzag path as shown in Figure 6.10. This is clearly visualized from the animated movie clips from the simulations. The maximum pressure at the bottom of the bed due total particle weight and the air inflow [1]. All the air bubbles generated at the bottom of the bed are moving in to low pressure zones. Bubbles are moving upward because of the generated higher pressure at bottom of the bed. Bubbles are reducing the pressure inside while increasing the volume during the upward movement. It may be hard to move upwards directly due to the weight from the particles above the bubble. Then the bubbles have to flow to the low pressure areas compared to the pressure at top of the bubble. This means the right or left sides from its original path. When the bed is extremely narrow, bubbles have no 2 sides to flow as it is always end up by hitting a wall of the bed. This may be the reason these bubbles are having a Zigzag path to escape from the bed.

Figures 6.11, 6.12 and 6.13 have shown the fluidized bed behavior of 60%, 80% and 100% large particle samples respectively.

Figure 6.14 has shown the simulated fluidized beds by Fluent for glass particle mixtures with composition of 0%, 20%, 50%, 60%, 80% and 100% large particles. These all the simulations were done for $0.307m/s$ superficial air velocity. Bed height and the volume fractions of large and small particles are shown in the table 6.2.

One of the major observations is various bed expansions for difference particle mixtures. Higher bed expansion is observed for samples with higher composition of small particles than the particle samples with more large particles. According to the experimental results shown in Figure 6.2 the minimum fluidization velocity of each of these samples are reduced with the increased composition of contained small particles. Here all the samples are having the same superficial air velocity. This means excess air velocity is decreasing with the large particle percentage as shown in the Figure 6.15. Excess air velocity is one of the major factor which effecting on the bed expansion. Bubbling fluidized bed with higher excess velocity is converted to turbulent fluidized beds, which can be observed from Figure 6.15 with first and second particle samples. Last particle sample with 100% large particles are more behaving like a fluidized bed with axial slugs with isolated bubbles. It may be because of the relatively lower excess air velocity.

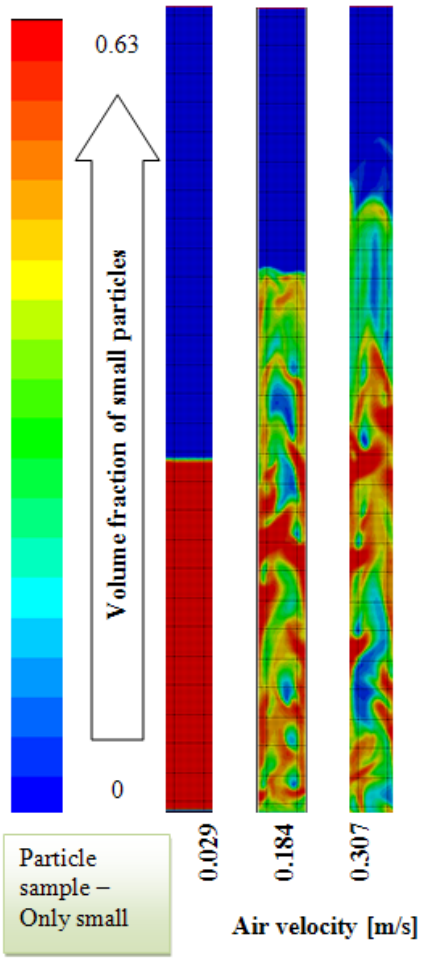

Figure 6.6: Simulated fluidized beds for several superficial air velocities for only small particle mixture

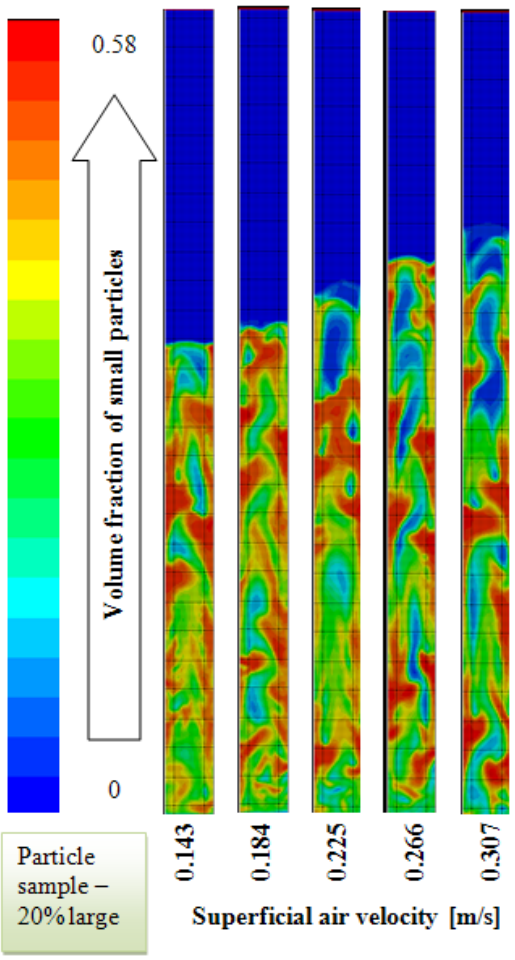

Figure 6.7: Simulated fluidized beds for several superficial air velocities for 20% large particle mixture

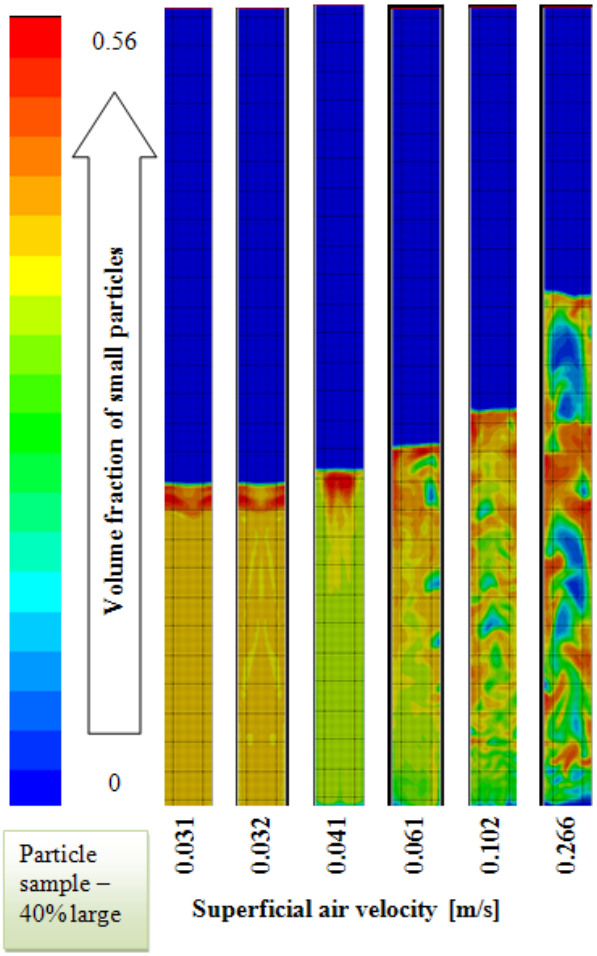

Figure 6.8: Simulated fluidized beds for several superficial air velocities for 40% large particle mixture

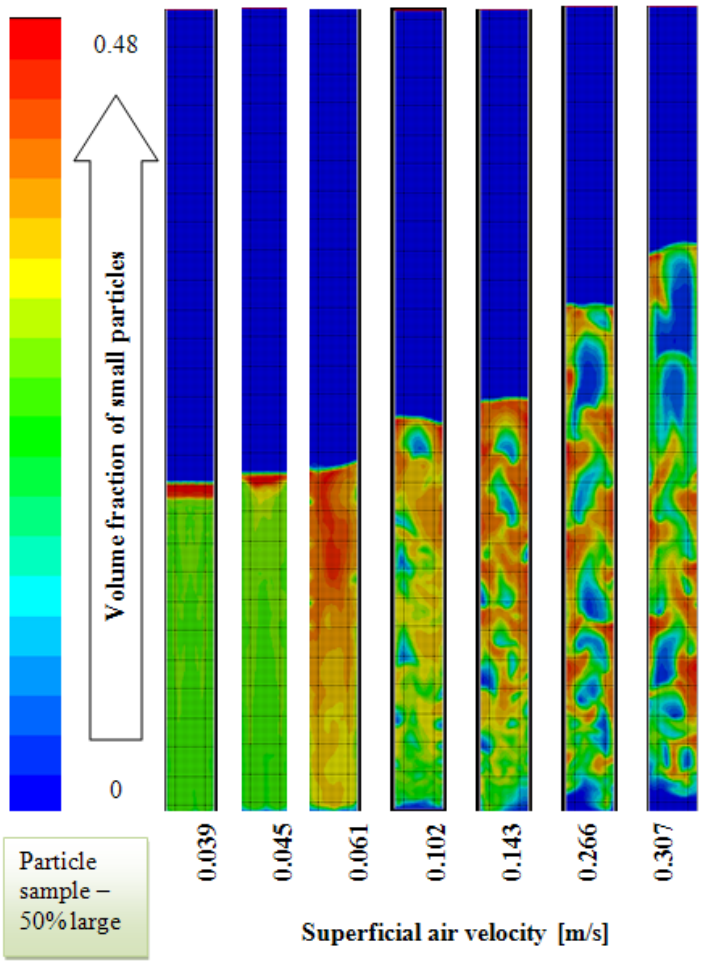

Figure 6.9: Simulated fluidized beds for several superficial air velocities for 50% large particle mixture

Figure 6.10: Zig zag bubble escaping pattern

Properties of the powder also effecting on the bed expansion. Geldart A particles are expanding more than the Geldart B particles at the same superficial air velocity [1]. The samples with 0%-50% large particles are contained Geldart B particles but it is very close to A particles. The sample with 50%-100% large particles are contained Geldart B particles. Therefore the bed expansions of the simulated fluidized beds can be explained by the Geldart particle properties.

Fluid like behavior of the fluidized bed is explained in chapter 2. The observations of the behavior of the bubbles in Figure 6.14 might be used as another proof for the fluid like behavior of a fluidized bed. That means, if the air can be sent though a low viscous fluid, bubbling may turn in to turbulent mode in higher superficial air velocity. If the same air velocity is used for a high viscous fluid the escaping bubbles will be the same as the bubbles in a large particle fluidized beds. All the escaping bubbles are converted to more spherical bubbles by the high surface tension in the media. Further investigations are needed for a better conclusion.

It is possible to observed similar behaviors in the fluidized beds with 0-60% large particles. Those are non spherical bubbles and a turbulent bed at high velocities. Fluidized bed with only large particles show axial slugs with more spherical bubbles for the velocities in the same range. The beds with 80% large particles are having both above mentioned properties as it formed bigger air bubbles while air has penitrated through particles.

According to the given bed properties it is possible to conclude that small particle are much more effecting on fluidization than large particles.

6.5 Pressure variation of the observations with computations

Figure 6.16 shows the variations in the pressure with respect to the percentage of large particles in the sample at different heights of the bed as found from the experiments and simulations. It is possible to observe that both experimental and computational results are little bit similar

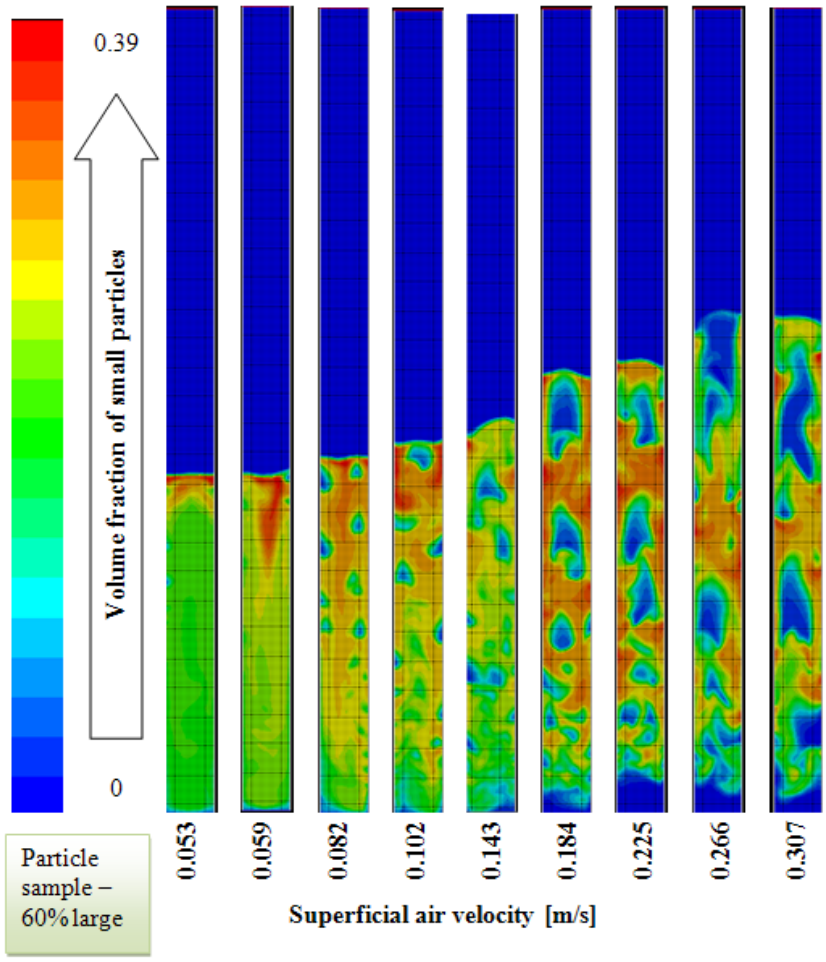

Figure 6.11: Simulated fluidized beds for several superficial air velocities for 60% large particle mixture

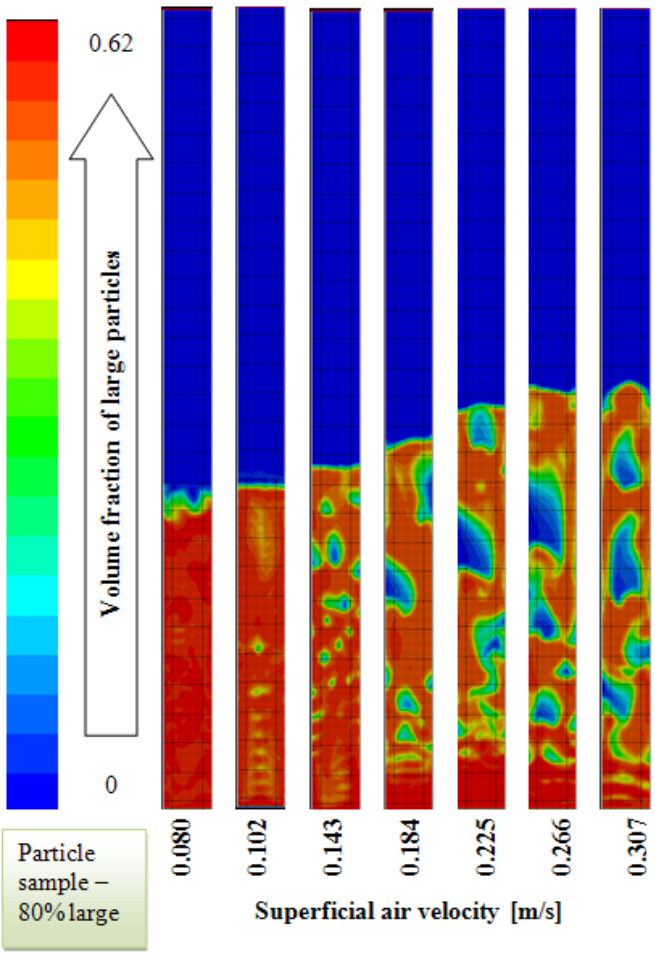

Figure 6.12: Simulated fluidized beds for several superficial air velocities for 80% large particle mixture

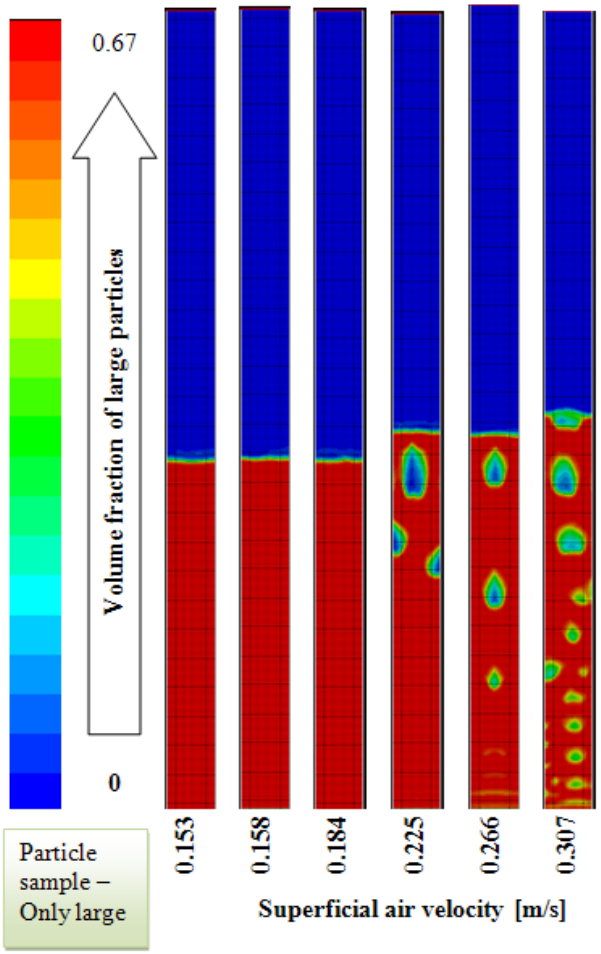

Figure 6.13: Simulated fluidized beds for several superficial air velocities for 100% large particle mixture

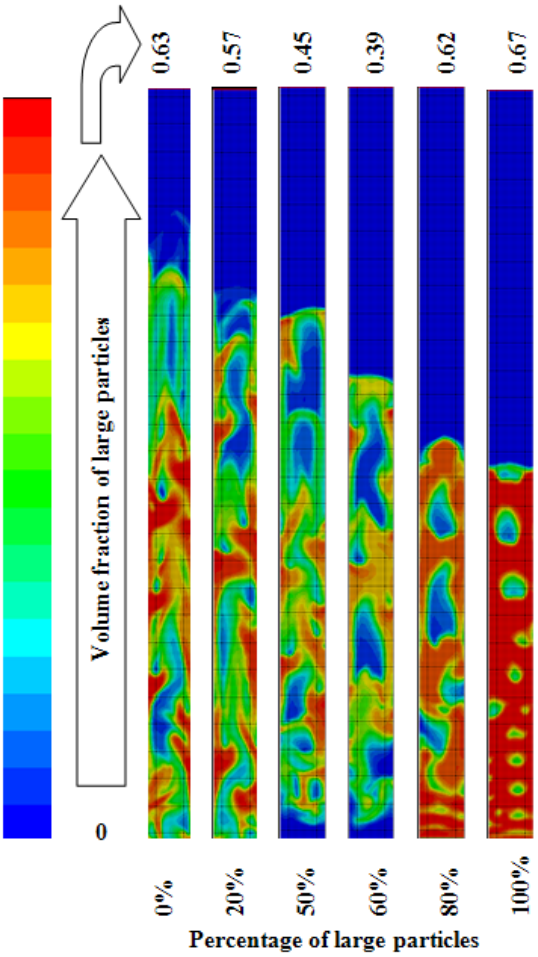

Figure 6.14: Simulated fluidized beds for several particle composition at 0.307m/s superficial air velocity

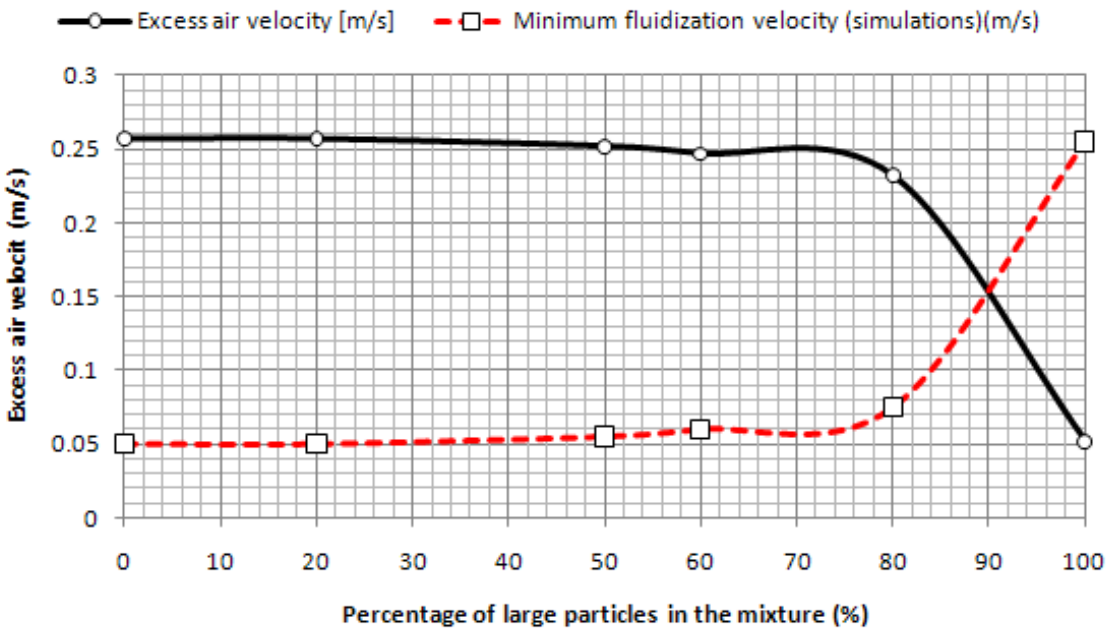

Figure 6.15: Variation of excess air velocity and the minimum fluidization velocity with respect to composition of the particle mixture

to each other at the same bed height. Still the pressure values found from the simulations are slightly lower than those from the experiments. This may be because the particle samples used for experiments consist of particle size distributions while the simulations consider only the mean particle size to represent each mixture.

Pressure values observed from the experiments for each particle sample, except the experiment for 100% large particles are higher than the predictions from the reference simulations. Both the experimental and computational pressure values are very close to each other for 100% large particles. The sample with 100% large particles is also consists of a size distribution since the particle type which is referred as large particles are not nomo-sized. Due to the closeness of the predictions and the observations of the pressure value with only large particles in the bad, it is possible to assume that the size distribution of the large particle group does not make a major influence on the results.

The total pressure along the bed is decreasing from the bottom to the top. This is mainly due to the weight of the particles which are above the measuring point [1].

Figure 6.17 shows the dependency of the total pressure at a certain bed height (23.5cm from bottom) on the superficial air velocity for several selected particle mixtures. The results presented in the figure are from both the experiments and simulations. The curves from the experimental results have steep gradients until they reach very high velocities while the gradients of the curves from the simulated results are not that steep. In both the experiments and simulations the total pressure has increased with the increasing superficial air velocity. The possible reason for this observation is that the measurement point is located close to the wall of the bed. Due to the appearance of the bubbles and the size of the bubbles in the bed, the particle bed close to the

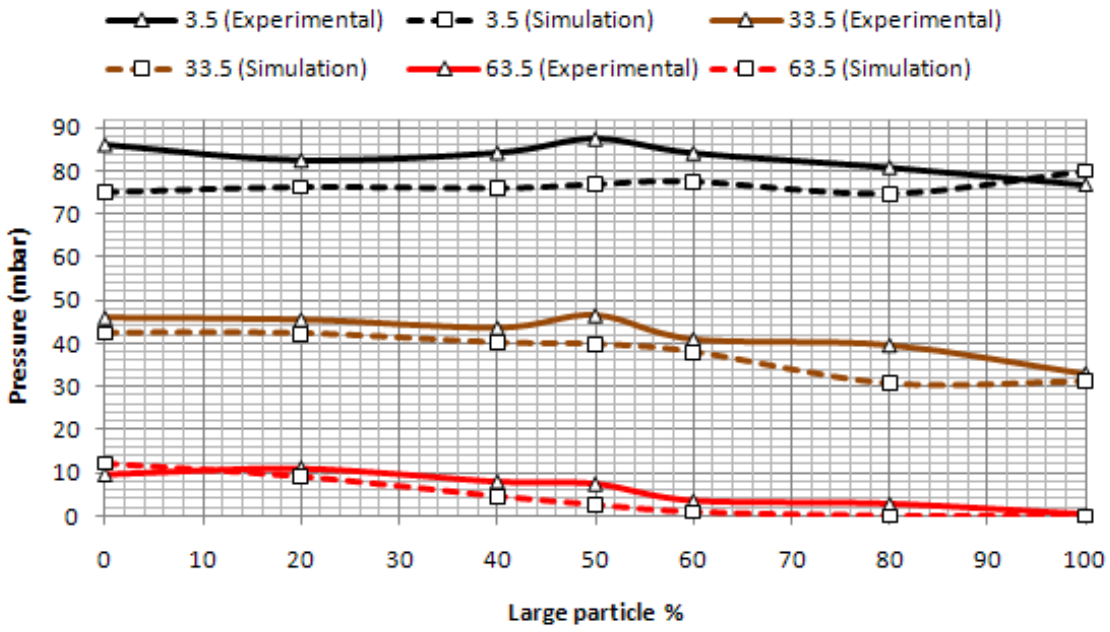

Figure 6.16: Pressure variations of, observations and computations at 3 different bed heights

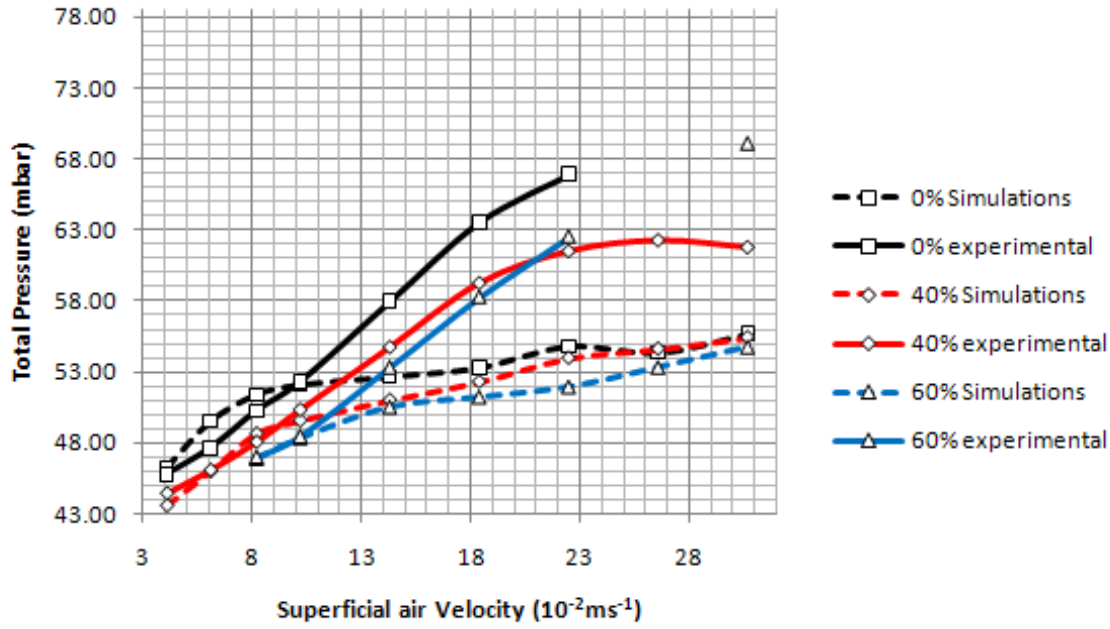

Figure 6.17: Pressure variations of observations and computations with respect to superficial air velocity at 23.5cm bed height. Results are shown from three different particle samples.

wall becomes more compact increasing the total pressure close to the wall. As the superficial air velocity increases, the number of bubbles in the bed increases and the size of the bubbles increases, and as a result the pressure close to the wall can be increased.

A decrease in the gradient of the 40% experimental curve can be seen in the figure at higher superficial air velocities, and the reason for that can be the transition of the bed from the bubbling mode to the turbulent mode at higher air velocities.

Chapter 7

Conclusion for computational and experimental studies of bubbling fluidized bed

The efficiency of the fluidized bed reactors depends on bubble distribution, bubble size and bubble velocity within the reactor. The bubble behavior depends on the amount of excess air introduced to the reactor. Excess air is the actual gas velocity minus the minimum fluidization velocity [1]. The minimum fluidization velocities for different mixtures of particles are studied. A series of experiments are and simulations are performed. Experiments are performed in a cylindrical bed with a uniform air distribution. Different mixtures of spherical glass particles with mean diameter of 154 μm (small particles) and 488 μm(large particles) and mixtures of the small and the large particles are used in the experiments.

Corresponding simulations are performed by using the commercial CFD code Fluent 6.3. Grid resolutions of the fluidized bed mesh is an important factor for more efficient computer simulations of bubbling fluidized bed. Computational studies are performed for several 2d grids with different resolutions and a high resolution 3D bed. Mesh with $2 \times 2mm$ grid resolutions is selected as the optimum mesh.

In addition to the minimum fluidization velocity, the experimental bed expansion is measured. The bed expansion for small particles and mixtures including up to 60% of large particles is about 20 mm at minimum fluidization velocity. This indicates that the fluidization properties in a fluidized bed reactor are significantly influenced of the smallest particles in the mixture. The bed expansion for 80 and 100% large particles is about 6 mm. This is a rather low bed expansion, which is typical for Group B particles.

The comparison between the experimental and computational results shows that the minimum fluidization velocities are strongly influenced of the smallest particles in the mixture. The experimental and computational results show the same tendency, that the minimum fluidization velocities are low and about constant for mixtures of 0 to about 60% of large particles. The computational minimum fluidization velocity is about double of the experimental fluidization velocity for small particles and mixtures with low concentrations of large particles. Mixture with 50, 60 and 80% large particles give good agreement between experimental and computational minimum fluidization velocities. The difference between the experimental and computational minimum fluidization velocity is significant for 100% large particles. The deviations are mainly due to the particle size range that is present in the experiments are not accounted for in the

simulations of 100% small and 100% large particles. The deviations observed in the studies of the mixtures, may be reduced by using more than two particle phases to get a more representative particle size distribution. Minimum fluidization for each sample is calculated by using the Ergun equation as void fractions are unknown. Theoretically predicted minimum fluidization velocity is far more deviating from experimental and computational minimum fluidization velocity specially for small and large particle mixtures.

Experimental void fractions are calculated and there are higher void fractions for only small and only large particles than the mixture of both particles phases. Lowest void fractions are observed from the mixtures with 50%-90% large particles. This may be due to the more packed bed because of well arrangement of the particles in the particle mixture with more larger particles.

Fluidized bed behavior is analyzed based on computer simulations for different particle mixtures. It has shown the highest bed expansion for only small particles and the lowest for only large particle samples. It is possible to observe bigger air bubbles and higher bed expansion of the 0%, 20%,40% and 60% large particle mixtures. More isolated and relatively small bubbles has created by the fluidized bed with only larger particles. There is more effect from the small particles on fluidization than large particles.

At the slugging conditions bubbles are moving upward by using a zigzag path. This can be clearly visualize from the computer animation. All the generated air bubbles at the bottom of the bed are moving in to low pressure zones. Bubbles are moving upward because of the generated highest pressure at bottom of the bed. When the bed is extremely narrow, bubbles are having a Zigzag path to escape from the bed as it is having obstacles to move directly up ward. According to the observation, experimental and computational fluidized bed behavior are relatively similar with each other.

Experimental pressure variations along the bed are slightly similar to the computational observations. it gives a slightly low pressure values for the simulations than the experimental values. This may be due to different particle sizes contained in the particle samples used for experiments. Both experimental and computational pressure values are providing the identical results for 100% large particles. Different particle phases containing in 100% large particles mixture are not effecting on the experimental results. Mostly it behaves as a unique size particle phase.

Experimental and computational pressure reading are analyzed. It gives a higher pressure increment vs superficial air velocity for experiments than the simulations. Experimental and computations results are similar at low superficial air velocities.

Bibliography

[1] Kunii,D. & Levenspiel, O.(1991) Fluidization Engineering, 2nd edition, Newton, US, Butterworth-Heinemann, pp (01-92).

[2] Caicedo,G.R., Ruiz,M.G., Marques,J.J.P. & Soler,J.G., Minimum fluidization velocities for gas /solid 2D beds,Chemical Engineering and Processing 41 (2002),pp 761-764

[3] Singh,P.K. & Roy,G.K., Prediction of minimum bubbling velocity, fluidization index and range of particulate fluidization for gas–solid fluidization in cylindrical and non-cylindrical beds,Powder Technology 159 (2005),pp 168 – 172

[4] Lin,C.L., Wey,M.Y. & You,S.D., The effect of particle size distribution on minimum fluidization velocity at high temperature, Powder Technology 126 (2002),pp 297– 301

[5] Girimonte,R. & Formisani, B., The minimum bubbling velocity of fluidized beds operating at high temperature, Powder Technology 189 (2009),pp74–81

[6] Wirsum, M., Fett,F., Iwanowa,N.& Lukjanow, G.,Particle mixing in bubbling fluidized beds of binary particle systems, Powder Technology 120 (2001),pp 63–69

[7] Rasul,M.G.,Rudolph,V., & Carsky,M., Segregation potential in binary gas fluidized beds, Powder Technology 103 (1999),pp 175–181

[8] Wang,Y.,Cheng,Y.,Jin,Y. & Bi,H.T., On impacts of solid properties and operating conditions on the performance of gas-solid fluidization systems, Powder Technology 172 (2007) ,pp167–176

[9] Werther,J., Measurement techniques in fluidized beds, Powder Technology 102 (1999),pp15–36

[10] Hayhurst,A.N. & Parmar,M.S.,Measurement of the Mass Transfer Coefficient and Sherwood Number for Carbon Spheres Burning in a Bubbling Fluidized Bed, Combustion and Flame130(2002),pp 361–375

[11] Ommen,J.R.,Schaaf,J.,Schouten,J.C.,Wachem,B.G.M., Coppens, M.O. & Bleek,M.,Optimal placement of probes for dynamic pressure measurements in large-scale fluidized beds, Powder Technology 139 (2004),pp 264– 276

[12] Kim,S.H. &Han,G.Y., An Analysis of pressure drop fluctuation in a circulating fluidized bed, Korean journel of Chemical Engineering16(5)(1999),pp 677-683

[13] Park,S.H., & Kim,S.D., Experimental, Statistical and stochastic studies of pressure fluctuations in a three-phase fluidized bed with a moderately large diameter,Korean journel of Chemical Engineering 20(1)(2003),pp 121-127

[14] Zhang, K.,Brandani, S., Bi, J. & Jiang, J., CFD simulation of fluidization quality in the three-dimensional fluidized bed, Progress in natural science 18(2008),pp 729-733

[15] Gidaspow,D., The Fluidized State. In Multiphase Flow and Fluidization, Continum and Kintic Theory Description, (1994), California: Academic press,Inc. pp 97-114

[16] Wong,A.C.Y., Use of angle of response and bulk densities for powder characterization and the prediction of minimum fluidization and minimum bubbling velocities. Chemical Engineering Science 57, (2002) No.14

[17] Davidson,J.F. & Harrison,D., Fluidization, (1971) Academic Press Inc. Ltd, London

[18] Abrahamsen,A.R., & Geldart,D., Powder Technol. 26 (1980),pp 35

[19] Rhodes,M.,Fluidization of Particles by Fluids,Classification of Powders (4), http://www.erpt.org/012Q/rhod-04.htm (15/05/2009)

[20] Bin,C., Cong,W. & Zhiwei,W.,Investigation of gas-solid two-phase flow across circular cylinders with discrete vortex method, Applied Thermal Engineering 29 (2009) ,pp1457–1466

[21] Patil,D.J.,Annaland,M.V.S., & Kuipers, J.A.M., Critical comparison of hydrodynamic models for gas solid fluidized beds-Part II: Freely bubbling gas-solid fluidized beds. Chemical Engineering Science 60 (2005).

[22] Gidaspow,D. & Ettehadleh, B., Fluidization in two-dimensional beds with a jet. II. Hydrodynamic modeling. I&EC Fundam 22(2):(1982),pp193–201.

[23] Zhang,K., Brandani S, Bi J. Computational fluid dynamics for dense gas–solid fluidized beds. Progr Nat Sci15,[special issue](2005),pp 42–51

[24] Geldart,D.,Gas Fluidization Technology, 1st edition, John Wiley & Sons, Ltd., Chap. 4.(1986), pp. 53–97

[25] Boemer,A.,Qi, H. & Renz, U.,Verification of Eulerrian simulation of spontaneous bubble formation in a flidized beds. Chemical Engineering Science, 53(10),(1998) pp 1835-1846

[26] Xie, N.,Battaglia, F.,& Pannala, S., Effects of using two-versus three-dimensional computational modeling of fluidized beds part1, Hydrodynamics. Powder Technology 182, (2008) pp. 1-13

[27] Patil,D.J.,Annaland,M.V.S., & Kuipers, J.A.M., Critical comparison of hydrodynamic models for gas solid fluidized beds-Part I:bubbling gas-solid fluidized beds operated witha jet. Chemical Engineering Science 60 (2005).

[28] Halvorsen,B.M.,An Experimental and Computational Study of Flow Behavior in Bubbling Fluidized Beds. In Thesis for the degree of Dr.Ing,(2005). pp.32-45

[29] Ariyarathna,D.G.A.S.U.,Recommendation of a model from simulating & analysis of the influence of particle size distribution on the simulations of bubbling fluidized beds, (Master thesis 2008), pp 06-70

[30] Lun, C.K.K., Savage, S.B., Jeffrey, D.J. & Chepurniy, N.,Kinetic theories for granular flow: inelastic particles in couette flow and slightly inelastic particles in a general flowfield. Fluid Mechanics, 140 (1984). pp.223-256

[31] Lun,C.K.K. & Bent, A.A., Numerical simulation of inelastic frictional spheres in simple shear flow, Journal of Fluid Mechanics. 258 (1994),pp 335–353

[32] Hoomans,B.P.B., Kuipers,J.A.M., Briels, W.J. & Swaaij, W.P.M., Discrete particle simulation of bubble and slug formation in a two dimensional gas-fluidized bed: a hard-sphere approach, Chemical Engineering Science. 51, (1996), pp 99–118

[33] Tsuji,Y.,Kwaguchi,T. & Tanaka,T., Discrete particle simulation of twodimensional fluidized bed, Powder Technology. 77 (1993),pp 79–87

[34] Chidambaram,N., Djamel,L. & George,Y., Linear stability analysis of particleladen mixing layers using Lagrangian particle tracking, Powder Technology. 125,(2002),pp 122–130

[35] Thomas,N.H., Entrainment and transport of bubbles by transient large eddies in multiphase turbulent shear flow, in: Proc. of the Int. Conf. on Physical Modeling of Multiphase Flows, Coventry, UK, 1983.

[36] Maxey,M.R. & Riley,J.J., Equation of motion for a small rigid sphere in a nonuniform flow, Phys. Fluids 26 (1983), pp 883–889

[37] Auton,T.R. & Hunt,C.J.R., The force exerted on a body in inviscid unsteady nonuniform rotational flow, Fluid Mechanics 197 (1988),pp 241–257.

[38] Sene,K.,Hunt,J.C.R. & Thomas, N.H., The role of coherent structures in bubble transport by turbulent shear flows, Fluid Mechanics, 259 (1994),pp 219–240

[39] Yang,X., Two-phase flow dynamics simulations and modeling, Ph.D Dissertation, University of Birmingham, UK, 1996

[40] Fluent (2006). Modelling Multiphase Flows. In Fluent 6.3 User's Guide, pp.37-71

Part III

Observations from experiments & simulations

Appendix A

Experimental observations of bed expansion

Table A.1: Bed height variations at different stages (*Mixture contained medium size particle with mean diameter of 488ţm and small particles with mean diameter of 154ţm. ** Total height from both small and medium particle layers without mixing.)

Percentage of large Particle in the mixture* [%]	**Compact bed height**** [mm]	**Filled bed height** [mm]	**Expanded bed height at minimum fluidization conditions** [mm]
0	491	540	558
20	491	518	530
40	491	510	521
50	491	511	524
60	491	513	530
80	491	532	539
100	491	548	554

Appendix B

Experimental observations of void fractions

Table B.1: Variation of void fraction with the composition of the particle mixture

Percentage of large Particle in the mixture* [%]	**Volume fraction of large particles at minimum fluidization condition**	**Volume fraction of small particles at minimum fluidization condition**	**Void fraction of the bed minimum fluidization condition**
0	0	0.6	0.4
20	0.13	0.49	0.38
40	0.26	0.38	0.36
50	0.33	0.32	0.35
60	0.40	0.26	0.34
80	0.53	0.13	0.34
100	0.62	0	0.38

Appendix C

Experimental observations of U_{mf} and U_{mb}

Table C.1: Experimental observations of minimum fluidization minimum bubbling velocity variations for particle mixtures

Percentage of large Particle in the mixture* [%]	**Minimum fluidization velocity (experimental)** $[ms^{-1}]$	**Minimum bubbling velocity (experimental)** $[ms^{-1}]$
0	0.025	0.029
20	0.028	0.030
40	0.031	0.032
50	0.039	0.045
60	0.053	0.059
80	0.080	0.083
100	0.153	0.158

Appendix D

Experimental observations of pressure variations along the bed with superficial air velocity

Figure D.1: Pressure variations along the bed with superficial air velocity for 100% small particles

0ml large with 2000ml small particles (Experimental) (0% large)										
Velocity (m/s)	Flow rate (Sl/min)	Pressure at different bed Height from bottom to top (mbar)								
		3.5cm	23.5cm	33.5cm	43.5cm	53.5cm	63.5cm	73.5cm	83.5cm	93.5cm
0.025	6.2	70	41.84	27.78	15.18	1.51	0.09	0.10	0.03	0.02
0.029	7	70.36	44.04	29.03	15.91	1.52	0.08	0.12	0.05	0.06
0.041	10	71.73	45.77	30.99	18.29	4.00	0.10	0.12	0.07	0.06
0.061	15	72.98	47.63	33.53	21.19	7.42	0.15	0.16	0.11	0.10
0.082	20	75.07	50.26	35.97	23.77	10.49	0.43	0.20	0.14	0.13
0.102	25	76.39	52.31	37.86	26.29	12.95	1.75	0.25	0.19	0.19
0.123	30	79.47	55.58	40.97	28.46	14.62	3.73	0.34	0.28	0.29
0.143	35	83.33	57.96	42.15	29.50	15.30	4.87	0.60	0.30	0.29
0.164	40	84.89	60.01	44.63	32.90	18.84	7.86	1.84	0.48	0.44
0.184	45	86.22	63.57	46.07	33.47	19.51	9.59	2.57	0.58	0.43
0.205	50	82.87	61.38	48.14	35.14	22.17	12.30	5.26	1.32	0.57
0.225	55	86.37	66.93	49.64	37.16	24.11	14.72	8.04	2.49	0.86
0.246	60	91.02	65.69	51.12	40.87	27.25	17.02	9.81	3.58	1.68
0.266	65	94.63	78.49	55.61	42.63	29.56	18.85	10.33	5.28	2.93
0.286	70	89.98	72.92	58.74	46.23	31.95	21.74	14.76	7.57	3.83
0.307	75	94.47	74.97	56.44	45.30	31.52	21.55	15.01	7.83	3.69

Figure D.2: Pressure variations along the bed with superficial air velocity for 20% large particles mixture

400ml large with 1600ml small particles (Experimental) (20% large)										
Velocity (m/s)	Flow rate (Sl/min)	Pressure at different bed Height from bottom to top (mbar)								
		3.5cm	23.5cm	33.5cm	43.5cm	53.5cm	63.5cm	73.5cm	83.5cm	93.5cm
0.028	6.8	64.95	40.86	26.43	13.19	0.09	0.05	0.08	0.02	0.01
0.030	7.4	70.23	43.73	28.19	14.24	0.10	0.07	0.08	0.03	0.05
0.041	10	71.84	44.77	29.31	15.57	1.09	0.08	0.09	0.04	0.03
0.061	15	73.24	46.90	31.77	18.56	4.11	0.11	0.11	0.07	0.06
0.082	20	74.51	48.92	33.97	21.21	6.74	0.49	0.15	0.09	0.10
0.102	25	75.93	50.62	36.29	23.97	9.58	0.52	0.17	0.13	0.12
0.123	30	77.33	53.31	38.75	25.84	11.62	1.81	0.23	0.18	0.18
0.143	35	81.60	55.97	41.36	28.72	15.05	3.83	0.39	0.26	0.25
0.164	40	83.43	59.27	43.31	29.96	16.87	6.18	1.48	0.31	0.30
0.184	45	82.63	59.94	45.62	34.69	22.92	10.98	3.61	0.55	0.34
0.205	50	88.61	61.55	46.39	33.57	20.78	12.86	5.44	1.28	0.54
0.225	55	87.94	63.85	49.28	37.27	22.76	14.58	7.58	2.15	0.61
0.246	60	89.71	67.35	51.44	38.81	24.21	17.14	7.97	4.14	1.52
0.266	65	88.65	67.80	53.08	41.72	27.10	20.28	10.54	6.49	4.29
0.286	70	86.61	67.72	53.95	43.06	29.56	21.65	13.56	6.88	4.27
0.307	75	97.75	71.64	55.74	45.32	32.46	25.00	17.97	10.24	6.44

Figure D.3: Pressure variations along the bed with superficial air velocity for 40% large particles mixture

800ml large with 1200ml small particles (Experimental) (40% large)										
Velocity (m/s)	Flow rate (Sl/min)	Pressure at different bed Height from bottom to top (mbar)								
		3.5cm	23.5cm	33.5cm	43.5cm	53.5cm	63.5cm	73.5cm	83.5cm	93.5cm
0.031	7.5	64.71	41.18	25.88	12.52	0.06	0.05	0.06	0.00	0.00
0.032	7.8	68.90	42.97	26.85	13.15	0.07	0.05	0.07	0.01	0.00
0.041	10	71.59	44.43	28.46	14.43	0.17	0.05	0.07	0.02	0.01
0.061	15	73.61	46.08	30.02	16.16	2.29	0.04	0.07	0.01	0.01
0.082	20	74.74	48.07	32.30	18.56	5.36	0.05	0.06	0.01	0.00
0.102	25	76.95	50.35	35.23	22.07	8.14	0.08	0.05	0.02	0.01
0.123	30	78.20	52.05	37.16	24.96	10.97	1.01	0.09	0.02	0.02
0.143	35	80.93	54.78	39.76	26.89	12.00	1.99	0.09	0.03	0.03
0.164	40	82.13	57.72	42.60	29.51	14.71	4.42	0.37	0.03	0.03
0.184	45	84.37	59.32	43.72	31.06	18.27	7.94	1.78	0.04	0.05
0.205	50	87.98	62.61	43.90	30.13	19.92	10.75	4.00	0.42	0.06
0.225	55	87.72	61.58	45.06	34.35	22.74	12.45	5.35	1.03	0.22
0.246	60	88.38	63.68	48.81	40.59	26.41	15.44	8.89	2.76	0.90
0.266	65	85.70	62.35	48.82	42.46	28.31	18.76	10.40	3.81	1.74
0.286	70	89.41	62.65	50.34	46.61	32.93	22.29	15.19	7.15	2.50
0.307	75	88.45	61.85	48.51	45.93	32.48	22.80	17.15	6.61	3.81

Figure D.4: Pressure variations along the bed with superficial air velocity for 50% large particles mixture

1000ml large with 1000ml small particles (Experimental) (50% large)										
Velocity (m/s)	Flow rate (Sl/min)	Pressure at different bed Height from bottom to top (mbar)								
		3.5cm	23.5cm	33.5cm	43.5cm	53.5cm	63.5cm	73.5cm	83.5cm	93.5cm
0.039	9.6	66.80	40.05	24.73	11.51	0.16	0.11	0.14	0.09	0.08
0.045	10.9	72.84	44.73	28.33	13.82	0.17	0.14	0.16	0.11	0.11
0.061	15	74.67	46.59	30.41	15.97	1.56	0.20	0.21	0.16	0.15
0.082	20	76.69	49.16	33.41	19.04	4.02	0.24	0.26	0.21	0.20
0.102	25	78.25	51.11	35.35	22.28	7.24	0.32	0.33	0.27	0.27
0.123	30	79.69	53.07	38.59	24.62	10.31	0.79	0.40	0.35	0.35
0.143	35	80.75	53.87	39.34	27.49	12.81	2.76	0.45	0.40	0.39
0.164	40	83.27	57.60	42.63	31.67	17.19	4.86	0.84	0.54	0.55
0.184	45	87.60	63.14	46.63	33.10	16.84	7.43	1.57	0.68	0.66
0.205	50	89.03	62.50	48.13	32.39	16.06	9.38	2.71	1.06	0.69
0.225	55	86.90	60.23	45.52	35.56	20.48	11.72	4.40	1.37	0.83
0.246	60	86.49	67.15	52.34	36.88	21.52	14.75	6.93	2.72	1.34
0.266	65	89.06	62.70	48.00	39.93	27.77	18.66	10.73	5.58	2.43
0.286	70	90.09	65.00	50.03	42.12	28.21	17.96	11.90	5.17	2.82
0.307	75	90.75	72.22	55.90	42.86	29.58	22.61	11.17	7.91	4.45

Figure D.5: Pressure variations along the bed with superficial air velocity for 60% large particles mixture

1200ml large with 800ml small particles (Experimental) (60% large)										
Velocity (m/s)	Flow rate (Sl/min)	Pressure at different bed Height from bottom to top (mbar)								
		3.5cm	23.5cm	33.5cm	43.5cm	53.5cm	63.5cm	73.5cm	83.5cm	93.5cm
0.053	13	68.90	42.98	26.79	12.57	0.09	0.05	0.06	0.00	0.00
0.059	14.5	71.69	43.97	28.10	13.52	0.09	0.09	0.06	0.00	0.02
0.082	20	75.57	46.96	30.88	16.27	1.22	0.07	0.07	0.00	0.02
0.102	25	76.75	48.41	32.60	18.52	3.48	0.09	0.08	0.02	0.03
0.123	30	78.78	50.02	34.53	21.00	6.40	0.08	0.08	0.02	0.05
0.143	35	80.01	53.30	37.18	23.48	9.01	0.31	0.11	0.04	0.07
0.164	40	82.89	55.36	39.80	25.77	12.00	1.56	0.15	0.04	0.06
0.184	45	84.27	58.26	41.07	27.58	14.48	3.50	0.15	0.06	0.09
0.205	50	83.40	58.53	41.44	30.66	17.12	5.75	0.50	0.07	0.08
0.225	55	87.87	62.53	46.70	32.87	18.07	7.81	1.39	0.28	0.13
0.246	60	87.68	63.62	51.23	38.39	22.09	11.63	4.18	0.72	0.22
0.266	65	82.81	55.11	40.68	38.16	25.90	14.02	7.79	0.69	0.12
0.286	70	89.69	64.38	46.36	39.59	29.56	18.90	12.82	3.71	1.60
0.307	75	92.69	69.10	53.74	42.92	29.65	19.58	10.59	4.55	1.94

Figure D.6: Pressure variations along the bed with superficial air velocity for 80% large particles mixture

1600ml large with 400ml small particles (Experimental) (80% large)										
Velocity (m/s)	Flow rate (Sl/min)	Pressure at different bed Height from bottom to top (mbar)								
		3.5cm	23.5cm	33.5cm	43.5cm	53.5cm	63.5cm	73.5cm	83.5cm	93.5cm
0.080	19.5	66.34	42.15	27.74	14.30	0.56	0.11	0.13	0.04	0.08
0.083	20.3	73.58	45.57	28.45	14.72	0.66	0.13	0.12	0.05	0.08
0.102	25	75.27	46.60	30.89	17.31	2.72	0.17	0.16	0.09	0.14
0.123	30	75.31	47.71	32.32	18.40	4.31	0.18	0.18	0.10	0.15
0.143	35	77.54	49.51	34.56	21.73	7.12	0.25	0.25	0.18	0.21
0.164	40	80.41	53.09	36.78	23.61	9.01	0.43	0.30	0.22	0.26
0.184	45	80.94	54.22	39.68	27.18	13.44	2.75	0.34	0.25	0.29
0.205	50	84.41	59.34	45.05	33.78	16.28	5.16	0.40	0.30	0.35
0.225	55	86.51	60.50	42.64	29.99	18.49	8.20	1.68	0.37	0.41
0.246	60	88.88	64.93	49.61	36.36	20.33	9.45	2.91	0.56	0.52
0.266	65	86.97	62.26	47.15	38.22	23.65	12.19	5.15	1.12	0.53
0.286	70	85.89	61.33	44.41	37.21	27.64	16.11	8.44	3.25	0.91
0.307	75	86.22	61.73	45.42	34.14	28.89	19.87	12.75	5.80	2.43

Figure D.7: Pressure variations along the bed with superficial air velocity for 100% large particles mixture (Experimental)

2000ml large with 0ml small particles (Experimental) (100% large)										
Velocity (m/s)	Flow rate (Sl/min)	Pressure at different bed Height from bottom to top (mbar)								
		3.5cm	23.5cm	33.5cm	43.5cm	53.5cm	63.5cm	73.5cm	83.5cm	93.5cm
0.153	37.5	72.56	46.23	30.75	17.09	2.35	0.24	0.24	0.13	0.20
0.158	38.5	74.86	47.29	31.53	18.02	3.20	0.26	0.26	0.16	0.22
0.164	40	75.15	47.60	31.65	18.13	3.37	0.27	0.26	0.17	0.23
0.184	45	76.91	49.29	33.02	19.88	5.30	0.29	0.30	0.21	0.27
0.205	50	78.38	51.58	35.74	22.52	8.12	0.38	0.36	0.26	0.33
0.225	55	79.47	52.75	37.51	24.77	11.38	1.16	0.41	0.32	0.37
0.246	60	80.91	55.76	39.54	28.57	15.63	4.81	0.50	0.39	0.46
0.266	65	86.15	62.32	46.33	31.15	16.11	5.96	1.76	0.43	0.50
0.286	70	85.08	63.48	47.60	32.48	16.95	7.09	2.17	0.64	0.58
0.307	75	92.95	68.98	50.34	34.30	17.78	6.75	1.87	0.60	0.61

Appendix E

Computational observations of pressure variations along the bed with superficial air velocity

Figure E.1: Pressure variations along the bed with superficial air velocity for 100% small particles mixture (computational)

0ml large with 2000ml small particles (Computational) (0% large)										
Velocity (m/s)	Flow rate (Sl/min)	Pressure at different bed Height from bottom to top (mbar)								
		3.5cm	23.5cm	33.5cm	43.5cm	53.5cm	63.5cm	73.5cm	83.5cm	93.5cm
0.025	6.2	74.99	44.17	28.99	13.37	0.00	0.00	0.00	0.00	0.00
0.029	7	74.99	44.16	28.97	13.33	0.00	0.00	0.00	0.00	0.00
0.041	10	75.28	46.25	31.95	17.20	2.91	0.00	0.00	0.00	0.00
0.061	15	75.68	49.51	36.62	23.46	10.51	0.00	0.00	0.00	0.00
0.082	20	75.70	51.40	39.33	26.85	14.71	2.90	0.00	0.00	0.00
0.102	25	75.68	52.09	40.03	27.76	16.38	5.65	0.00	0.00	0.00
0.143	35	75.29	52.66	41.37	30.47	19.97	10.09	1.08	0.00	0.00
0.184	45	74.98	53.30	42.32	31.27	21.86	12.14	4.00	0.00	0.00
0.225	55	75.11	54.81	45.00	34.79	24.06	15.16	7.21	1.40	0.00
0.266	65	74.97	54.35	46.63	35.23	25.90	17.37	9.46	3.54	0.10
0.307	75	75.59	55.68	46.82	37.06	27.97	17.62	10.28	4.79	0.54

Figure E.2: Pressure variations along the bed with superficial air velocity for 20% large particles mixture (computational)

400ml large with 1600ml small particles (Computational) (20% large)										
Velocity (m/s)	Flow rate (Sl/min)	Pressure at different bed Height from bottom to top (mbar)								
		3.5cm	23.5cm	33.5cm	43.5cm	53.5cm	63.5cm	73.5cm	83.5cm	93.5cm
0.028	6.8	75.33	42.72	26.67	10.14	0.00	0.00	0.00	0.00	0.00
0.03	7.4	75.32	42.72	26.67	10.13	0.00	0.00	0.00	0.00	0.00
0.041	10	75.52	44.74	29.62	14.06	0.00	0.00	0.00	0.00	0.00
0.061	15	75.82	47.94	34.11	19.84	6.20	0.00	0.00	0.00	0.00
0.082	20	76.08	49.99	37.01	24.00	10.94	0.00	0.00	0.00	0.00
0.102	25	76.07	51.56	38.91	26.31	13.89	2.09	0.00	0.00	0.00
0.143	35	75.79	52.61	40.58	28.41	17.00	5.47	0.00	0.00	0.00
0.184	45	76.23	53.45	42.21	30.93	19.92	9.07	0.56	0.00	0.00
0.225	55	75.93	54.22	43.74	33.74	22.88	12.46	3.62	0.01	0.00
0.266	65	75.72	54.76	45.23	34.58	23.92	14.71	5.33	0.11	0.00
0.307	75	75.77	55.79	45.76	36.13	26.58	16.75	8.84	2.41	0.00

Figure E.3: Pressure variations along the bed with superficial air velocity for 40% large particles mixture (computational)

800ml large with 1200ml small particles (Computational) (40% large)										
Velocity (m/s)	Flow rate (Sl/min)	Pressure at different bed Height from bottom to top (mbar)								
		3.5cm	23.5cm	33.5cm	43.5cm	53.5cm	63.5cm	73.5cm	83.5cm	93.5cm
0.031	6.8	76.18	42.27	25.58	8.39	0.00	0.00	0.00	0.00	0.00
0.032	7	76.21	42.32	25.65	8.46	0.00	0.00	0.00	0.00	0.00
0.041	10	76.38	43.56	27.36	10.68	0.00	0.00	0.00	0.00	0.00
0.061	15	76.43	45.98	30.01	14.65	0.83	0.00	0.00	0.00	0.00
0.082	20	76.99	48.63	34.41	19.35	5.09	0.00	0.00	0.00	0.00
0.102	25	76.48	49.56	36.32	22.43	8.65	0.00	0.00	0.00	0.00
0.143	35	76.37	51.00	38.52	25.38	12.67	1.04	0.00	0.00	0.00
0.184	45	75.94	52.30	40.12	27.84	15.99	4.53	0.00	0.00	0.00
0.225	55	76.38	53.98	42.18	29.70	18.66	7.17	0.12	0.00	0.00
0.266	65	76.60	54.62	43.75	32.07	21.05	10.71	2.35	0.00	0.00
0.307	75	77.03	55.43	44.46	34.02	24.43	13.25	3.87	0.08	0.00

Figure E.4: Pressure variations along the bed with superficial air velocity for 50% large particles mixture (computational)

1000ml large with 1000ml small particles (Computational) (50% large)										
Velocity (m/s)	Flow rate (Sl/min)	Pressure at different bed Height from bottom to top (mbar)								
		3.5cm	23.5cm	33.5cm	43.5cm	53.5cm	63.5cm	73.5cm	83.5cm	93.5cm
0.039	7	77.38	43.34	26.56	9.21	0.00	0.00	0.00	0.00	0.00
0.045	10	77.50	44.00	27.38	10.18	0.00	0.00	0.00	0.00	0.00
0.061	15	78.23	46.34	30.35	13.63	0.00	0.00	0.00	0.00	0.00
0.082	20	78.18	48.02	32.87	15.12	1.80	0.00	0.00	0.00	0.00
0.102	25	78.14	49.62	35.46	20.46	6.17	0.00	0.00	0.00	0.00
0.143	35	76.37	51.00	38.60	25.46	12.67	1.04	0.00	0.00	0.00
0.184	45	76.86	52.21	39.77	26.55	13.80	2.55	0.00	0.00	0.00
0.225	55	76.93	53.24	41.58	29.12	16.79	5.67	0.00	0.00	0.00
0.266	65	77.00	54.25	43.51	31.86	19.89	8.50	0.96	0.00	0.00
0.307	75	76.98	55.55	44.09	33.44	23.11	12.64	3.78	0.01	0.00

Figure E.5: Pressure variations along the bed with superficial air velocity for 60% large particles mixture (computational)

1200ml large with 800ml small particles (Computational) (60% large)										
Velocity (m/s)	Flow rate (Sl/min)	Pressure at different bed Height from bottom to top (mbar)								
		3.5cm	23.5cm	33.5cm	43.5cm	53.5cm	63.5cm	73.5cm	83.5cm	93.5cm
0.053	10	77.97	44.41	27.66	10.18	0.00	0.00	0.00	0.00	0.00
0.059	15	78.33	44.94	28.25	10.97	0.00	0.00	0.00	0.00	0.00
0.082	20	79.35	46.86	30.30	13.28	0.01	0.00	0.00	0.00	0.00
0.102	25	78.90	48.35	32.82	17.02	2.13	0.00	0.00	0.00	0.00
0.143	35	78.34	50.54	35.95	20.83	7.61	0.00	0.00	0.00	0.00
0.184	45	77.50	51.24	37.98	24.84	11.97	0.86	0.00	0.00	0.00
0.225	55	76.83	51.96	39.80	27.15	14.64	3.55	0.00	0.00	0.00
0.266	65	76.96	53.34	41.58	29.35	18.25	6.90	0.22	0.00	0.00
0.307	75	77.32	54.78	43.16	31.16	20.62	9.44	1.39	0.00	0.00

Figure E.6: Pressure variations along the bed with superficial air velocity for 80% large particles mixture (computational)

1600ml large with 400ml small particles (Computational) (80% large)										
Velocity (m/s)	Flow rate (Sl/min)	Pressure at different bed Height from bottom to top (mbar)								
		3.5cm	23.5cm	33.5cm	43.5cm	53.5cm	63.5cm	73.5cm	83.5cm	93.5cm
0.080	10	73.86	40.15	23.44	6.03	0.00	0.00	0.00	0.00	0.00
0.102	15	74.29	40.78	24.64	8.51	0.00	0.00	0.00	0.00	0.00
0.143	20	75.10	43.21	27.65	11.83	0.02	0.00	0.00	0.00	0.00
0.184	25	74.65	45.32	30.80	15.30	2.44	0.00	0.00	0.00	0.00
0.225	35	73.62	45.05	31.46	17.91	4.78	0.00	0.00	0.00	0.00
0.266	45	73.78	46.71	33.70	21.01	8.36	0.20	0.00	0.00	0.00
0.307	55	73.56	47.84	35.13	22.36	10.39	1.19	0.00	0.00	0.00

Figure E.7: Pressure variations along the bed with superficial air velocity for 100% large particles mixture (computational)

2000ml large with 0ml small particles (Computational) (100% large)										
Velocity (m/s)	Flow rate (Sl/min)	Pressure at different bed Height from bottom to top (mbar)								
		3.5cm	23.5cm	33.5cm	43.5cm	53.5cm	63.5cm	73.5cm	83.5cm	93.5cm
0.153	20	79.89	47.24	31.19	14.66	0.03	0.00	0.00	0.00	0.00
0.184	25	80.00	47.39	31.32	14.77	0.02	0.00	0.00	0.00	0.00
0.225	35	80.40	48.16	32.51	16.72	1.88	0.00	0.00	0.00	0.00
0.266	45	79.60	47.79	32.37	17.01	3.01	0.00	0.00	0.00	0.00
0.307	55	79.81	49.95	35.21	20.38	6.65	0.00	0.00	0.00	0.00

Appendix F

Comparison of experimental and computational pressure variations along the bed

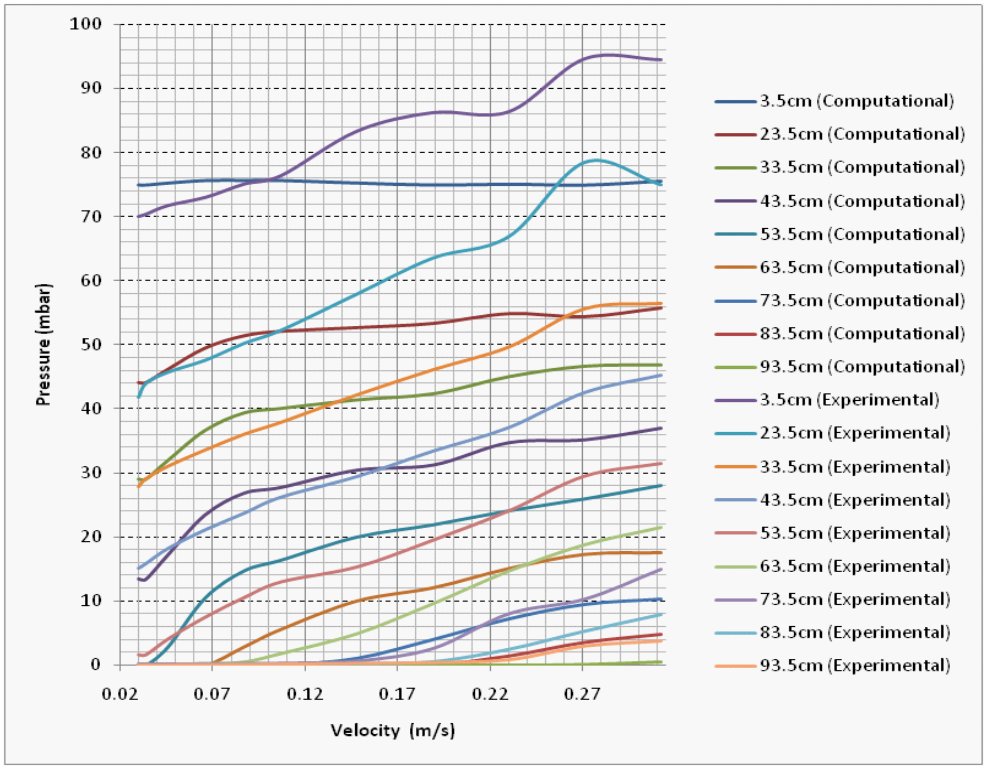

Comparison of experimental and computational pressure variations along the bed with superficial air velocity 100% small particles

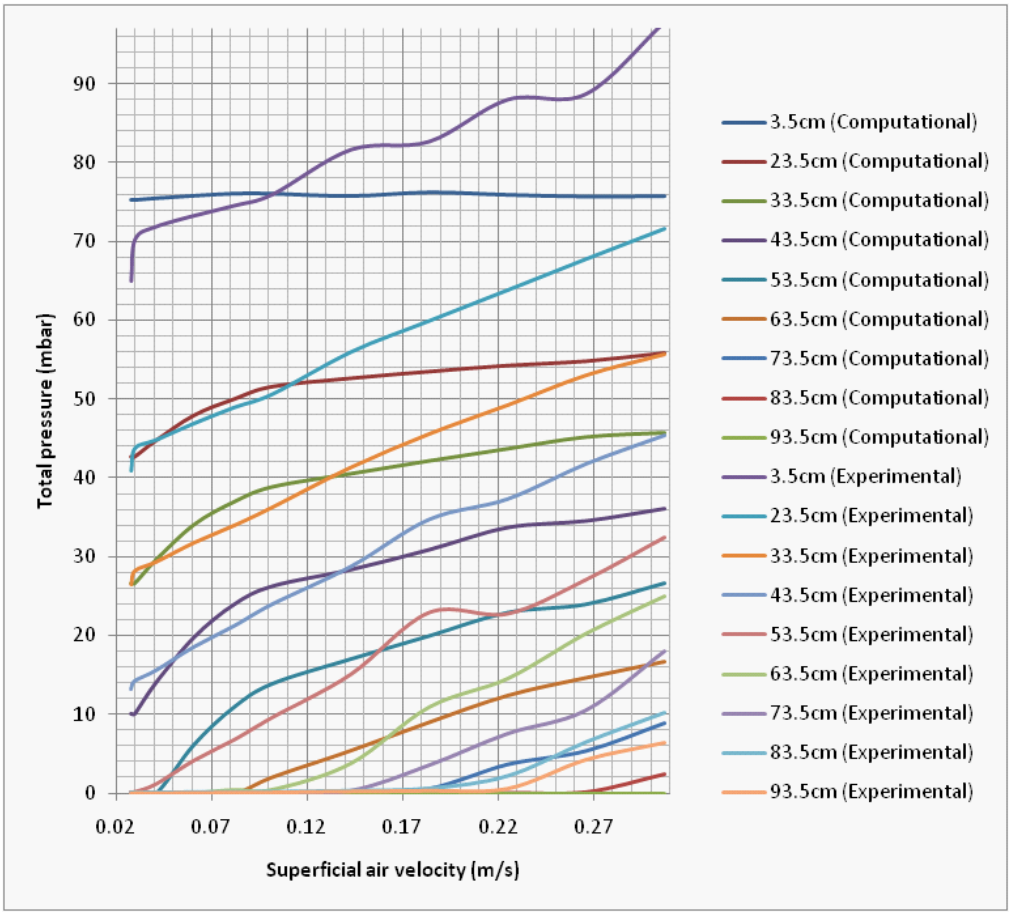

Figure F.1: Comparison of experimental and computational pressure variations along the bed with superficial air velocity 20% large particles

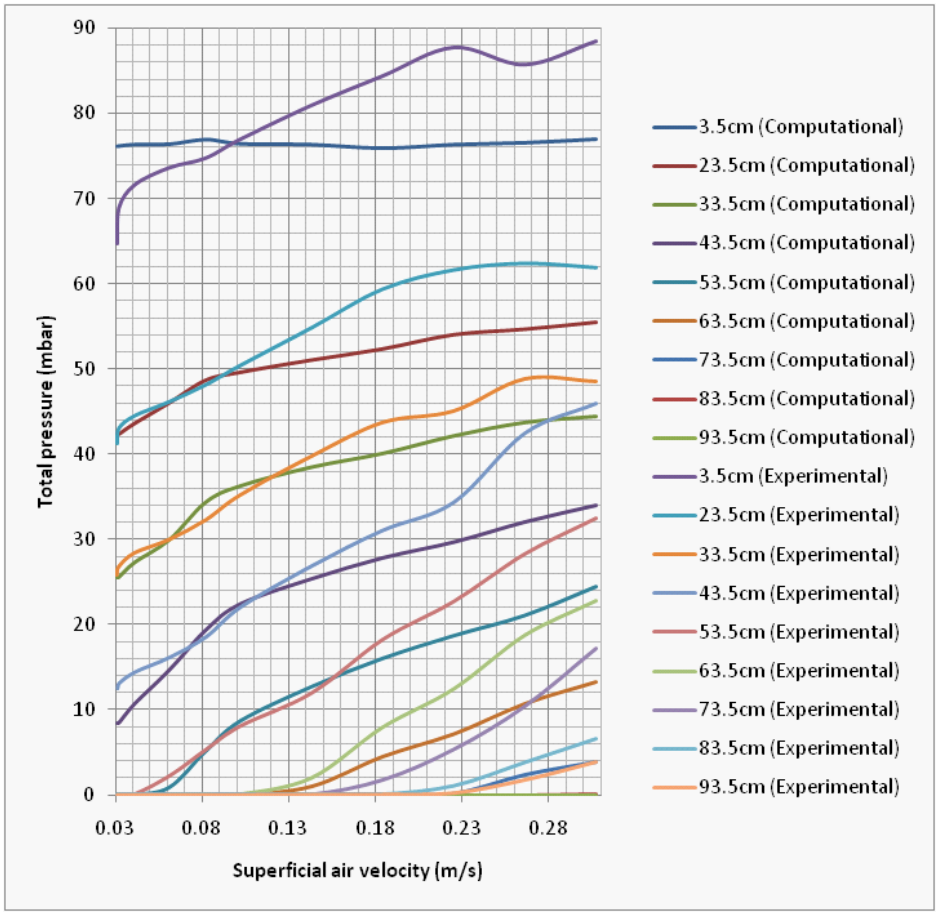

Figure F.2: Comparison of experimental and computational pressure variations along the bed with superficial air velocity 40% large particles

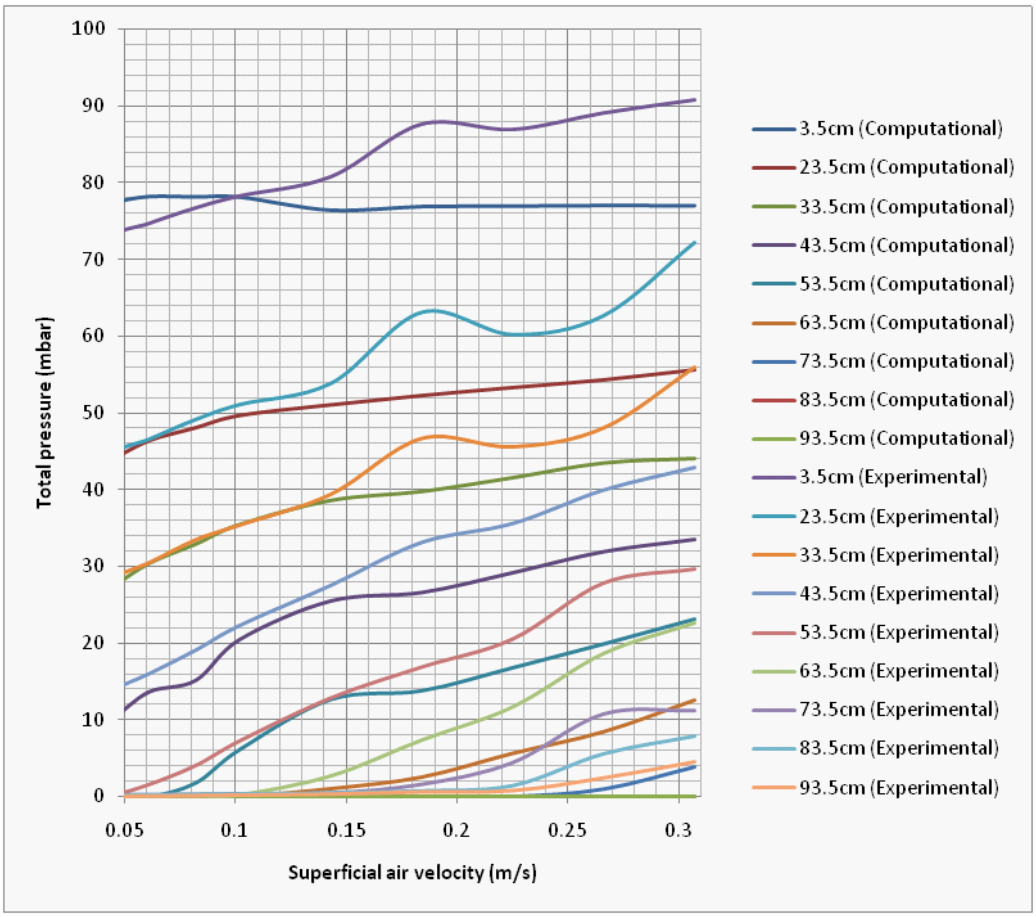

Figure F.3: Comparison of experimental and computational pressure variations along the bed with superficial air velocity 50% large particles

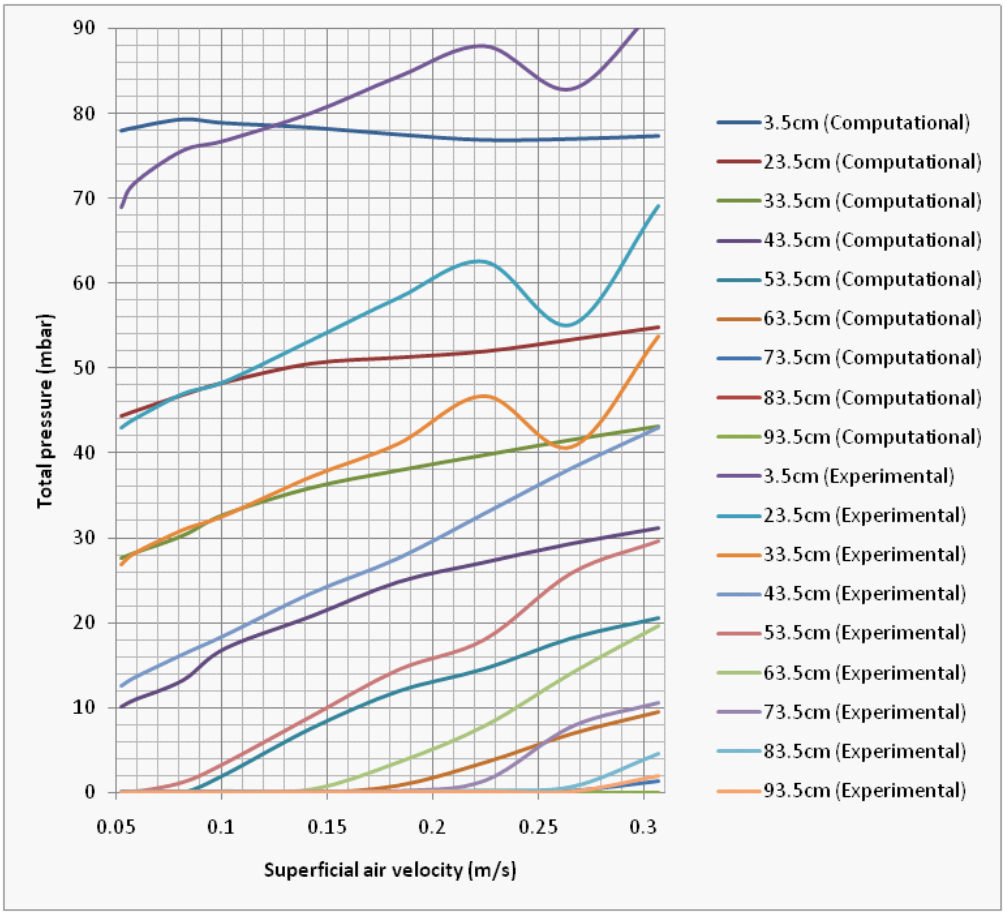

Figure F.4: Comparison of experimental and computational pressure variations along the bed with superficial air velocity 60% large particles

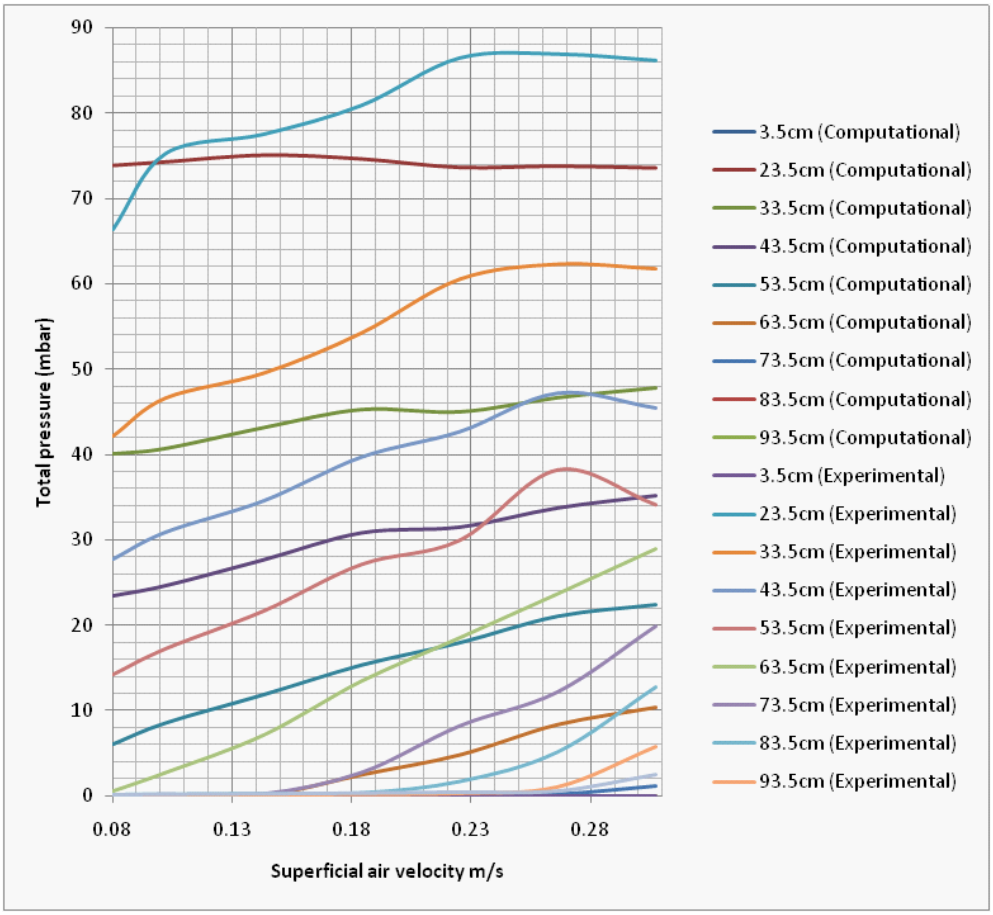

Figure F.5: Comparison of experimental and computational pressure variations along the bed with superficial air velocity 80% large particles

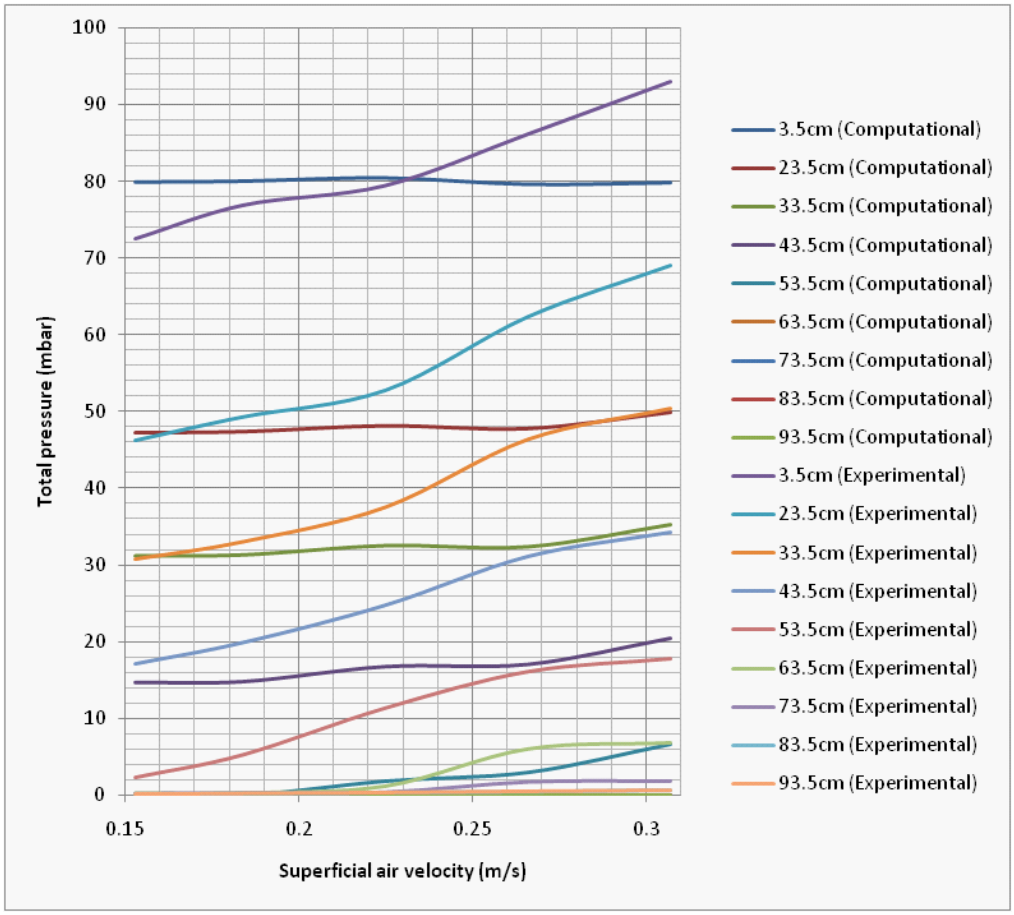

Figure F.6: Comparison of experimental and computational pressure variations along the bed with superficial air velocity 100% large particles

Appendix G

Particle size distribution

The particles have the size range 100˜200 μm (small particles) and 400˜600 μm (large particles). Particle size distribution of each particle samples are shown in the Table G.1 and the Table G.2. S. Ariyarathna et al performed and experiment to analyze the particle size distribution for several particle samples. The mean sizes of the particles for each sieve and the weight of the particles on each sieve are analyzed in order to get the mean particle diameter of the particle group.

Table G.1: Particle size distribution for small particles [29]

100˜200 [μm] **(small)**	
Average Screen size [μm]	**Mass on the screens** [g]
40	0.09
84.5	9.44
128	42.17
175	46.16
225	2.12
300	0.01

Table G.2: Particle size distribution for large particles [29]

400˜600 μm **(Large)**	
Average Screen size [μm]	**Mass on the screens** [g]
200	0.35
327.5	2.45
390	22.56
462.5	47.68
565	26.77
700	0.31

Appendix H

Calculations of Umf

In this study the analytical method has used in order to calculate the minimum fluidization velocities of the above mentioned particle groups. Those two groups are introduced as small and large. Densities of the glass particles and gas are known as $2485kg/m^3$ and $1.2kg/m^3$ respectively. And the viscosity of gas is known as $1.8 * 10^{-5}Pa.s$.

H.1 For small particles

Particle mean diameter = 154 μm

Using the Eq. 2.9 ;

$$U_{mf} = \frac{\left(154 \cdot 10^{-6}\right)^2 \cdot (2485 - 1.2) \cdot 9.81}{1650 \cdot 1.8 \cdot 10^{-5}} = 1.9 \times 10^{-2} ms^{-1} \tag{H.1}$$

Have to check whether the Reynolds number of the flow is in the required value region in order to be able to use Eq. 2.9 for calculating the minimum fluidization velocity.

$$\mathrm{Re} = \frac{\rho \cdot U \cdot d}{\mu} = \frac{1.2 \cdot 1.95 \times 10^{-2} \cdot 154 \cdot 10^{-6}}{1.8 \cdot 10^{-5}} = 0.195 \tag{H.2}$$

Re, number has a value which is well bellow the limit.

$\therefore$ The theoretical $U_{mf} = 1.9 \times 10^{-2} ms^{-1}$

H.2 For large size particles

Particle mean diameter = 488 μm

Using the Eq. 2.9 ;

$$U_{mf} = \frac{\left(488 \cdot 10^{-6}\right)^2 \cdot (2485 - 1.2) \cdot 9.81}{1650 \cdot 1.8 \cdot 10^{-5}} = 0.195 ms^{-1} \tag{H.3}$$

Have to check whether the Reynolds number of the flow is in the required value region in order to be able to use Eq. 2.9 for calculating the minimum fluidization velocity.

$$\mathrm{Re} = \frac{\rho \cdot U \cdot d}{\mu} = \frac{1.2 \cdot 0.195 \cdot 488 \cdot 10^{-6}}{1.8 \cdot 10^{-5}} = 6.2013 \tag{H.4}$$

Re, number has a value which is well bellow the limit.
$\therefore$ The theoretical $U_{mf} = 0.192\,19 ms^{-1}$

Appendix I

Observations of excess air velocity

Table I.1: Excess air velocity for each particle samples when the computational auperficial air velocity is 0.307 m/s

Large particle percentage [%]	**Minimum fluidization velocity (simulations)**$[m/s]$	**Excess air velocity** $[m/s]$
0	0.05	0.257
20	0.05	0.257
50	0.055	0.252
60	0.06	0.247
80	0.075	0.232
100	0.255	0.052

EXPERIMENTAL AND COMPUTATIONAL STUDY OF PARTICLE MINIMUM FLUIDIZATION VELOCITY AND BED EXPANSION IN A BUBBLING FLUIDIZED BED

Chameera K. Jayarathna[1], Britt M. Halvorsen[1,2]

[1] Telemark University College, Porsgrunn, Norway
[2]Telemark Technological R&D Centre, Porsgrunn, Norway

chameera80@yahoo.com (Chameera Jayarathna)

ABSTRACT

The aim of this work is to study flow behavior in a fluidized bed with different mixtures of particles. The efficiency of fluidized bed reactors depends on bubble distribution, bubble size and bubble velocity within the reactor. The bubble behavior depends on the amount of excess air introduced to the reactor. Experiments are performed in a cylindrical bed with a uniform air distribution. Spherical glass particles with different mixtures of particles are used in the experiments. The minimum fluidization velocity and the bed expansion are observed for two different powders and mixtures of the powders. Corresponding simulations are performed by using the commercial CFD code Fluent 6.3. The computational results are compared to the experimental data and the discrepancies are discussed.

1 INTRODUCTION

Fluidized beds are widely used in industrial operations. Good mixing and large contact area between phases, enhances chemical reactions, heat transfer and mass transfer. Fluidized beds have the ability to operate smoothly because of a liquid like behavior of particles. In a well mixed bed, isothermal conditions are obtained and hence the operation can be controlled simply and consistently. Fluidized bed is used in chemical industry in two main types of reactions, in catalytic gas phase reactions where the particles influence on the reaction velocity without being consumed, and in gas-particle reactions. Pure silicon is needed in the production of solar cells and a gas-particle reaction in a fluidized bed can be used in one term of the purification process. The fluidized bed replaces the highly energy consuming process term that is commonly used today. The gas-particle reaction is a continuous process where the particles are fully consumed during the reaction and the particles in the reactor have large range of particle sizes. In a reactor like this, the temperature becomes very high, and it is extremely important to keep the particles fluidized and well mixed.

Fluidization and bubble formation depend very much on the particle characteristics.The behaviour of particles in fluidized beds depends on a combination of the particle size and density. Geldart fluidization diagram [1] is used to identify characteristics associated with fluidization of powders. Powders characterized within Group A are easily fluidized and give a high bed expansion before bubbles appear.

This type of powders has the most desirable properties for fluidization, and is mostly used as catalyst in fluidization system. For group B particles the bed expansion is low, and bubbles will appear as soon as the gas velocity reaches the minimum fluidization velocity [2]. The Geldart diagram is based on mean particle diameters, but earlier studies have shown that powders with a range of particle sizes cannot be characterized from the mean diameter only [3, 4, 5, 6]. The fluidization properties are highly influenced of the bulk density, and the bulk density change with the particle distribution. The bubble behavior depends on the amount of excess air introduced to the reactor. The excess air is the actual superficial velocity minus the minimum fluidization velocity. The excess air is also defined as the air leaving the bed with the bubbles.

The amount of excess air should be sufficient to give a good mixing of the bed. In this work the minimum fluidization velocities for different mixtures of particles are studied.

2 COMPUTATIONAL MODEL

Two dimensional computational studies have been performed on the fluidized bed. The simulations are performed by using the commercial CFD code Fluent 6.3. The model is based on an Eulerian description of the gas and the particle phases. The combinations of models used in this work are presented in Table 1. Jayaratna et al. [7] did a computational studied of the influence of particle size distribution on flow behavior in fluidized beds, and by studying different combinations of models they concluded that this combination give the most realistic flow behavior.

Drag model	Syamlal&O'Brien
Granular viscosity	Syamlal&O'Brien
Granular bulk viscosity	Constant
Frictional viscosity	Schaeffer
Frictional pressure	Based-ktgf
Solid pressure	Ma-ahmadi
Radial distribution function	Ma-ahmadi

Table 1: Recommended combination of models [7]

The Syamlal &O'Brien drag model is used to express the solid-gas interaction. The Syamlal & O'Brien drag model is expressed in Eq (1) [8]:

$$\Phi_{sg} = C_D \frac{3\varepsilon_s \varepsilon_g \rho_g \left|\vec{U}_g - \vec{U}_s\right|}{4 v_r^{\,2} d_s} \tag{1}$$

where ε_g and ε_s are the gas and solid fractions, ρ_g is the gas density, U_g and U_s are the gas and solid velocities and d_s is the particle diameter. The terminal velocity correlation for the solid phase, v_r, is a function of void fraction and Reynolds number [9]. In Eq. (2) the drag factor is expressed [10]:

$$C_D = \left(0.63 + \frac{4.8}{\sqrt{\mathrm{Re}_s / v_r}}\right)^2 \tag{2}$$

The granular viscosity includes a collisional and a kinetic viscosity term. The collisional term is given in Eq (3):

$$\mu_{s,kin} = \frac{\varepsilon_s d_s \rho_s \sqrt{\Theta_s \pi}}{6(3e_{ss} - 1)} \left[1 + \frac{2}{5}(1 - e_{ss})(3e_{ss} - 1)\varepsilon_s g_{0,ss}\right] \tag{3}$$

and in Eq (4) the collisional term is presented:

$$\mu_{col} = \frac{4}{5}\varepsilon_s d_s \rho_s g_{0,ss}(1 + e_{ss})\sqrt{\frac{\Theta_s}{\pi}} \tag{4}$$

where d_s e_s and Θ_s are the particle diameter, elasticity coefficient and the granular temperature of solid phase s respectively. The radial distribution function is presented by $g_{0,ss}$. The radial distribution function included in the Syamlal-O'Brien-symmetric equation is expressed by Ma and Ahmadi [11].

The minimum fluidization velocity can be developed from the buoyant-equals-drag balance. The relation is expressed in Eq. (5)

$$(1 - \varepsilon_g)(\rho_s - \rho_g)g = \frac{\Phi_{sg}}{\varepsilon_g}(u_g - u_s) \tag{5}$$

where the drag coefficient is developed by Syamlal&O'Brien. Eq (6) express the equation for minimum fluidization velocity [12]:

$$U_{mf} = \frac{\varepsilon_{mf}^{\,2}(1 - \varepsilon_{mf})(\rho_s - \rho_g)g}{\Phi_{sg}} \tag{6}$$

Two particle phases are included in the simulations of mixtures. Syamlal-O'Brien-symmetric, is used to express the particle-particle momentum exchange [13].

3 EXPERIMENTAL & COMPUTATIONAL SET-UP

Experiments and corresponding simulations are performed. The set-up is given in this chapter.

3.1 Experimental set up

A lab-scale fluidized bed with a uniform air distribution is constructed. The bed is cylindrical and is made of Lexan glass. The diameter and the height of the bed are 0.072 and 1.4 m respectively. The experimental rig is shown in Figure. 1. The gas flow rate is controlled by a pressure reduction valve, and measured by a digital flow meter. The pressure can be measured at eight positions in the bed.

Glass particles with two different mean particle sizes are used in this study. The particles have the size range 100~200 μm (small particles) and 400~600 μm (large particles).

The particle density is 2485 kg/m^3. The bed and particle parameters are presented in Table. 2.

Experiments have been performed with 100% small particles, 100% large particles and mixtures of small particles with 20, 40, 50, 60 and 80% of large particles. The aim is to study how the different fractions of particle sizes influence on the minimum fluidization velocity and the bed expansion. Before the experiments with the mixtures started, the powders were well mixed and 2 liter of a compact mixture was weighted and filled into the bed. The void fractions at start and at minimum fluidization were calculated based on the weight and the volume.

Bed design			
Height Diameter		1.4 m 0.072 m	
Particles (Spherical glass)			
Density		2485 kg/m^3	
Powder, particle range	100~200 µm (small)	400~600 µm (medium)	Mixture
Mean particle size (µm)	154	488	
% large particles			20, 40, 50, 60, 80

Table. 2: Experimental data

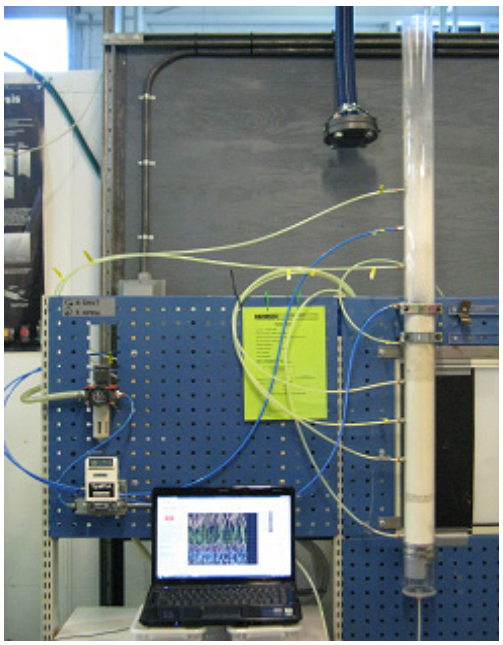

Figure. 1 Experimental set-up

3.2 Computational set-up

The simulations are performed with particles with diameters equal to the mean diameters of the glass powders used in the experiments. The simulations of the mixtures are performed with two particle phases. The data are given in Table. 3. Two particle sizes are used to simulate the mixtures of two powders with different mean particle size. The simulations are run with the same velocities and initial bed heights as in the experiments. Two-dimensional Cartesian co-ordinate system is used to describe the geometry. The dimensions of the computational bed are width 0.072 m and height 1.2 m. A grid resolution test is performed to find a suitable grid size. The grid is uniform and the size of a cell is 3x3 mm. The simulations have been run for 7 seconds. The simulations have been run with different gas flow rates, starting with low flow rates to determine the minimum fluidization velocities.

Simulation no.	% small particles. Mean diameter 153 µm	% large particles. Mean diameter 488 µm
1	100	0
2	80	20
3	60	40
4	50	50
5	40	60
6	20	80
7	0	100

Table. 3: Simulation martrix

4 RESULTS

This chapter presents the experimental bed expansion and the comparison of the experimental and computational minimum fluidization velocities.

4.1 Bed expansion

The bed expansion has been measured in the experimental rig for 100% small particles, 100% large particles and 5 different mixtures of small and large particles. The small particles have a mean diameter of 154 µm, and according to Geldarts characterization diagram, the particles are characterized as Group B particles, but very close to Group A particles. Due to inter-particle forces, Group A particles expand significantly before bubbles appear.

Inter-particle forces are due to wetness, electrostatic charges and Van der Waals forces. For Group B particles the inter-particle forces are neglectible, and the bed expansion is at minimum fluidization velocity is rather low [2]. The small particles have a range of particle sizes from 100-200 μm.

The bed height as a function of fraction of large particles is shown in Figure. 2. The curves present the initial bed height and the bed height at minimum fluidization. Initially two liters of well mixed and maximum packed particles are filled into the experimental rig. This corresponds to a initial bed height of 491 mm as plotted with a dotted line. During the filling, the powder expanded, and the initial height of the bed therefore varies with the concentration of small and large particles. The initial bed height is 540 mm for 100% small particles and decreases to about 510 mm for mixtures with 40, 50 and 60% large particles, and increases to 548 mm for 100% large particles. The difference between maximum packed powder and bed height after filling are significant for all the mixtures, about 50, 20 and 60 mm for 100% small, 40-60% large and 100% large respectively. For the small particles this is due to the inter-particle forces as described above. The large particles are getting random packed during the filling, and the void fraction increases compared to maximum packing. In the mixtures, the properties of small and large particles influence on each other. The large particles settle and is randomly packed, and the small particles fill the spaces between the large particles.

The bed expansion for the small particles at minimum fluidization velocity is about 20 mm. About the same bed expansion is also observed for the mixtures with 20, 40, 50 and 60% large particles. This indicates that the fluidization properties in a fluidized bed reactor are significantly influenced of the smallest particles in the mixture. The bed expansion for 80 and 100% large particles is about 6 mm. This is a rather low bed expansion, which is typical for Group B particles.

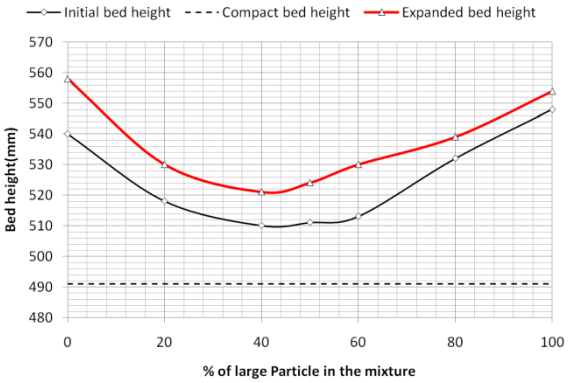

Figure. 2 Bed height as a function of particle mixtures.

4.2 Minimum fluidization velocity

Experiments are performed to study the minimum fluidization velocities for different mixtures of small and large particles. Corresponding studies have earlier been performed with mixtures of 50% small and large particles which showed that the flow behavior is influenced of the smallest particles in the mixture [14]. The aim of this work is to study the flow behavior for the whole range of mixtures. The experiments are performed by starting with low velocities and increase the velocity until the minimum fluidization velocity is obtained and the powder starts to float. Corresponding simulations were performed, starting with the minimum fluidization velocities determined in the experiments. The comparison between the experimental and computational results is presented in Figure. 3.

The experimental minimum fluidization velocity is about 0.025 m/s for 100% small particles and 0.15 m/s for large particles. For the mixtures the minimum fluidization velocities increase from 0.027 to 0.039 m/s when the fraction of large particles is increased from 20 to 50%. The minimum fluidization velocities are 0.05 and 0.08m/s for the mixtures with 60 and 80% large particles. The minimum fluidization velocity is almost doubled when the fraction of large particles are increased from 80 to 100% large particles. This shows that the smallest particles in the mixture influence strongly on the fluidization behavior.

The results from the simulations show the same tendency as the experimental results. The minimum fluidization velocity for 100% small particles is 0.05 m/s.

When the fraction of large particles are changed from 0 to 40% no change in minimum fluidization velocity are observed. The minimum fluidization velocity increases slightly when the volume fraction of large particles is increased from 40 to 80%. The computational minimum fluidization velocities are 0.055, 0.06 and 0.075 for 50, 60 and 80% large particle mixtures respectively. The simulation with 100% large particles gives a minimum fluidization velocity of 0.255 m/s. This is more than three times the fluidization velocity observed for the mixture with 80% large particles.

The comparison between the experimental and computational results shows that the minimum fluidization velocities are strongly influenced of the smallest particles in the mixture. The computational minimum fluidization velocity is about double of the experimental fluidization velocity for small particles and mixtures with low concentrations of large particles. For the mixture with 50% large particles the deviation is smaller, and for the 60 and 80% mixtures the deviation between experimental and computational results are less than 10%. The difference between the experimental and computational minimum fluidization velocity is significant for the large particles.

The large deviation between the simulations and experiments for 100% small and 100% large particles can be explained by the difference in particle distribution. The small and the large particles used in the experiments are not mono sized particles but powders with a particle range of 100-200 µm and 400-600 µm respectively. This means that in the experiments many particle sizes are included, and this influence on the fluidization properties. In the simulations with 100%small and 100%large particles, the bed contains of mono sized particles, and this influence on the void fractions, packing of the bed and thereby on the fluidization properties. The minimum void fraction is significantly higher for mono sized particles than for a mixture of particle sizes. Higher void fraction in the bed requires a higher gas velocity to get the particles fluidized. To get a better agreement between simulations and experiments for the small and large particles, the simulations for these cases can be run with multiple particle phases to give a particle size distribution that corresponds to the experimental powder.

More than two particle phases can also be included in the simulations of the mixtures.

The deviation between the computational and experimental results may also partly be due to that the simulations are performed in a two dimensional system.

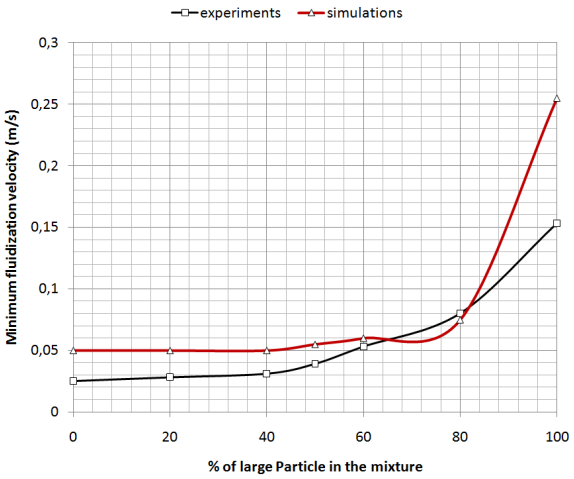

Figure. 3 Experimental and computational minimum fluidization

5 CONCLUSION

The efficiency of fluidized bed reactors depends on bubble distribution, bubble size and bubble velocity within the reactor. The bubble behavior depends on the amount of excess air introduced to the reactor. Excess air is the actual gas velocity minus the minimum fluidization velocity. The minimum fluidization velocities for different mixtures of particles are studied. A series of experiments are and simulations are performed. Experiments are performed in a cylindrical bed with a uniform air distribution. Different mixtures of spherical glass particles with mean diameter of 154 µm (small particles) and 488 µm (large particles) and mixtures of the small and the large particles are used in the experiments. Corresponding simulations are performed by using the commercial CFD code Fluent 6.3. In addition to the minimum fluidization velocity, the experimental bed expansion is measured. The bed expansion for small particles and mixtures including up to 60% of large particles is about 20 mm at minimum fluidization velocity. This indicates that the fluidization properties in a fluidized bed reactor are significantly influenced of the smallest particles in the mixture.

The bed expansion for 80 and 100% large particles is about 6 mm. This is a rather low bed expansion, which is typical for Group B particles. The comparison between the experimental and computational results shows that the minimum fluidization velocities are strongly influenced of the smallest particles in the mixture. The experimental and computational results show the same tendency, that the minimum fluidization velocities are low and about constant for mixtures of 0 to about 60% of large particles. The computational minimum fluidization velocity is about double of the experimental fluidization velocity for small particles and mixtures with low concentrations of large particles. Mixture with 50, 60 and 80% large particles give good agreement between experimental and computational minimum fluidization velocities. The difference between the experimental and computational minimum fluidization velocity is significant for 100% large particles. The deviations are mainly due to the particle size range that is present in the experiments are not accounted for in the simulations of 100% small and 100% large particles. The deviations observed in the studies of the mixtures, may be reduced by using more than two particle phases to get a more representative particle size distribution.

REFERENCES

[1] Geldart, D., *Gas Fluidization Technology*, John Wiley & Sons Ltd., 1986.

[2] Kunii, D., Levenspiel, O., *Fluidization Engineering,* Second Edition, Butterworth-Heinemann, Newton, US, 1991.

[3] Halvorsen, B.M., Lundberg J., Mathiesen, V. (2008), Computational study of fluidized bed, Conference on Heat Transfer, Fluid Mechanics and Thermodynamics, HEFAT 2008, June 30. –July 2., Pretoria, South Africa.

[4] Ariyarathna, D.G.A.S.U, Wo, W.J., Halvorsen, B.M. (2008), Verifification of the importance of introducing particle size distributions to bubbling fluidized bed simulations, SIMS 2008, October 7th-8th, Oslo, Norway.

[5] Wu, W.J., Ariyarathna, D. G. A. S. U., Halvorsen, B. M.(2008), Experimental study of effects of particle size distribution on bubble behaviour for validation of CFD modelling of bubbling fluidized bed, SIMS 2008, October 7th-8th, Oslo, Norway.

[6] Jayarathna, S.A., Jayarathna, C.K., Wu, W.J., Halvorsen, B.M., (2008), Influence of particle size distributions on CFD simulations and experiments of bubbling fluidized beds. AIChE Annual Meeting 2008, November 16-21, Philadelphia, US.

[7] Ariyarathna, D.G.A.S.U (2008).Recommendation of a Model for Simulating & Analysis of the Influence of Particle Size Distribution on the Simulations of Bubbling Fluidized Beds. In Thesis for the degree of MSc. Ing, pp. 22-46.

[8] Syamlal, M., The Particle-Particle Drag Term in a Multiparticle Model of Fluidization., National Technical Information Service, Springfield, VA, 1987.

[9] Garside, J. & Al Dibuouni, M.R., Velocity-Voidage Relationships for Fluidization and Sedimentation, I&EC Process Des. Dev., **16**, pp. 206-214, 1977

[10] Dalla Valle, J.M., Micromeritics, Pitman, London, 1948.

[11] Ma, D., Ahmadi, G., Thermodynamical Formulation for Dispersed Multi-phase Turbulent Flows*, Int. J. Multiphase Flow,* **16**, pp. 323-351, 1990.

[12] Gidaspow, D., *Multiphase Flow and Fluidization*, Academic Press, Boston, 1994.

[13] Syamlal, M., O'Brien, T.J., A Generalized Drag Correlation for Multi-particle Systems, Morgantown Energy Technology Center, 1987.

[14] Halvorsen. B. M. (2005), An experimental and computational study of flow behaviour in bubbling fluidized beds.NTNU, 2005.